

Bone regeneration by tuning the drug release from the Calcium Phosphate Scaffolds

Dissertation

zur Erlangung des Grades

des Doktors der Ingenieurwissenschaften

der Naturwissenschaftlich-Technischen Fakultät

der Universität des Saarlandes

von

Kanupriya Khurana

Saarbrücken, 2017

Tag des Kolloquiums:

Dekan:

Berichterstatter:

.....

.....

Vorsitz:

Akad. Mitarbeiter:

Dedicated to my mom

“You may encounter many defeats, but you must not be defeated. In fact it may be necessary to encounter the defeats, so you can know who you are, what you can rise from, how you can still come out of it.”

Maya Angelou

Acknowledgements

Someone once told me, life during PhD is something unique, yet it is pretty much like its literal full form i.e. “Doctor of Philosophy”. A journey where one’s life is basically at the mercy of results obtained and four years of sleeping, eating or even vacations are with thoughts like what, why and how subconsciously. I am so used to live my life in this PhD box that it would be challenging to get back to normal life again. Interesting part of life in a PhD box is people, from supervisors to colleagues and so many people came along the way. I have to admit each life has gave me one or other reason to work on my personal growth and so much more. Believe it or not, every single person has taught me something and i am blessed to know all of you in your own special way. I want to sincerely thank you, by you, i mean:

-You, Pau and Cristina for your time, guidance and continuous support throughout this extraordinary journey. Thank you.

-You, Mucklich, Guido and Flavio, for your commitment, and guidance to make my german stay fruitful. Thank you

-You, Angelica, Carles, Daniel, Daniela, Daniela, Doreen, Edgar, Elisa, Erica, Joaquim, Jordi, Jose Maria, Kim, Marta, Mireia, Miquel, Monica, Monste, Monste, Noelia, Romain, Sergi, Triffon, Xell, Yago, colleagues from BBT research group for help, laughter and making the work life more fun.

-You, Ana, Idris, Jonas, Kathy, Nadine, Ray, Sebastian, Vincente, friends and colleagues from Saarland, for making my stay here warmer with your help and lovely time even in cold winters.

-You, Zhitong for your friendship and faith in me, Judit for giving me a beautiful and most amazing catalan family, Elia for being friend, lovely neighbour, and listening each day, Anna for our deep conversations, Joanna for adding fun in my life with your laugh, you all made my journey special and words are not enough to say how grateful i am for each one of you. Romain thanks for being a great partner in finishing this thesis together.

-You, all the interns who came for short time but you all added more life in my life.

-You, names’ which are not here but who all have supported me behind the scenes with most sincere thanks to you all.

Table of contents

Acknowledgements	v
List of Tables	ix
List of figures	xi
Abstract	xv
Kurzzusammenfassung	xvii
Objectives and Structure of the thesis	xix
<i>Objectives</i>	<i>xix</i>
<i>Structure</i>	<i>xx</i>
Chapter 1	1
State of the art	1
<i>Introduction</i>	<i>2</i>
<i>Bone</i>	<i>2</i>
<i>Bone Diseases</i>	<i>6</i>
<i>Bone Grafts</i>	<i>10</i>
<i>Calcium phosphate cements</i>	<i>15</i>
<i>Plasma Treatment</i>	<i>20</i>
Chapter 2	31
Simvastatin as an osteogenic drug: facts and future perspectives	31
<i>Abstract</i>	<i>32</i>
<i>Introduction</i>	<i>32</i>
<i>Role of simvastatin in bone metabolism and bone regeneration</i>	<i>35</i>
<i>Effects of simvastatin in the cell fate in vitro: cell culture studies</i>	<i>35</i>
<i>Effects of simvastatin in vivo</i>	<i>37</i>
<i>Systemic administration</i>	<i>38</i>
<i>Local administration</i>	<i>40</i>
<i>Conclusions</i>	<i>44</i>
Chapter 3	65

Design of calcium phosphate scaffolds with controlled simvastatin release by plasma polymerization	65
<i>Abstract</i>	66
<i>Introduction</i>	66
<i>Experimental</i>	68
<i>Results</i>	72
<i>Discussion</i>	79
<i>Conclusions</i>	83
Chapter 4	89
Effect of plasma polymerization coating of tricalcium phosphate ceramics on antibiotic delivery and biological performance	89
<i>Abstract</i>	90
<i>Introduction</i>	90
<i>Experimental</i>	92
<i>Results</i>	98
<i>Discussion</i>	106
<i>Conclusions</i>	110
Chapter 5	117
Injectable Calcium Phosphate Foams for the delivery of Pitavastatin as osteogenic and angiogenic agent	117
<i>Abstract</i>	118
<i>Introduction</i>	118
<i>Materials and methods</i>	120
<i>Results</i>	125
<i>Discussion</i>	131
<i>Conclusions</i>	135
Chapter 6 Conclusions	141

List of Tables

Table 1-1 Various pharmacological interventions that have been involved in the treatments of osteoporosis as vertebral, non-vertebral and hip fractures and their associated efficacy [20].	10
Table 1-2 Properties of the biologically relevant calcium phosphates [46], [47].	14
Table 1-3 Different strategies and approaches to manipulate the setting reactions [58]. ..	17
Table 2-1 Comparison of the lipophilicity of statins, simvastatin being among the most lipophilic. [19], [20].	36
Table 2-2 In vitro studies conducted to study the effect of the simvastatin on bone formation.....	46
Table 2-3 In vivo systemic administration of simvastatin to study the effect on bone formation. (P.O: Oral administration, IM: Intramuscular, IP: intraperitoneal).	48
Table 2-4 Local delivery of simvastatin through local injections (INJ) (Subcutaneous (SC), Intradermal (ID) or Intramuscular (IM)) at defect site.	50
Table 2-5 Local delivery of simvastatin by incorporating in implantable biomaterial carriers.	51
Table 3-1 Static contact angle and X-ray photoelectron spectroscopy (atomic concentration and atomic ratio) of the different CaP discs either untreated or after plasma polymerization.....	74
Table 3-2 C1s peak deconvolution.	74
Table 3-3 Simvastatin acid loaded and final amount released (11 days) from CDHA and b-TCP scaffolds with different plasma polymerization times.	77
Table 4-1 Polymerization conditions evaluated on β -TCP, static contact angle and Dynamic advancing and receding contact angles and contact angle hysteresis of β -TCP samples untreated (UT) or with different plasma treatments.	99
Table 4-2 Elemental composition obtained by XPS. β -TCP samples with different plasma treatments.....	100

Table 4-3 Ampicillin or Gentamicin released percentage β -TCP discs after 24 h and kopcha kinetics for the release kinetics.....	105
Table 5-1 Table 1: DNA sequences of forward (fw) and reverse (rv) primers for the selected genes used for real – time qPCR.....	123
Table 5-2 Degradation of PITA at pH 8 and pH 9.5 with the function of time (t = 24 h) and total degradation when loaded in i-CPFs 24 h, calculated according to eq. (3).....	126
Table 5-3 Specific surface area (SSA), skeletal density and Porosity of i-CPFS with and without PITA at 100 μ M, each measurement was conducted with 4 cylinders.....	128
Table 5-4 Percentage of total release of PITA in each i-CPF specimen after 72 h and values of R^2 and n with Kosermeier Peppas model for the release kinetics.....	131

List of figures

Figure 1-1 Hierarchical structure of bone: collagen fibrils, lamellae, osteons and trabecular, cortical and trabecular bone [8].	4
Figure 1-2 Bone remodeling process [10].	5
Figure 1-3 Micro-organisms (left) and pathogenic factors (right) behind the chronicity of a bone infection [16].	7
Figure 1-4 Etiology of osteoporosis and osteoporotic fractures [18].	9
Figure 1-5 During injury, adequate cells differentiate for the bone repair [25].	11
Figure 1-6 Different type of grafts that can be possible [28].	13
Figure 1-7 Schematic diagram for the process of formulation of cements.	15
Figure 1-8 Classification of the most common formulations of Calcium Phosphate Cements from [49].	16
Figure 1-9 Microporosity and microstructure of CPCs can be adjusted by varying some processing parameters such as the liquid-to-powder ratio or particle size [49].	18
Figure 1-10 Schematic diagram of the possible strategies to load drugs in calcium phosphate cements [49].	19
Figure 1-11 Scheme of plasma polymerization process.	21
Figure 2-1 Graphic representation of the conversion of simvastatin (SIM) to simvastatin acid (SVA) [16], [17].	34
Figure 2-2 Role of Simvastatin (SIM) in the bone regeneration.	35
Figure 3-1 SEM images of the different materials before (top images) and after plasma polymerization with PCL-PEG (4:1). β -TCP (a), CDHA (b), β -TCP-90CW (c), and CDHA-90CW (d). FIB-SEM cross-section of the surface of both polymerized materials β -TCP-90CW (e) and CDHA-90CW (f).	73
Figure 3-2 X-ray Photoelectron Spectroscopy C1s peak deconvolution, of (a) β -TCP and (b) CDHA with PCL-co-PEG (1:4) plasma coating 90CW.	75

Figure 3-3 Scanning electron micrographs of transversal sections of β -TCP and CDHA scaffolds after 90 min CW plasma polymerization at different depths. Views of the surface of pores found on the top surface layer (top image), at a depth of 550 μ m, and at 1500 μ m (lower image).	76
Figure 3-4 Pore entrance size distribution of β -TCP and CDHA obtained by Mercury Intrusion Porosimetry.	77
Figure 3-5 Cumulative release of SVA in (%) from β -TCP (a) or CDHA (b) scaffolds either untreated or after 90 min coating in continuous wave mode with hypothesis on the possible phenomena taking place (below).	78
Figure 3-6 Release pattern for SVA from CDHA scaffolds at (a) different treatment times with continuous wave mode (CW) or (b) different power supply mode being either continuous (CW) or pulsed (PW).	79
Figure 4-1 Chemical structure of ampicillin sodium salt (a) and gentamicin sulphate (b). .	92
Figure 4-2 Scheme of the experimental layout employed to obtain PEG-like coatings on β -TCP discs. Low pressure plasma: 1st activation of the surface by O_2 plasma and 2 nd plasma polymerization Ar as carrier with Diglyme monomer, with 10 min sequential treatments named as single polymerization (SP10), double polymerization (DP10), triple polymerization (TP10) and quadruple polymerization (QP10).	94
Figure 4-3 FTIR spectra of the plasma polymer (QP10) obtained on Si wafer as model surface.	98
Figure 4-4 Wettability of two plasma-polymerized substrates: silicon wafer (employed as flat model surface) and β -TCP samples (UT and SP10 were not measurable due to hydrophilicity). Images of the droplet on the surface of QP10 with the sample lying flat, or held vertical.	99
Figure 4-5 C1s spectra of the PEG-like plasma polymer coating on β -TCP for QP10. ...	100
Figure 4-6 Scanning Electron Micrographs of β -TCP untreated at two different magnifications (top) surfaces and of the surface of β -TCP at different polymerization conditions (left) with their corresponding transversal sections obtained by FIB. Arrows indicate the polymer coatings. (Other plasma polymer coatings: DP10, TP10 not shown).	101

Figure 4-7 Thickness of the PEG-like layer obtained by different plasma polymerization treatments on the surface of β -TCP as a function of the total treatment time.	102
Figure 4-8 SaOS-2 cells relative fold growth on untreated β -TCP and plasma-polymerized β -TCP at different cell culture times. (A indicates significant differences with respect to β -TCP, $P > 0.05$). TCPS accounts for "Tissue culture polystyrene" which is taken as a positive control.....	102
Figure 4-9 Scanning electron micrographs of untreated and plasma-coated β -TCP seeded with SaOS-2 cells for either 6 h (left) or 72 h (right).....	103
Figure 4-10 Evaluation of release kinetics of ampicillin and gentamicin (top) for 24 hours, total quantity released for both ampicillin and gentamicin (labelled with "D" for drug) for untreated and different treatments (bottom).	104
Figure 4-11 Continuous monitoring of the optical density of Staphylococcus Aureus bacterial suspensions in contact with ampicillin (AMP) and gentamicin (GENTA) loaded β -TCP ceramics either untreated (UT) or plasma polymerized (UT_P40m, SP10-D, DP10-D, TP10-D and QP10-D) or the suitable controls (in contact with <i>S. aureus</i> growth activity during 26 hours.	105
Figure 4-12 Representation of the wetting behaviour of β -TCP bioceramics before and after plasma polymerization of PEG-like layers.	108
Figure 5-1 Chemical structure of the Pitavastatin used in this study.....	121
Figure 5-2 Influence of temperature (5 & 37 °C) (top) and pH (8 & 9.5) (37 °C) on the stability of PITA solutions at different concentrations (Standard deviation was calculated with three replicates, error bars are really small to be seen clearly).	126
Figure 5-3 Influence of PITA on the gene expression of OCN, Col Type1, BMP-2 by rMSCs and VEGFR1, VEGFR2, VEGFA by EPCs and at 6, 24, 48 and 72 h. The statistical difference with TCPS and 0.1 μ M are represented as A and B respectively for each time point.....	127
Figure 5-4 FESEM images of i-CPF of control and Pitavastatin loaded i-CPF with 100 μ M h (top). μ CT images of control i-CPF and Pitavastatin loaded i-CPF at 100 μ M (bottom)..	129
Figure 5-5 MIP pore size entry distribution (n=4) of i-CPF and PITA loaded i-CPF.	129

Figure 5-6 Release curves of i-CPFs containing different amounts of PITA for 6 days (a), zoom of the initial 5 hours (b) and total amount of PITA released by 72 h is plotted for each specimen of PITA loaded i-CPFs such as 50-PITA, 75-PITA, 100-PITA & 200-PITA (c) with a proposed scheme of the release of PITA during the setting reaction..... 130

Abstract

Bone is among the most transplanted tissues with more than a million surgical procedures annually in Europe, and around two million worldwide. The regeneration of bone defects, caused by trauma, congenital deformities, age-related bone loss or bone infections represents an urgent challenge for today's healthcare system. This has fueled the demand of more efficient synthetic bone substitutes.

Due to their similar characteristics to the mineral phase of bone, calcium phosphates (CaPs) have raised a lot of interest. Some properties of calcium phosphates, like biodegradability, biocompatibility, bioactivity and osteoconduction represent a great potential for this application. Among them, calcium phosphate cements (CPCs) have additional advantages like injectability and in situ hardening ability. Moreover, the possibility to tune the porosity of CaPs in general and of CPCs in particular makes them suitable vehicles for local delivery of drugs. Loading CaPs with drugs allows conferring additional functionalities to the synthetic bone grafts, which is of great interest.

The main aim of this thesis is to explore CaP bioceramics as vehicles for local delivery of drugs, covering both low temperature biomimetic ceramics, like calcium deficient hydroxyapatite (CDHA), and high temperature sintered ceramics, like beta tricalcium phosphate (β -TCP), in the form of microporous and macroporous substrates. The physicochemical nature of these bioceramics, their porosity and textural properties plays an essential role in their drug delivery properties.

In order to be able to tailor the drug release kinetics of the bioceramics beyond their intrinsic properties, plasma polymerization has been investigated. Plasma is a particular state of a gas, electrically neutral, which is formed by ions, electrons, radicals, metastables, UV and visible radiation and can be employed in different applications. Although plasma polymerization has been widely studied for biomedical applications, its combination with bioceramics is rather unexplored.

To select a suitable drug for bone regeneration, an extensive literature review was done on statins, and more particularly on simvastatin as a potential osteogenic and angiogenic promoter (Chapter 2). This drug was evaluated within macroporous scaffolds of either CDHA or β -TCP as drug delivery vehicles. The drug-loaded materials were plasma-coated with polycaprolactone:poly ethylene glycol (PCL:PEG) co-polymers. The coating covered

the micro and nanopores of the CaPs surface and produced complex geometries presenting a nano and micro rough morphology which led to low wettability despite the hydrophilicity of the copolymer. Plasma coating with PCL-co-PEG on scaffolds loaded with simvastatin acid allowed delaying and modulating the drug release from the bone scaffolds depending on the thickness of the layer deposited, which, in turn depended on the initial specific surface area of the CaP (Chapter 3). To further investigate the fundamentals of plasma polymerization on bioceramics, PEG-like polymer coatings of different thickness were deposited on microporous β -TCP loaded with antibiotics. The rough β -TCP surface was associated to strong hydrophobic surface properties, which nevertheless retained their suitable biological behavior with regard to human osteoblast cells. The microbiological activity of the antibiotics was preserved, and the coatings reduced the total amount of drug released as a function of the increasing plasma treatment time (Chapter 4).

In another approach, a statin that had never before been employed in combination with CaPs, Pitavastatin (PITA), was investigated as potentially osteogenic and angiogenic promoter through in vitro studies which revealed dose-dependent enhancement of mineralization and vascularization. The incorporation of PITA to the liquid phase of an injectable CDHA foam allowed obtaining injectable local drug delivery scaffolds, without altering their macroporosity or textural properties. The drug release kinetics was affected by the evolving microstructure of the setting of the macroporous cement. Overall the results obtained proved that PITA seems to be a suitable novel candidate to enhance the osteogenic potential of synthetic bone grafts and identified the required doses to obtain the desired biological effects (Chapter 5).

Kurzzusammenfassung

Knochen gehört zu den am meisten transplantierten Geweben mit mehr als einer Million chirurgischen Verfahren jährlich in Europa und rund zwei Millionen weltweit. Die Regeneration von Knochenfehlern verursacht durch Trauma, angeborene Deformitäten, altersbedingter Knochenverlust oder Knocheninfektionen, stellt eine dringende Herausforderung für das heutige Gesundheitssystem dar. Dies hat zu einer gestiegenen Nachfrage nach effizienteren synthetischen Knochenersatzstoffen geführt.

Aufgrund ihrer ähnlichen Eigenschaften zu der Mineralphase des Knochens haben Calciumphosphate (CaPs) ein großes Interesse geweckt. Einige Eigenschaften von Calciumphosphaten, wie biologische Abbaubarkeit, Biokompatibilität, Bioaktivität und Osteokonduktion stellen ein großes Potenzial für diese Anwendung dar. Unter ihnen haben Calciumphosphat-Zemente (CPCs) zusätzliche Vorteile wie Injektionsfähigkeit und in situ Härtungsfähigkeit. Darüber hinaus macht die Möglichkeit, die Porosität von CaPs im Allgemeinen und von CPCs zu stimmen, insbesondere geeignete Fahrzeuge für die lokale Abgabe von Medikamenten. Das Laden von CaPs mit Medikamenten erlaubt es, den synthetischen Knochentransplantaten zusätzliche Funktionalitäten zu verleihen, was von großem Interesse ist.

Das Hauptziel dieser Arbeit ist es, CaP-Biokeramiken als Vehikel für die lokale Verabreichung von Arzneimitteln zu erforschen, die sowohl biologimetrische Tieftemperatur-Keramiken wie Kalzium-defiziente Hydroxyapatite (CDHA) und hochtemperaturgesinterte Keramiken wie Beta-Tricalciumphosphat (β -TCP), in Form von mikroporösen und makroporösen Substraten. Die physikalisch-chemische Natur dieser Biokeramiken, ihre Porosität und ihre strukturellen Eigenschaften spielen eine wesentliche Rolle bei ihren Arzneimittelabgabeeigenschaften.

Um die Arzneimittelfreisetzungs kinetik der Biokeramiken über ihre intrinsischen Eigenschaften hinaus anzupassen, wurde die Plasmopolymerisation untersucht. Plasma ist ein besonderer Zustand eines gases, elektrisch neutral, der durch Ionen, Elektronen, Radikale, Metastables, UV und sichtbare Strahlung gebildet wird und in verschiedenen Anwendungen eingesetzt werden kann. Obwohl die Plasmopolymerisation für biomedizinische Anwendungen weitgehend untersucht wurde, ist ihre Kombination mit Biokeramiken eher unerforscht.

Zur Auswahl eines geeigneten Arzneimittels zur Knochenregeneration wurde eine umfangreiche Literaturrecherche auf Statine und insbesondere auf Simvastatin als

potentieller osteogener und angiogenetischer Promotor durchgeführt (Kapitel 2). Dieses Arzneimittel wurde in makroporösen Gerüsten von entweder CDHA oder β -TCP als Arzneimittelabgabe-Vehikel untersucht. Die mit Arzneistoff beladenen Materialien wurden mit Polycaprolacton: Polyethylenglykol (PCL: PEG) -Kopolymere plasmabeschichtet. Die Beschichtung bedeckte die Mikro- und Nanoporen der CaPs-Oberfläche und erzeugte komplexe Geometrien, die eine nano- und mikro-raue Morphologie darstellten, die trotz der Hydrophilie des Copolymers zu einer geringen Benetzbarkeit führte. Die Plasmabeschichtung mit PCL-co-PEG auf mit Simvastatinsäure beladenen Gerüsten ermöglichte die Verzögerung und Modulation der Arzneimittelfreisetzung aus den Knochengerüsten in Abhängigkeit von der Dicke der abgeschiedenen Schicht, die wiederum von der anfänglichen spezifischen Oberfläche des CaP abhängt (Kapitel 3). Zur weiteren Untersuchung der Grundlagen der Plasmapolymerisation auf Biokeramiken wurden PEG-artige Polymerbeschichtungen unterschiedlicher Dicke auf mikroporösem β -TCP, das mit Antibiotika beladen war, abgeschieden. Die raue β -TCP-Oberfläche war mit starken hydrophoben Oberflächeneigenschaften verbunden, die dennoch ihr geeignetes biologisches Verhalten gegenüber menschlichen Osteoblastenzellen beibehielten. Die mikrobiologische Aktivität der Antibiotika wurde konserviert, und die Beschichtungen reduzierten die Gesamtmenge des Arzneimittels, die als Funktion der zunehmenden Plasmabehandlungszeit freigesetzt wurde (Kapitel 4).

In einem anderen Ansatz wurde das Pitavastatin (PITA), das noch nie in Kombination mit CaPs eingesetzt wurde, als potentiell osteogener und angiogenetischer Promotor durch In-vitro-Studien untersucht, die eine dosisabhängige Verstärkung der Mineralisierung und Vaskularisierung aufwiesen. Der Einbau von PITA in die flüssige Phase eines injizierbaren CDHA-Schaums ermöglichte die Gewinnung injizierbarer lokaler Arzneimittelabgabegerüste, ohne deren Makroporosität oder texturale Eigenschaften zu verändern. Die Arzneimittelfreisetzungskinetik wurde durch die sich entwickelnde Mikrostruktur der Einstellung des makroporösen Zements beeinflusst. Insgesamt zeigten die erzielten Ergebnisse, dass PITA ein geeigneter neuer Kandidat zu sein scheint, um das osteogene Potential von synthetischen Knochentransplantaten zu verbessern und die erforderlichen Dosen zu identifizieren, um die gewünschten biologischen Effekte zu erhalten (Kapitel 5).

Objectives and Structure of the thesis

Objectives

The main aim of this PhD thesis is to investigate new strategies for controlled drug delivery from calcium phosphate (CaP) bone substitutes (sintered CaP ceramic scaffolds and injectable calcium phosphate foams), which might contribute to enhanced bone regeneration.

Specifically, the following objectives have been set and constitute the different parts of this thesis:

- To conduct a thorough research on the existing literature on simvastatin, an osteogenic and angiogenic promoter, covering both *in vitro* and *in vivo* effects, to provide a basis for further advancements.
- To evaluate the potential of plasma polymerization in the modulation of drug release from CaP scaffolds. The issues tackled here are the design and thorough physico-chemical characterization of macroporous calcium deficient hydroxyapatite (CDHA) and β -tricalcium phosphate (β -TCP) scaffolds, their modifications by plasma polymer layers and the evaluation of loading and release of simvastatin acid (SVA) from the aforementioned scaffolds.
- To investigate in-depth the surface modification produced by plasma polymerization on β -TCP ceramics coated with PEG-like polymers, its effects on the biological behavior of the materials, and on the release properties of two antibiotics (ampicillin or gentamicin) loaded therein.
- To investigate a novel candidate drug, i.e. Pitavastatin (PITA) as an osteogenic and angiogenic promoter, in combination with injectable calcium phosphate foams (i-CPFs). This includes the investigation of the effects of PITA *in vitro* with relevant cell lines, the effects of PITA addition on the physical and chemical properties of i-CPFs, and the drug release patterns.

Structure

The present work involves the investigation of CDHA and β -TCP scaffolds, including injectable scaffolds (i-CPFs) as bone substitutes and drug delivery vehicles. Plasma polymerization has been investigated as a novel tool to modulate the drug release from the scaffolds. This thesis has been divided into four main parts. The schematic diagram of the structure of the present thesis is shown in Figure 1. In the beginning, a general state of the art including bone, bone substitutes, drug delivery vehicles and plasma polymerization has been discussed (Chapter 1). Chapter 2 presents a literature review for simvastatin, as osteogenic and angiogenic promoter. Chapter 3 introduces the development of SVA-loaded calcium phosphate scaffolds (CDHA or β -TCP) where controlled release was aimed at using plasma polymerization. The findings of the latter led to further interest in the effects of plasma polymerization found on the surface properties of calcium phosphates. Thus, Chapter 4 focuses upon the fundamentals of plasma polymerization on β -TCP loaded with two different antibiotics, Ampicillin and Gentamicin. In the end, Chapter 5 introduces i-CPFs as potential drug delivery vehicles for a novel drug candidate, Pitavastatin to investigate it as osteogenic and angiogenic promoter.

Chapter 1

State of the art

Bone, bone grafts, calcium phosphates, drug delivery & plasma polymerization

Chapter 2

Literature review: Simvastatin an osteogenic and angiogenic promoter

Chapter 3

CaPs (CDHA or β -TCP) as tunable drug delivery vehicle

CDHA

β -TCP

Simvastatin acid

PCL:PEG

Drug delivery

Chapter 4

Fundamentals of Plasma polymerization

β -TCP

Ampicillin or Gentamicin

PEG

Drug delivery

Biocompatibility

Anti-bacterial

Chapter 5

Injectable calcium phosphate foams (i-CPFs) as drug delivery vehicle

i-CPFs

Pitavastatin

in vitro

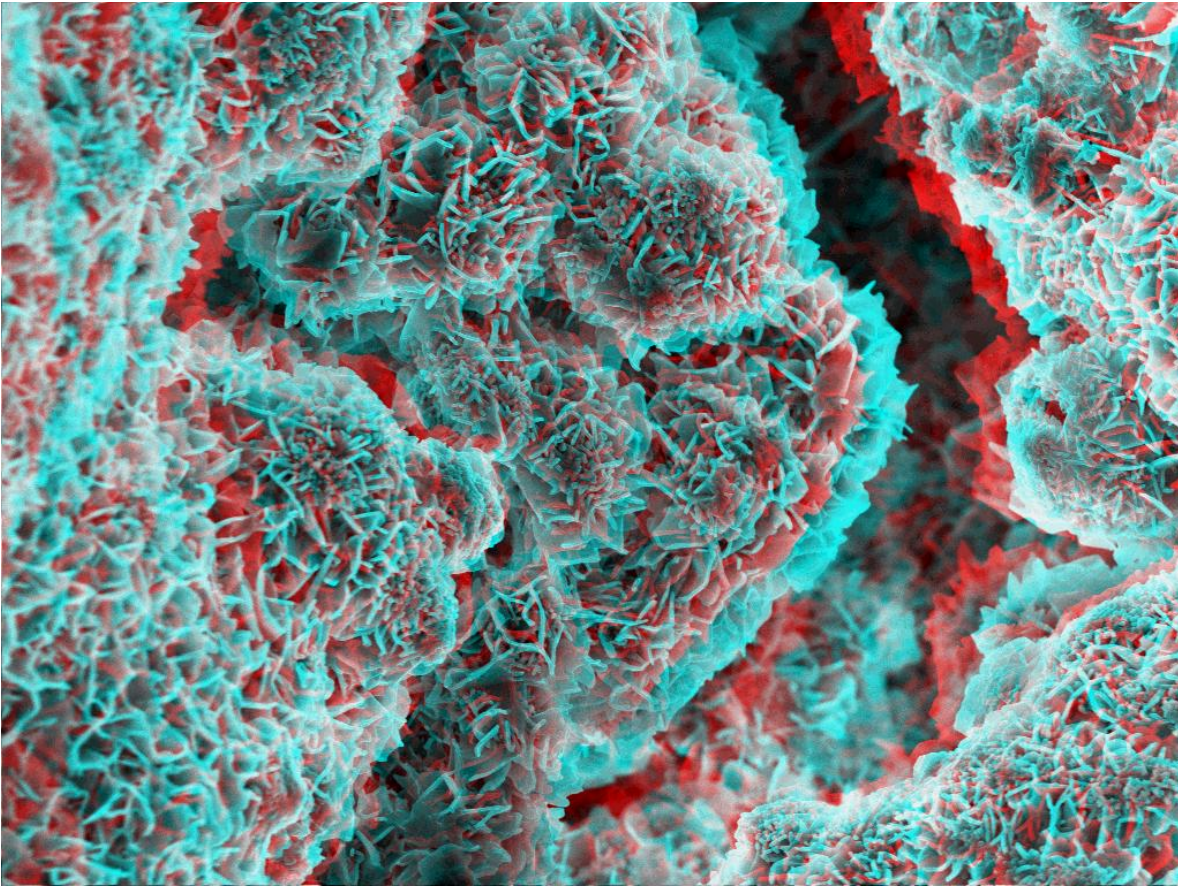
Drug delivery

Chapter 6

Conclusions

Chapter 1

State of the art



3D SEM image of calcium deficient hydroxyapatite (CDHA)

Introduction

Bone is among the most transplanted tissues with more than a million surgical procedures annually in Europe. Bone defects may be due to trauma, congenital deformities, bone loss due to ageing and bone infections. Bone replacement materials are currently estimated for a worldwide market of € 5 billion, with a 10 % annual growth. In 2010, estimated costs for osteoporotic and fragility fractures were € 37 billion including 66 % of this cost for incident fractures, 29% for long term fracture and 5 % for prevention. By 2025, these estimated costs are expected to shoot with a 25 % increase [1]. According to the World Health organization, musculoskeletal diseases are expected to be the fourth main disability by the year 2020 [2]–[4].

In the following sections, the composition, structure and functions of bone will be described. The understanding of the hierarchal structure and processes like modeling and remodeling of bone will provide the necessary information that can help designing of the biomaterials for the bone regeneration process. Apart from this, bone features like osteoinduction, osteoconduction or osteointegration can support the understanding of the grafts that have been used and will be used in future. Ultimately, an important facet of this thesis being local or controlled delivery of the selected drug by plasma polymerization to enhance bone regeneration, angiogenesis or antibiotics for osteomyelitis will be discussed in the further sections.

Bone

Bones in our body are living tissues. A child is born with about 300 soft bones. During childhood and adolescence, the cartilage grows and is slowly replaced by hard bone. Some of these bones later fuse together; eventually the adult skeleton has 206 bones. This characteristic reflects the capability of bone to grow or repair with help of the bone marrow. Bones are vascularized with their own blood vessels and are made of living cells in bone marrow. Bones are innervated organs made up of bone tissue, bone marrow, and a surrounding connective tissue called periosteum [5]. The skeleton serves as structural support while protecting the vital organs. Bones act as the ion, growth factors, nutrients, and proteins reservoir and are highly responsible for the calcium/phosphate balance and detoxification of the heavy metals [6]. Composition of the bone makes them a suitable provider for an environment for marrow where blood cells are produced. Due to osteogenesis, mineralization and degradation / resorption bone can go through modeling

and remodeling [6].

Bone Architecture:

Bone is a highly hierarchical structure from the nano to the macro size scale as shown in Figure 1-1. A general classification includes two types of bones; compact or cortical bone and trabecular or cancellous or spongy bone. The hard outer layer called cortical (compact) bone is strong, dense and tough. The spongy inner layer called trabecular (cancellous) bone is lighter and less dense than compact bone.

Cortical bone comprises 80 % of the total mass of the skeleton and is generally found in the shaft of long bones and outer shells. Trabecular bone is located inside the cortical tissues, in medullary cavities at the end of long bones and within the interior of short bones like spinal vertebrae. One of the major microstructural parameters in cortical bone is its porosity around 5-10%. This porosity is contributed by Haversian canals, Volkmann's canal and resorption cavities. Trabecular bone is a three-dimensional structure of interconnected plates and rods known as trabeculae of around 200µm thick. The porosity of trabecular bone is between 75-95%. The pores in trabecular bone are interconnected and filled with bone marrow [7], [8].

Microscopically, these two structures, cortical or spongy are consequences of a specific arrangement of collagen fibers at lower scale: as lamellar bone or as woven bone.

- **Lamellar bone** is characterized by a regular parallel alignment of collagen into sheets (lamellae) and is mechanically strong.
- **Woven bone** is characterized by a haphazard organization of collagen fibers and is mechanically weak.

Woven bone is produced when osteoblasts produce osteoid rapidly. This occurs initially in all foetal bones, but the resulting woven bone is replaced by remodeling and the deposition of more resilient lamellar bone. In adults, woven bone is formed when there is very rapid new bone formation, as occurs in the repair of a fracture. Following a fracture, woven bone is remodelled and lamellar bone is deposited. Virtually all bone in the healthy mature adult is lamellar bone.

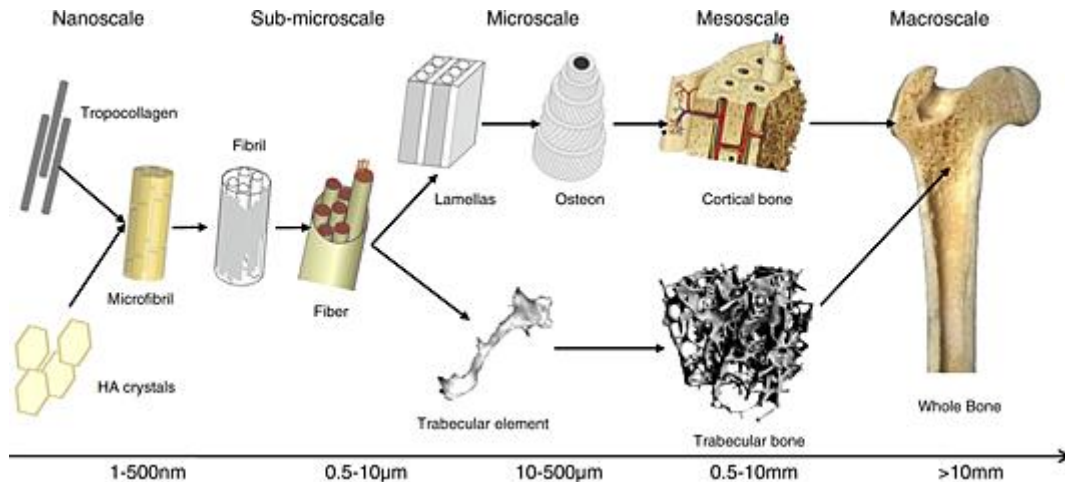


Figure 1-1 Hierarchical structure of bone: collagen fibrils, lamellae, osteons and trabecular, cortical and trabecular bone [8].

Bone Matrix Composition:

Bone is a composite material formed by an inorganic component (70%) and an organic matrix (30%). On the other hand, the inorganic part of bone consists of poorly crystalline calcium-deficient hydroxyapatite (95%). The mineral hydroxyapatite phase (calcium phosphate crystal) contains multiple ionic substitutions. Hydroxyapatite has an open and hospitable structure which allows several ionic substitutions such as sodium, magnesium, fluoride or citrate, being the most common carbonate-substituted. On the other hand, the remaining organic matrix is constituted by collagen (90%) and non-collagen structural proteins such as proteoglycans, sialoproteins, growth factors and cytokines, including bone forming cells, such as osteoblasts, osteoclasts and osteocytes [7], [9]. These bone forming cells and their biological cascades derived from them will be deeply described in the following sections.

Bone cells

Bone cells (Figure 1-2) are responsible for bone production, maintenance and modeling:

- **Osteoblasts:** These cells are derived from mesenchymal stem cells and are responsible for bone matrix synthesis and its subsequent mineralization.
- **Osteocytes:** These cells are osteoblasts that become incorporated within the newly formed osteoid, which eventually becomes calcified bone. They are thought to be ideally situated to respond to changes in physical forces upon bone and to transduce messages to cells on the bone surface, directing them to initiate resorption or formation responses.

- Osteoclasts:** These cells are large multinucleated cells, like macrophages, derived from the hematopoietic lineage. Osteoclasts function in the resorption of mineralized tissue and are found attached to the bone surface at sites of active bone resorption. One of their characteristic features is a ruffled edge where active resorption takes place with the secretion of bone-resorbing enzymes, which digest bone matrix.

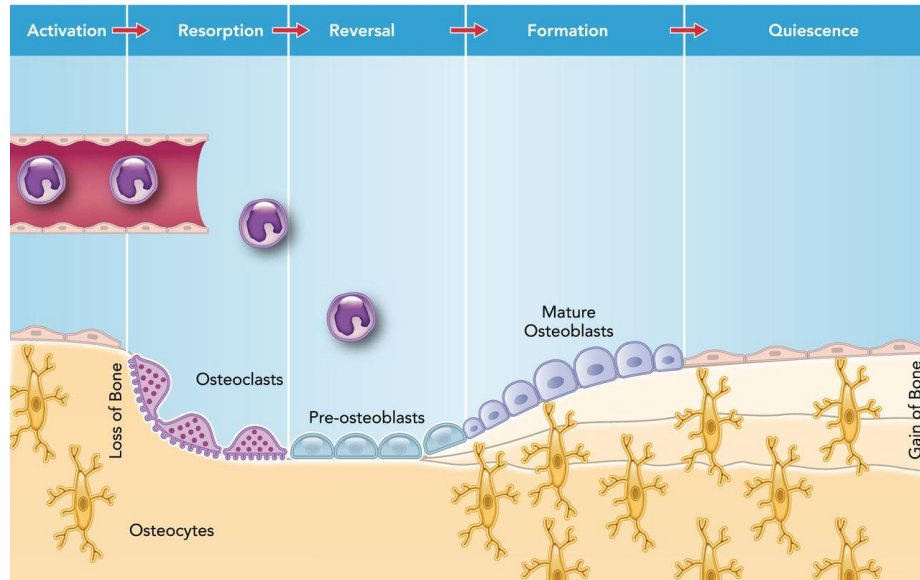


Figure 1-2 Bone remodeling process [10].

Bone modeling

Modeling occurs when bone resorption and bone formation occur on separate surfaces (i.e. formation and resorption are not coupled). During birth to adulthood, long bone grows in length and diameter and is also responsible for gain in skeletal mass and changes in skeletal form.

Bone remodeling

Replacement of old tissue by new bone tissue is known as bone remodeling process. This mainly occurs in the adult skeleton to maintain bone mass. This process consists of five phases as shown in Figure 1-2:

- Activation:** Under the influence of cytokines and growth factors pre-osteoclasts are stimulated and differentiate into mature active osteoclasts.
- Resorption:** Osteoclasts digest mineral matrix (old bone) and produce an acid environment.

3. **Reversal:** Resorption finishes by the osteoclast apoptosis while activation of the pre-osteoblast takes place.
4. **Formation:** Pre-osteoblasts differentiate to osteoblasts and synthesize new bone matrix.
5. **Quiescence:** This phase is also called as resting phase because osteoblasts become resting bone lining cells on the newly formed bone surface.

Bone Diseases

As bone is a critical component and being involved in so many functions and processes it is highly prone to diseases from osteoporosis to bone infections, ranging through a number of bone cancers. One of the reasons known behind bone diseases is imbalance in the ions or growth factors or proteins like vascular endothelial growth factor (VEGF) or bone morphogenetic protein-2 (BMP-2). Other major issues and pathologies are known to be caused by the accidental trauma, infections due to surgery or other causes or age related causes.

Traumatic bone defects

One of the most frequent musculoskeletal injuries that are recorded is fractures of long bone. Fractures, bone dislocations or severe bone damage due to accidental injuries are recorded in high numbers worldwide. Fractures are defined as a single or multi-fragmentary circumferential disruption of a diaphysis or metaphysis or a single disruption of an articular surface [11]. Among most common traumatic fractures are long-bone fractures, pelvic fracture in pediatric or adult trauma patients, forearm or elbow injuries, cranio-maxillofacial trauma, spinal injuries or traumatic brain injuries (TBI) etc. [12], [13]. In 1986, Schmitz and Hollinger introduced the term of critical size bone defects referring to the defects that are unable to heal completely during the lifetime of an animal [14]. To heal the critical size defects different grafting options are available. The increasing number of trauma has raised the demand of bone grafts.

Bone infection, Osteomyelitis

Osteomyelitis (*osteo-* derived from the Greek word *osteon*, meaning bone, *myelo-* meaning marrow, and *-itis* meaning inflammation) is the appellation used for bone infection. Osteomyelitis is common bone pathology of bone infection mostly caused by bacteria or other germs. Most common bacteria known for the osteomyelitis are *S. aureus*

and *S. epidermidis*. Infection can be caused by different pathologies as discussed below [15]:

- **Devascularization:** Originated from trauma, surgical intervention (mechanical damage or overheating) and leads to bone necrosis. In the case that necrosis exists in both sides of a fracture, an infected non-union is inevitable [15].
- **General infection:** Bacterial infection may come from damaged soft tissues or travel through blood stream and spread to the bone. This occurs when the patient has an infection elsewhere such as pneumonia etc.
- **Implant associated infection:** Any foreign body is capable of retaining bacteria on its surface protected by a biofilm [15]. Despite, the sterilization of the implant surfaces and proper handling during the surgery, there is still certain percentage of infections.

In 200, Ciampolini and Harding summarized the micro-organisms and pathogenic factors behind the chronicity of a bone infection as shown in Figure 1-3 [16]. Axford presented in 2010 a complete study of joint and bone infections and a special focus on osteomyelitis [17].

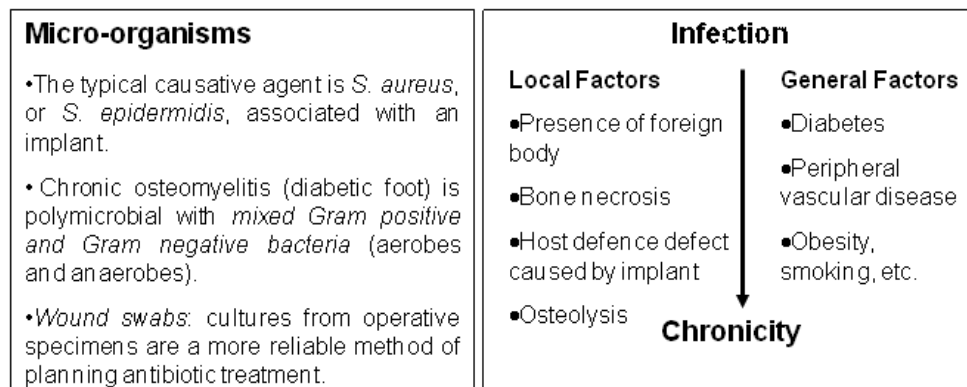


Figure 1-3 Micro-organisms (left) and pathogenic factors (right) behind the chronicity of a bone infection [16].

Mainly literature shows two routes of administration (oral and intravenous (IV)) among others. However, this has different disadvantages, such as side effects or low patient compliance. Local drug delivery in musculoskeletal disorder treatments can address some of the critical issues more effectively and efficiently than the systemic delivery. It ensures

delivery of the drug to the surrounding tissue at the target site, allowing decreasing the dosage which reduces associated toxicity to other non-target sites.

In this thesis, two antibiotic drugs will be evaluated: ampicillin (pencillin) and gentamicin (aminoglycoside), which will be incorporated to calcium phosphate bone grafts to evaluate novel methods to achieve controlled release.

Osteoporosis

Osteoporosis is known as the major cause for the disability and death in the elderly population. It causes an increased risk of fracture, disruption of bone micro architecture and reduction in non-collagenous proteins. Osteoporosis is a growing issue in the modern world. 30% of Caucasian woman over 50 years old suffer osteoporosis at the hip, spine or forearm. An osteoporotic fracture due to a major or minor trauma is due to a bone that has lower bone quantity and quality. The major reasons for the bone loss can be hormonal changes after menopause, estrogen deprivation, vitamin D or calcium deficiency and many other factors as shown in Figure 5. Many comprehensive approaches to the therapy of Osteoporosis have been taken. Successful therapy includes mainly aspects like treatment of pain, initiation of physical activity, nutrition, Vitamin D or calcium supplements, and Hormonal replacement therapy (HRT). List of some most common pharmaceutical treatment options is shown in Table 1-1.

Three major therapies include anti-resorptive therapy, osteoanabolic therapy and other medications [19]. Presently these treatments of osteoporosis rely on the systemic administration (generally oral) of some drugs from the following families are here as examples:

- **Anti-resorptive therapy**

Bisphosphonates: Bisphosphonates present an inhibitory effect on osteoclast-mediated bone resorption and are widely used to treat increased bone turnover such as osteoporosis but also Paget's disease of bone or metastatic bone tumor.

Calcitonin and parathyroid hormone: Whereas administration of parathyroid hormone stimulates bone formation in fracture healing, calcitonin presents the opposite effect by reducing the activity of osteoclasts, i.e. bone resorption, modulating the levels of calcium in serum and kidney.

- **Osteoanabolic therapy**

Strontium ranelate: Strontium ranelate increases both bone formation by promoting differentiation of osteoblast precursors and decreases bone resorption limiting the activation of osteoclasts.

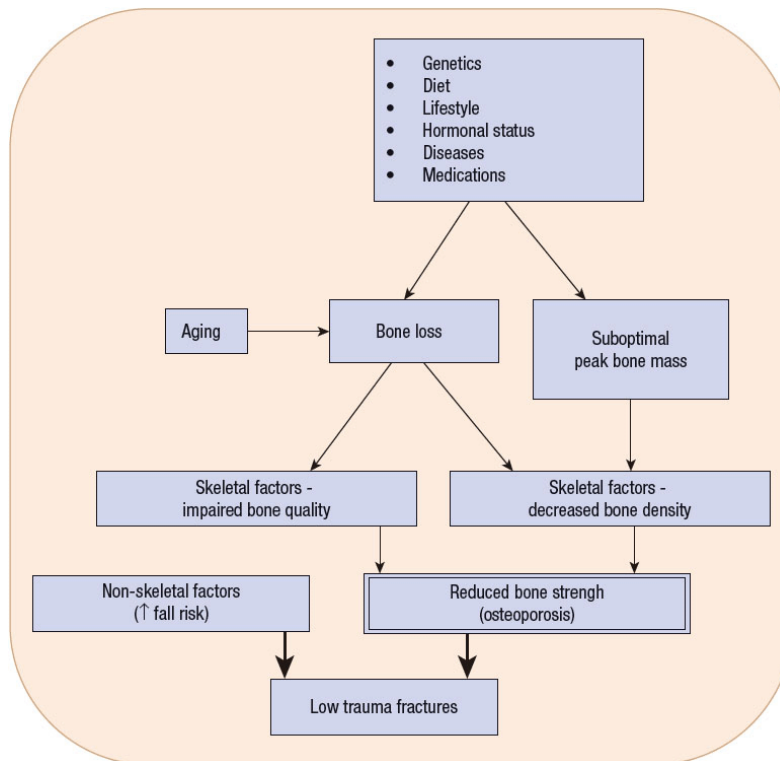


Figure 1-4 Etiology of osteoporosis and osteoporotic fractures [18].

Nevertheless, prevention of osteoporosis by following patient presenting risk factors is the approach chosen nowadays to prevent fractures and increase bone density by lifestyle advices (balanced diet, adequate calcium and vitamin D intake, mobility) or light drug therapies with bisphosphonates or selective estrogen receptor modulator raloxifene, particularly in post-menopausal woman [19], [21], [22].

Table 1-1 Various pharmacological interventions that have been involved in the treatments of osteoporosis as vertebral, non-vertebral and hip fractures and their associated efficacy [20].

Agent	Route and Frequency of Administration	BMD Response		Fracture Risk Reduction in Postmenopausal Osteoporosis		
		Spine	Hip	Spine	Hip	Nonvertebral
Alendronate	PO, daily or weekly	+++	++	+	+	+
Ibandronate	PO, daily or monthly; IV infusion, q3mo	+++	++	+		
Risedronate	PO, daily or weekly	+++	++	+	+	+
Zoledronic acid	IV, yearly	+++	++	+	+	+
Calcitonin	Intranasal spray, daily			+		
Estrogen/hormone replacement	PO, daily; transdermal patch, twice weekly	+++	++	+	+	+
Raloxifene	PO, daily	++	+	+		
Teriparatide	SC injection, daily	++++	+	+		+

BMD, bone mineral density; +, modest response; ++, moderate response; +++, good response; +++++, very good response.

By understanding the above information it is clearly seen that anti-resorptive drugs are not sufficient if osteoporosis is chronic. Thereby, a localized drug delivery system can be more suitable for the chronic osteogenesis.

In this PhD thesis, two drugs, simvastatin and Pitavastatin from the family of statins, will be loaded with the prepared biomaterials, with the focus on traumatic bone injuries or osteoporosis in views of fostering bone regeneration.

Bone Grafts

A bone graft is the replacement or augmentation of a fracture or diseased part of a bone by transplanting a biomaterial substitute. It is a surgical procedure generally done to reverse loss or resorption of bone due to trauma or diseases such as osteoporosis or Paget's disease. Surgeons use bone grafts to repair and rebuild diseased bones in patient's hips, knees, spine, and sometimes other bones and joints. Grafts can also repair bone loss caused by some types of fractures or cancers. Once your body accepts the bone graft, it should provide a framework for growth of new, living bone. Different types of bone grafts will be discussed in further section. Before discussing the types of bone grafts, it is important to understand the physiology of the bone grafting.

The Physiology of Bone-Grafting

The biology of bone grafts and their substitutes is based on the clear understanding of the bone formation processes of *osteogenesis*, *osteinduction*, and *osteoconduction*. After considering these parameters, the success rate of the bone graft can be estimated theoretically.

Graft osteogenesis: The cellular elements within a donor graft, which survive transplantation and synthesize new bone at the recipient site. Osteogenesis is highly dependent on the osteoinductive properties of the graft or on the site of transplantation [23], [24].

Graft osteoinduction: It is a process to activate osteogenesis. While new bone forms through the active recruitment of host mesenchymal stem cells from the surrounding tissue, which differentiate into bone-forming cell lineage / osteoblast cells. This process is facilitated by the presence of growth factors within the graft, principally bone morphogenetic proteins (BMPs). In addition to the differentiated bone cells, some less differentiated cells are also present in the bone and adjacent tissues. These undifferentiated cells play a very important role in bone healing and anchorage of an implant since they can form osteoprogenitor cells as well (Figure 1-5). Later, with the correct stimulus from growth factors as already mentioned they can help in bone growth through bone forming cells [23], [24].

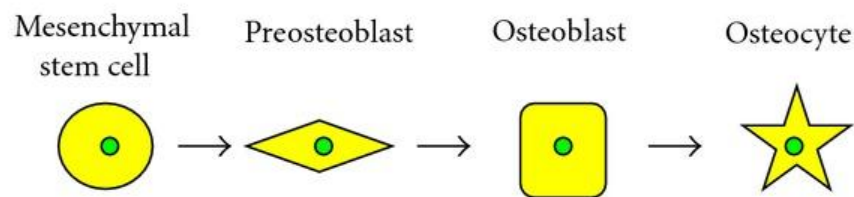


Figure 1-5 During injury, adequate cells differentiate for the bone repair [25].

Graft osteoconduction: The process of bone growth on the surface or down into pores or channels of the transplant is known as osteoconductivity. Such three-dimensional structural graft is conducive for on growth and/or ingrowth of newly formed bone [26]. This behavior directs the bone growth to conform to the material's surface. It involves facilitation of blood-vessel incursion and new-bone formation into a defined passive trellis structure. Though the bone growth is completely dependent on the action of differentiated bone cells,

without a proper blood supply bone growth and bone conduction both are not possible [23], [24]. Thus, angiogenesis is of uttermost importance.

Autogenous bone grafts

Autogenous grafts are considered “gold standard,” as a solution to the bone tissue engineering paradigm. Autografts are sections or fragments of bone removed from one site on the patient, typically the iliac crest, and implanted to another site based on need. Autografts harvested from the iliac crest are mostly trabecular bone with a thin shell of cortical bone. Since autografts originate within the patient, they are readily incorporated at the implant site and rarely elicit any immune responses, which allow autografts to have excellent wound healing properties [5], [27].

The major advantage of autologous grafts is that only potential progenitor cells transfer to the site of transplantation. Other advantages are low rate of transmission diseases and excellent success rate. However, autografts have a few drawbacks; there is often donor site morbidity indicated by necrosis and infection at the location of autograft harvest that may cause the patient more pain from the harvest site than the implant site. Additionally, autografts are limited in availability to the amount of tissue that can be harvested from the donor site. It is these shortcomings plaguing the autograft that has increased the effort to find other bone graft substitutes.

Allogenic bone grafts

Allogenic grafts are also known as allografts, and this technique is based on the harvesting of bone from one organism to another between the same species. In other words, a lack of similar genetic is avoided. One of the major advantages of allografts is their availability in different shapes and sizes, harvested from the cadavers. This avoids the problems with the donor-site morbidity and sacrifice of the host structure. Allogenic bone can be provided as demineralized bone matrix, morsellized or cancellous chips, cortical grafts, osteochondral and others like whole bone segments. Literature has shown that structural allografts are more stable mechanically. The major disadvantage or cause of concern is the fact that they are documented for HIV and hepatitis C virus transmissions [27].

Xenogenic bone grafts

As a parallel to the allograft, the xenograft uses harvested bone from other species, generally pig or cows. The obvious problem in this case is the huge genetic variation

existing between the donor and the patient. Therefore, there is a high probability of immune rejection or consequent rejection of the implant.

Allografts and Xenografts are generally preferred by patients and professionals as it avoids a potentially painful harvesting procedure. However, bone regeneration is likely to take somewhat longer than in an autografts case due to the lack of osteogenic and osteoinductive properties.

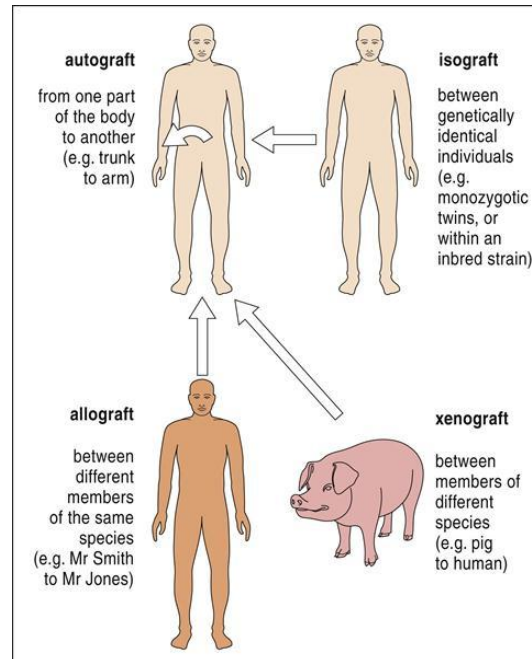


Figure 1-6 Different type of grafts that can be possible [28].

Synthetic bone grafts

Current commercial substitute materials to replace or repair teeth and bones include metals, polymers (natural or synthetic), corals, and coral derived, synthetic ceramics (calcium phosphates, calcium sulphate, calcium carbonate, bioactive glasses), and composites [29]. Depending on their ability to stimulate a response from the tissue, materials are classified into bio inert (e.g.: metals some polymers, some ceramics) and bioactive materials (including natural polymers, calcium phosphates, calcium carbonate, calcium sulphate and bioactive glasses).

Ceramic based bone graft substitutes

Calcium orthophosphates have been studied as bone repair materials for the last 80 years. The first in vivo use of calcium orthophosphates was performed in 1920, when researchers implanted tricalcium phosphate (TCP) into animals to test its efficacy as a bone substitute

[30]. However, in 1951 it was Ray et al., when for the first time hydroxyapatite (HA) was implanted in rats and guinea pigs. Those attempts might be characterized as the initial medical trials with the first generation of bone substituting biomaterials. In the 1970s other calcium orthophosphates were synthesized, characterized, investigated and tried in medicine [31], [32]. Nowadays the most commonly used ceramics are hydroxyapatite and β -TCP as synthetic bone grafts. These grafts are of importance due to their characteristics such as solubility shown in Table 1-2.

Table 1-2 Properties of the biologically relevant calcium phosphates [46], [47].

Ca/P molar ratio	Compound	Formula	Solubility at 25°C, -log(K _s)	Solubility at 25°C, g/L	pH stability range in aqueous solutions at 25°C
0.5	Monocalcium phosphate monohydrate (MCPM)	Ca(H ₂ PO ₄) ₂ ·H ₂ O	1.14	~ 18	0.0 – 2.0
0.5	Monocalcium phosphate anhydrous (MCPA or MCP)	Ca(H ₂ PO ₄) ₂	1.14	~ 17	[6]
1.0	Dicalcium phosphate dihydrate (DCPD), mineral brushite	CaHPO ₄ ·2H ₂ O	6.59	~ 0.088	2.0 – 6.0
1.0	Dicalcium phosphate anhydrous (DCPA or DCP), mineral monentite	CaHPO ₄	6.90	~ 0.048	[6]
1.33	Octacalcium phosphate (OCP)	Ca ₈ (HPO ₄) ₂ (PO ₄) ₄ ·5H ₂ O	96.6	~ 0.0081	5.5 – 7.0
1.5	α -Tricalcium phosphate (α -TCP)	α -Ca ₃ (PO ₄) ₂	25.5	~ 0.0025	[6]
1.5	β -Tricalcium phosphate (β -TCP)	β -Ca ₃ (PO ₄) ₂	28.9	~ 0.0005	[6]
1.2 – 2.2	Amorphous calcium phosphates (ACP)	Ca _n H _n (PO ₄) _n ·nH ₂ O, n = 3 – 4.5; 15 – 20% H ₂ O	[6]	[6]	~ 5 – 12 [6]
1.5 – 1.67	Calcium-deficient hydroxyapatite (CDHA or Ca-def HA) [6]	Ca _{10-x} (HPO ₄) _x (PO ₄) _{6-x} (OH) _{2-x} (0 < x < 1)	~ 85	~ 0.0094	6.5 – 9.5
1.67	Hydroxyapatite (HA, HAp or OHAp)	Ca ₁₀ (PO ₄) ₆ (OH) ₂	116.8	~ 0.0003	9.5 – 12
1.67	Fluorapatite (FA or FAp)	Ca ₁₀ (PO ₄) ₆ F ₂	120.0	~ 0.0002	7 – 12
1.67	Oxyapatite (OA, OAp or OXA) [6]	Ca ₁₀ (PO ₄) ₆ O	~ 69	~ 0.087	[6]
2.0	Tetracalcium phosphate (TTCP or TetCP), mineral hilgenstockite	Ca ₄ (PO ₄) ₂ O	38 – 44	~ 0.0007	[6]

[6] These compounds cannot be precipitated from aqueous solutions.

[7] Cannot be measured precisely. However, the following values were found: 25.7±0.1 (pH = 7.40), 29.9±0.1 (pH = 6.00), 32.7±0.1 (pH = 5.28). The comparative extent of dissolution in acidic buffer is: ACP >> α -TCP >> β -TCP > CDHA >> HA > FA.

[8] Stable at temperatures above 100°C.

[9] Always metastable.

[10] Occasionally, it is called "precipitated HA (PHA)".

[11] Existence of OA remains questionable.

In 2008, LeGeros [29] listed some properties of CaPs that are relevant to achieve adequate bone regeneration, like interconnecting porosity, biodegradability, bioactivity, osteoconductivity and osteoinductivity. The osteoconductive CaP biomaterials allow the cell colonization, and the associated cellular events like migration, proliferation, attachment and differentiation to bone-forming cells. These bone substitutes have additional advantages such as long shelf life, availability and no risk of disease transfer [27], [45].

Calcium phosphate cements

In 1980s Brown and Chow patented self-setting Calcium phosphate cements (CPC) [33]. In general, CPC are formed by a combination of one or more calcium phosphate powders and an aqueous solution to form a paste that is able to set and harden after being implanted within the body. Properties like setting times, compressive strength, porosity, solubility or *in vivo* resorption etc. are affected by processing parameters like liquid to powder (L/P) ratio or particle size [48], [49]. The cement sets as a result of a dissolution and precipitation process as shown in Figure 1-7. The entanglement of the precipitated crystals is responsible for cement hardening. Based on the initial formulations either single or multicomponent, there can be two types of apatitic cements that yield the most stable calcium phosphate at $\text{pH} > 4.2$ which is hydroxyapatite and brushite formed at $\text{pH} < 4.2$ with multicomponent (Figure 1-8) [49], [50].

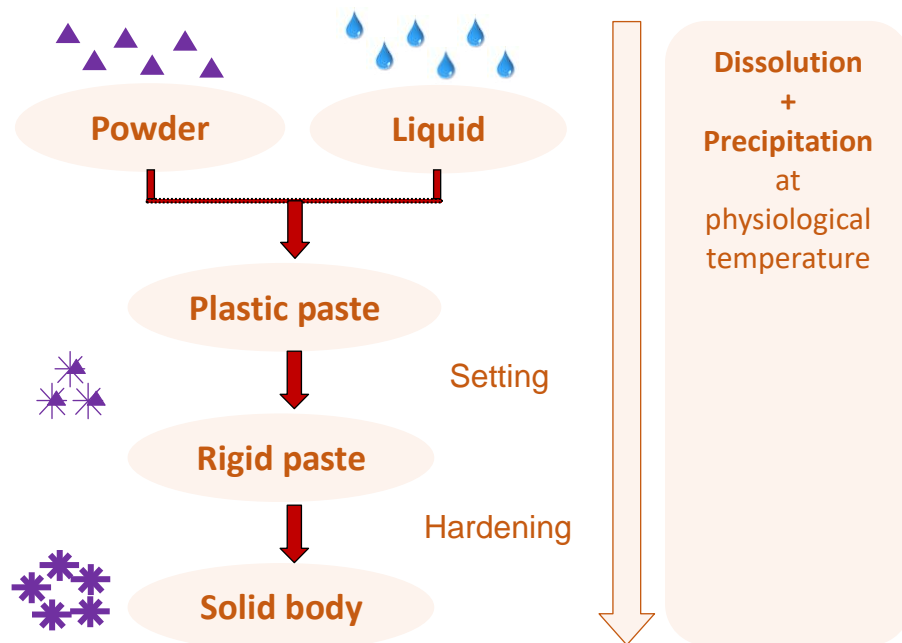


Figure 1-7 Schematic diagram for the process of formulation of cements.

The relevance of hydroxyapatite as a bone substitute arises from the fact that the mineral in bone is a poorly crystalline carbonate- and other substituent-containing analogue of apatite. As mentioned in Section 1.1.2, 90% of the inorganic bone matrix is made up of hydroxyapatite. Therefore, hydroxyapatite is the synthetic graft closest in chemical composition to the natural bone [51], [52]. When set, CPC consist of a network of calcium phosphate crystals, which closely resemble the mineral phase of the bone tissue [52]–[56].

	Apatitic Cement		Brushitic Cement
	Single Component	Multiple Components	
Reactives	α -TCP	TTCP + DCPA/DCPD	β -TCP + MCPM/MCPA
Reaction	$3\alpha\text{-Ca}_3(\text{PO}_4)_2 + \text{H}_2\text{O} \rightarrow \text{Ca}_9(\text{HPO}_4)_4(\text{PO}_4)_6(\text{OH})$	$2\text{Ca}_3(\text{PO}_4)_2\text{O} + 2\text{CaHPO}_4 \rightarrow \text{Ca}_{10}(\text{PO}_4)_6(\text{OH})_2$	$\beta\text{-Ca}_3(\text{PO}_4)_2 + \text{Ca}(\text{H}_2\text{PO}_4)_2 \cdot \text{H}_2\text{O} + 7\text{H}_2\text{O} \rightarrow 4\text{CaHPO}_4 \cdot 2\text{H}_2\text{O}$
Type of Reaction	Hydrolysis	Acid-Base	Acid-Base
Setting mechanism and crystal morphology			
SEM		<div style="display: flex; align-items: center; justify-content: center;"> <div style="writing-mode: vertical-rl; transform: rotate(180deg);">APATITE</div> <div style="writing-mode: vertical-rl; transform: rotate(180deg);">BRUSHITE</div> </div>	

Figure 1-8 Classification of the most common formulations of Calcium Phosphate Cements from [49].

In this PhD Thesis, apatitic cements will be used. The starting material selected will be α -Tricalcium Phosphate, which after mixing with water hydrolyzes to calcium deficient hydroxyapatite (CDHA), a low temperature ceramic and after sintering transforms to beta-tricalcium phosphate (β -TCP).

The setting reaction that gives rise to the solid cement consists in three stages: dissolution of the reactants, nucleation of the new phase (in this case apatite) and crystal growth. Therefore, the setting reaction is a dissolution-precipitation process [48]–[50], [57]. During dissolution, the raw powders release calcium and phosphate ions, generating a supersaturated solution. Once the ionic concentration reaches a critical value, the nucleation of the new phase occurs, generally surrounding the powder particles, the latter acting as nucleation dots. Afterwards, the new phase keeps growing as the dissolution of the reagents goes on. During the first hours the setting process is controlled by the dissolution kinetics of the raw materials, but once the new phase surrounds the reactants, the process is controlled by diffusion across the new phase [57]. In 2007, Bohner et al

explained that by modulating these three stages we can modify the CPC reactivity as listed below (Table 1-3.) [58]

CPCs can be processed using many different approaches to obtain modified porosity and textural properties. Total porosity, microporosity and specific surface area (SSA) vary with the processing conditions of the cements, such as the liquid to powder (L/P) ratio and the particle size of the starting powder, as shown in Figure 1-9. Thus, the total porosity increases when the L/P ratio is increased, and otherwise the particle size of the starting powder conditions the shape and size of the precipitated crystals. It has been shown that HA needle-like crystals are obtained when fine α -TCP powder is used, whereas plate-like crystals with leading to materials are obtained using coarser powder [49], [58]. It is therefore important to stress the need of a thorough characterization of these textural features of CPC in order to achieve a precise knowledge in views of controlling the resorption and biological response of calcium phosphate cements.

Table 1-3 Different strategies and approaches to manipulate the setting reactions [58].

Strategy	Approach	Sub-approaches
1. Dissolution rate	1.1. Change contact area between reagent and mixing liquid	1.1.1. Change milling duration 1.1.2. Use nano/micro powder
	1.2. Change solubility in the mixing liquid	1.2.1. Use more/less soluble phase 1.2.2. Change of reaction pH
	1.3. Change saturation of the mixing liquid	
	1.4. Use dissolution inhibitors in the mixing liquid	
	1.5. Modify reagent surface	1.5.1. Chemical change (pre-reaction) 1.5.2. Physical change (dissolution pits)
2. Nucleation rate	2.1. Use crystallization nuclei	
	2.2. Change the saturation of the reaction product in the mixing liquid	2.2.1. Change of saturation 2.2.2. Change of end-product solubility
3. Growth rate	2.3. Use nucleation inhibitors	
	3.1. Change the saturation of the reaction product in the mixing liquid	3.1.1. Change of saturation 3.1.2. Change of end-product solubility
	3.2. Use crystal growth inhibitors	

Apatitic CPCs are intrinsically microporous but display very slow resorption rates in vivo. To solve this problem, macroporosity may be introduced in CPCs. Macroporosity is sought to enhance the material's resorbability and the extent of bioactivity by increasing the surface area available for reaction, enhancing fluid circulation within the material and allowing cell colonization. To introduce macroporosity, different approaches such as foaming, leaching, or air entraining agents among others can be used [59]–[62].

Different synthetic routes may lead to the obtention of macroporous calcium phosphate cements although porosity can be a limitation for the use in high load bearing applications. The incorporation of a water soluble porogen (Mannitol) in the calcium phosphate cement

is clearly the most used approach [63]–[65]. Porogens are subsequently removed by dissolution, degradation or temperature variation to let free space: the macroporosity. Gas

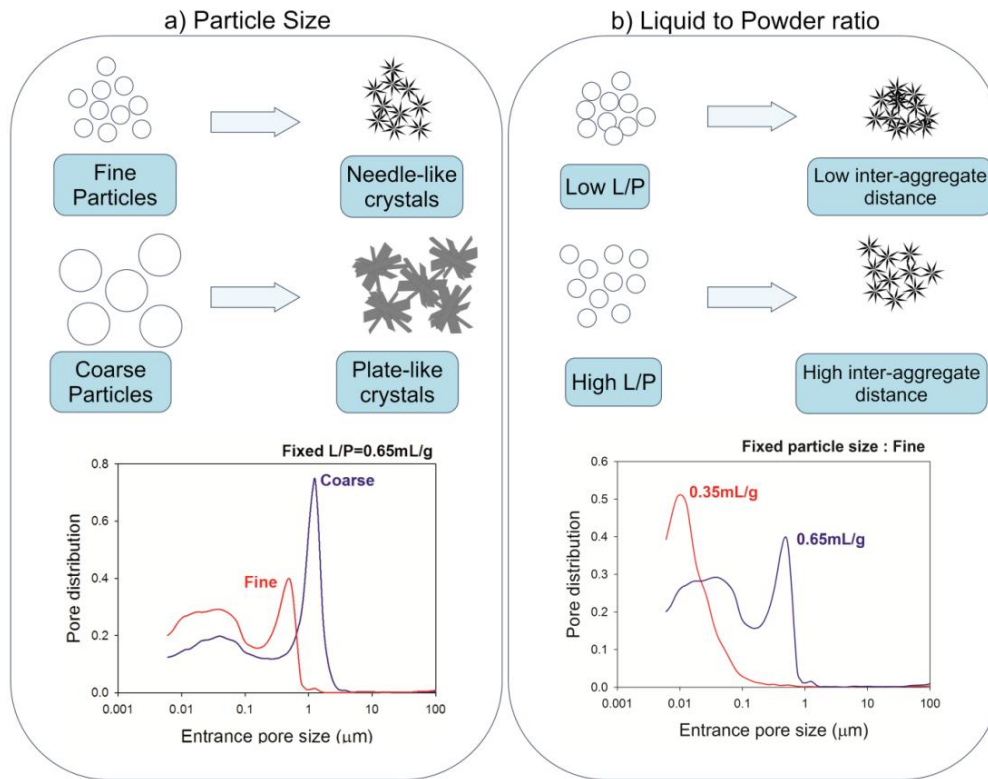


Figure 1-9 Microporosity and microstructure of CPCs can be adjusted by varying some processing parameters such as the liquid-to-powder ratio or particle size [49].

generating porogen present another alternative to generation of macroporous CPCs. For example, a mixture of sodium hydrogen carbonate and acetic acid produces CO_2 and thus, macropores [63]. A major drawback of using porogens is that relevant interconnectivity between pores can be achieved only with high proportion of porogens like 40% mannitol, resulting in increase in the setting time [66], and introduction of macroporosity leads to decrease in density, and thus fragility of the material.

Another option to introduce macroporosity in CPCs is by foaming liquid phase [67]. Adding a surfactant at low concentration to the liquid phase of the cement allows the generation of stable foam by mechanical agitation. The foam acts as a template and will keep all or part of its structure while mixing with the powder phase to lead to CPCs with high macroporosity and interconnections [68], [69]. Macroporosity of the material doesn't just replicate the trabecular bone rather it can play role in guiding the tissue growth and vessel

colonization. In fact Yin et al has shown the cell growth inside the macropores of the structure [70].

Considerable effort and large number of studies have been devoted in the last decades in order to combine the intrinsic bone regeneration potential of CPC with their ability to incorporate drugs or other active molecules which are therapeutically relevant [45], [60], [71]–[77]. Other studies have even reported the relevant property of injectability of CPCs for in vivo in soft tissue [78], trabecular bone [79], [80] and many more [43], [64], [81]–[84]. Many drugs have been combined with Calcium phosphates cements while the interaction between drug and material is a topic of interest, but it has not been tackled always.

The adequate composition of CPCs providing them with important regenerative properties once set in parallel with its intrinsic porosity, non-thermal setting reaction and ease of preparation make them excellent drug carriers for bone and musculoskeletal regeneration [71].

Based on the different bone pathologies and musculoskeletal diseases, calcium phosphates have been combined with different types of drugs including antibiotics [73], [85]–[87], anti-osteoporosis [37], [88]–[90], anti-inflammatory [91], [92], growth factors [93]–[96] and anti-cancer [76], [77], [97] drugs.

As already mentioned, combination of solid powders of calcium phosphates in an aqueous solution leads to setting and hardening of the cements (Figure 1-7). Understanding the process of cement formulation can give a clear understanding of possible approaches to load the drugs (Figure 1-10).

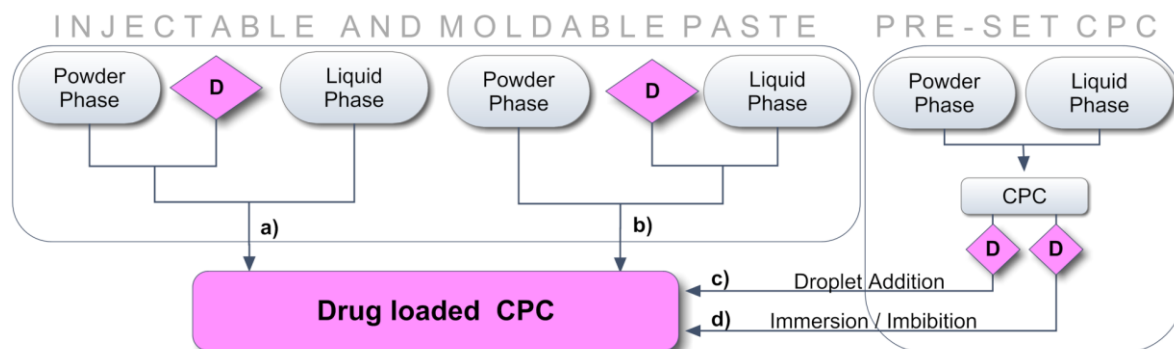


Figure 1-10 Schematic diagram of the possible strategies to load drugs in calcium phosphate cements [49].

Ginebra et al. [49] explained the loading of drugs in calcium phosphate cements according to three possible strategies: i) by adding the drug either in the powder phase, ii) in the liquid phase or iii) after preparation of the cements by droplet addition or immersion. The choice of strategy depends on different factors like drug-material interaction, solubility of drug, stability of drug or whether CPC is already set or not.

In this PhD thesis, different methods of incorporation of drug i.e. either by mixing with liquid phase or by adsorption after immersion in a drug solution will be investigated.

Plasma Treatment

The physical definition of a "plasma " is a state of mixed ions, free radicals, electrons, excited molecules, UV and visible radiation that preserves electrical neutrality. Roughly, the three main effects of plasmas on the surface of a material are: i) functionalization or grafting (covalent bonding of new chemical species); ii) etching (removal of surface material); and iii) thin film deposition (deposition of thin layers). Plasma allows selection of the treatment gas and has the advantage of controlled conditions leading to highly reproducible results. It is generated with electric discharges on gases. Coating by plasma polymerization refers to the deposition of polymer films due to the excitation of an organic monomer in the gas state and the subsequent deposition and polymerization of the excited species on the surface of a substrate. The deposition of solid polymer coatings under plasma conditions has been well studied since the 1960s, with a very wide range of materials now accessible [98].

The working principle for plasma polymerization involves two-step process: activation and coating. Before plasma treatments, an activation step by plasma reaction is generally carried out to remove contaminants or finishing agents from the surface and to generate surface radicals which may then react with the precursor monomers and generate a stronger bond on the surface. In the plasma polymerization process, a monomer gas is pumped into a vacuum chamber where it is polymerized by plasma to form a thin film on the surface. The monomer, which starts out from a liquid fed into an external recipient, is converted to a gas in an evaporator or dragged by bubbling with an inert gas, and is

pumped into the vacuum chamber. A glow discharge initiates the polymerization. The excited electrons created in the glow discharge ionize the monomer molecules. The monomer molecules break apart creating free electrons, ions, excited molecules and radicals. The radicals absorb or react with the previously activated surface, condense, and polymerize on the substrate. The electrons and ions crosslink, or create a chemical bond, with the already deposited molecules to form a polymer (Figure 1-11).

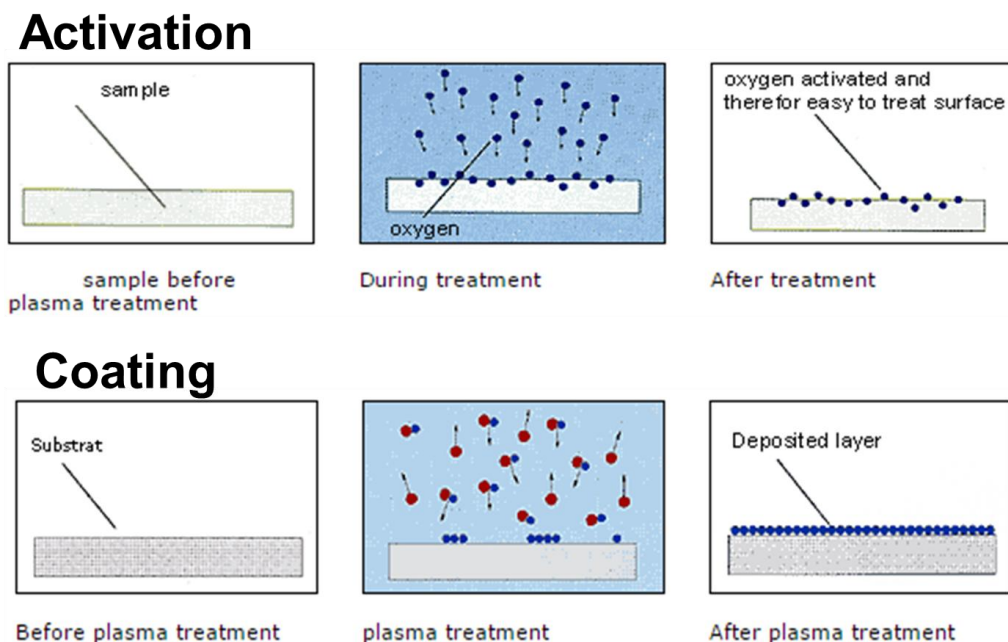


Figure 1-11 Scheme of plasma polymerization process.

In the past decade, the use of non-thermal plasmas for selective surface modification for controlled drug delivery has been a rapidly growing research field. One of the major applications of this technique that has been used is for surface modification with plasma polymers to act as a barrier for a controlled drug delivery. Many studies have shown that through multilayer coatings, a controlled drug release can be obtained [99]–[102]. The coating can be used either to regulate the incorporation of the active principle, or to act as a shield to delay its release. Stability of a polymeric coating (as in this case) is controlled by the physic-chemical properties of the polymer such as composition, crosslinking and coating thickness. All these variables can be tuned through the initial composition of the gas and plasma parameters such power and time of the treatment. In this work, low pressure plasma polymerization (hereinafter plasma polymerization) has been investigated in two ways: i) in soft conditions (Pulsed Wave (PW) polymerization) in order to retain the functionalities of the precursor or ii) in a Continuous Wave (CW mode) to

deposit cross linked thicker layers. It is an important parameter involved in the surface modification as the prime objective of this thesis.

To the best of our knowledge, in the field of CaP materials for drug delivery applications, plasma polymerization has not been investigated yet. Therefore, in the present work, we have investigated the possibility of applying a biocompatible polymer on the surface of calcium phosphates (CDHA and β -TCP) to investigate the principles behind surface modification using different plasma treatments for a controlled drug delivery system.

In this PhD thesis, plasma polymerization will be investigated for CaPs (CDHA and β -TCP) using low pressure plasma to design a tunable drug release system.

References:

- [1] E. Hernlund, A. Svedbom, M. Ivergård, J. Compston, C. Cooper, J. Stenmark, E. V McCloskey, B. Jönsson, and J. A. Kanis, "Osteoporosis in the European Union: medical management, epidemiology and economic burden. A report prepared in collaboration with the International Osteoporosis Foundation (IOF) and the European Federation of Pharmaceutical Industry Associations (EFPIA).," *Arch. Osteoporos.*, vol. 8, no. 1–2, p. 136, Jan. 2013.
- [2] A. D. Woolf and B. Pfleger, "Burden of major musculoskeletal conditions," *Bull. World Health Organ.*, vol. 81, no. 9, pp. 646–656, 2003.
- [3] E. Gómez-Barrena, C. A. Solá, and C. P. Bunu, "Regulatory authorities and orthopaedic clinical trials on expanded mesenchymal stem cells.," *Int. Orthop.*, vol. 38, no. 9, pp. 1803–9, Sep. 2014.
- [4] C. Mock and M. N. Cherian, "The global burden of musculoskeletal injuries: challenges and solutions.," *Clin. Orthop. Relat. Res.*, vol. 466, no. 10, pp. 2306–16, Oct. 2008.
- [5] A. S. Hoffman, "Biomaterials Science," in *An Introduction to Materials in Medicine 3rd Edition*, Elsevier Academic Press, 2004, pp. 535–539.
- [6] J. Khurana, E. McCarthy, and P. Zhang, *Essentials in bone and soft-tissue pathology*. 2010.
- [7] X. Wang, J. S. Nyman, X. Dong, H. Leng, and M. Reyes, *Fundamental Biomechanics in Bone Tissue Engineering*, vol. 2, no. 1. 2010.
- [8] A. Barkaoui, A. Chamekh, T. Merzouki, R. Hambli, and A. Mkaddem, "Multiscale approach including microfibril scale to assess elastic constants of cortical bone based on neural network computation and homogenization method," *Int. j. numer. method. biomed. eng.*, vol. 30, no. 3, pp. 318–338, Mar. 2014.
- [9] A. Bigi, G. Cojazzi, S. Panzavolta, A. Ripamonti, N. Roveri, M. Romanello, K. Noris Suarez, and L. Moro, "Chemical and structural characterization of the mineral phase from cortical and trabecular bone," *J. Inorg. Biochem.*, vol. 68, no. 1, pp. 45–51, Oct. 1997.
- [10] J. A. Siddiqui and N. C. Partridge, "Physiological Bone Remodeling: Systemic Regulation and Growth Factor Involvement," *Physiology*, vol. 31, no. 3, 2016.
- [11] T. Meling, K. Harboe, and K. Søreide, "Incidence of traumatic long-bone fractures requiring in-hospital management: a prospective age- and gender-specific analysis of 4890 fractures.," *Injury*, vol. 40, no. 11, pp. 1212–9, Nov. 2009.
- [12] R. Gassner, T. Tuli, O. Hächl, A. Rudisch, and H. Ulmer, "Cranio-maxillofacial trauma: a 10 year review of 9,543 cases with 21,067 injuries.," *J. Craniomaxillofac. Surg.*, vol. 31, no. 1, pp. 51–61, Feb. 2003.
- [13] D. Demetriades, M. Karaiskakis, G. C. Velmahos, K. Alo, J. Murray, and L. Chan, "Pelvic fractures in pediatric and adult trauma patients: are they different injuries?," *J. Trauma*, vol. 54, no. 6, p. 1146–51; discussion 1151, Jun. 2003.
- [14] J. P. Schmitz and J. O. Hollinger, "The critical size defect as an experimental model for craniomandibulofacial nonunions.," *Clin. Orthop. Relat. Res.*, no. 205, pp. 299–308, Apr. 1986.
- [15] P. E. Ochsner and S. Hailemariam, "Histology of osteosynthesis associated bone infection.," *Injury*, vol. 37 Suppl 2, no. 2, pp. S49-58, May 2006.
- [16] J. Ciampolini and K. G. Harding, "Pathophysiology of chronic bacterial osteomyelitis. Why do antibiotics fail so often?," *Postgrad. Med. J.*, vol. 76, no. 898, pp. 479–483, Aug. 2000.
- [17] J. S. Axford, "Joint and bone infections," *Medicine (Baltimore)*, vol. 38, no. 4, pp. 194–201, Apr. 2010.
- [18] O. Page, "Osteoporosis Page 1," pp. 1–9.

- [19] R. Bartl and B. Frisch, *Osteoporosis*, 2nd ed. Springer, 2010.
- [20] "Approved Treatments for Osteoporosis and What's in the Pipeline | Patient Care Online." [Online]. Available: <http://www.patientcareonline.com/drug-benefit-trends/approved-treatments-osteoporosis-and-what's-pipeline>. [Accessed: 12-Jul-2017].
- [21] J. E. Compston and C. J. Rosen, "Fast facts on osteoporosis," 2010.
- [22] A. N. Tsartsalis, C. Dokos, G. D. Kaiafa, D. N. Tsartsalis, A. Kattamis, A. I. Hatzitolios, and C. G. Savopoulos, "Statins, bone formation and osteoporosis: hope or hype?," *Hormones (Athens)*, vol. 11, no. 2, pp. 126–39, 2012.
- [23] T. Albrektsson and C. Johansson, "Osteoinduction, osteoconduction and osseointegration," *Eur. Spine J.*, vol. 10 Suppl 2, pp. 96–101, Oct. 2001.
- [24] for the C. on B. Implants, A. S. Greenwald, S. D. Boden, V. M. Goldberg, Y. Khan, C. T. Laurencin, and R. N. Rosier, "Bone-Graft Substitutes: Facts, Fictions, and Applications," *J. Bone Jt. Surg.*, vol. 83, no. 2 suppl 2, pp. S98-103, Nov. 2001.
- [25] M. Senba, K. Kawai, and N. Mori, "Pathogenesis of Metastatic Calcification and Acute Pancreatitis in Adult T-Cell Leukemia under Hypercalcemic State," *Leuk. Res. Treatment*, vol. 2012, pp. 1–9, Dec. 2012.
- [26] D. J. Hak, "The Use of Osteoconductive Bone Graft Substitutes in Orthopaedic Trauma," *J. Am. Acad. Orthop. Surg.*, vol. 15, no. 9, pp. 525–536, Sep. 2007.
- [27] G. Zimmermann and A. Moghaddam, "Allograft bone matrix versus synthetic bone graft substitutes.," *Injury*, vol. 42 Suppl 2, pp. S16-21, Sep. 2011.
- [28] "Transplantation | Clinical Gate." [Online]. Available: <https://clinicalgate.com/transplantation/>. [Accessed: 12-Jul-2017].
- [29] R. Z. LeGeros, "Calcium phosphate-based osteoinductive materials.," *Chem. Rev.*, vol. 108, no. 11, pp. 4742–53, Nov. 2008.
- [30] F. H. Albee, "Studies in bone growth: triple calcium phosphate as a stimulus to osteogenesis," *Ann. Surg.*, vol. 71, no. 1, pp. 32–9, Jan. 1920.
- [31] D. M. ROY and S. K. LINNEHAN, "Hydroxyapatite formed from Coral Skeletal Carbonate by Hydrothermal Exchange," *Nature*, vol. 247, no. 5438, pp. 220–222, Jan. 1974.
- [32] B. V. Rejda, J. G. Peelen, and K. de Groot, "Tri-calcium phosphate as a bone substitute.," *J. Bioeng.*, vol. 1, no. 2, pp. 93–7, Jan. 1977.
- [33] W. Brown and L. Chow, "A new calcium-phosphate setting cement," *J. Dent. Res.*, vol. 62, no. 19, pp. 672–672, 1983.
- [34] E. A. Monroe, W. Votava, D. B. Bass, and J. McMullen, "New calcium phosphate ceramic material for bone and tooth implants.," *J. Dent. Res.*, vol. 50, no. 4, pp. 860–861, 1971.
- [35] L. C. Chow, "Next generation calcium phosphate-based biomaterials.," *Dent. Mater. J.*, vol. 28, no. 1, pp. 1–10, Jan. 2009.
- [36] C. G. Finkemeier, "Bone-grafting and bone-graft substitutes.," *J. Bone Joint Surg. Am.*, vol. 84–A, no. 3, pp. 454–64, Mar. 2002.
- [37] A. C. Killeen, P. a Rakes, M. J. Schmid, Y. Zhang, N. Narayana, D. B. Marx, J. B. Payne, D. Wang, and R. a Reinhardt, "Impact of local and systemic alendronate on simvastatin-induced new bone around periodontal defects.," *J. Periodontol.*, vol. 83, no. 12, pp. 1463–71, Dec. 2012.
- [38] B. S. McAllister and K. Haghghat, "Bone augmentation techniques.," *J. Periodontol.*, vol. 78, no. 3, pp. 377–96, Mar. 2007.
- [39] S. V. Dorozhkin, "Calcium Orthophosphate Cements and Concretes," *Materials (Basel)*, vol. 2, no. 1, pp. 221–291, Mar. 2009.
- [40] K. Chen, S. Sahoo, P. He, K. S. Ng, S. L. Toh, and J. C. H. Goh, "A hybrid silk/RADA-based

- fibrous scaffold with triple hierarchy for ligament regeneration.,” *Tissue Eng. Part A*, vol. 18, no. 13–14, pp. 1399–409, Jul. 2012.
- [41] L. E. Mermelstein, L. C. Chow, C. Friedman, and J. . Crisco, “The Reinforcement of Cancellous Bone Screws with Calcium Phosphate Cement,” *J. Orthop. Trauma*, vol. 10, no. 1, pp. 15–20.
- [42] Z. Du, J. Chen, F. Yan, and Y. Xiao, “Effects of Simvastatin on bone healing around titanium implants in osteoporotic rats.,” *Clin. Oral Implants Res.*, vol. 20, no. 2, pp. 145–50, Feb. 2009.
- [43] T.-H. T. Lim, G. G. T. Brebach, S. Renne, W.-J. W. Kim, J. G. J. Kim, S. M. Renner, R. E. Lee, G. B. J. Andersson, and H. S. An, “Biomechanical evaluation of an injectable calcium phosphate cement for vertebroplasty.,” *Spine (Phila. Pa. 1976).*, vol. 27, no. 12, pp. 1297–1302, 2002.
- [44] M. Nakano, N. Hirano, K. Matsuura, H. Watanabe, H. Kitagawa, H. Ishihara, and Y. Kawaguchi, “Percutaneous transpedicular vertebroplasty with calcium phosphate cement in the treatment of osteoporotic vertebral compression and burst fractures,” *J. Neurosurg. Spine*, vol. 97, no. 3, pp. 287–293, Oct. 2002.
- [45] M. P. Ginebra, T. Traykova, and J. a Planell, “Calcium phosphate cements as bone drug delivery systems: a review.,” *J. Control. Release*, vol. 113, no. 2, pp. 102–110, Jun. 2006.
- [46] S. V. Dorozhkin, “Calcium Orthophosphates in Nature, Biology and Medicine,” *Materials (Basel).*, vol. 2, no. 2, pp. 399–498, Apr. 2009.
- [47] S. V. Dorozhkin, “Self-Setting Calcium Orthophosphate Formulations: Cements, Concretes, Pastes and Putties,” *Int. J. Mater. Chem.*, vol. 1, no. 1, pp. 1–48, Aug. 2012.
- [48] E. Fernánde z, F. J. Gil, M. P. Ginebra, F. C. M. Driessens, J. A. Planell, and S. M. Best, “Calcium phosphate bone cements for clinical applications. Part I: Solution chemistry,” *J. Mater. Sci. Mater. Med.*, vol. 10, no. 3, pp. 169–176, Mar. 1999.
- [49] M.-P. Ginebra, C. Canal, M. Espanol, D. Pastorino, and E. B. Montufar, “Calcium phosphate cements as drug delivery materials.,” *Adv. Drug Deliv. Rev.*, vol. 64, no. 12, pp. 1090–110, Sep. 2012.
- [50] E. Fernánde z, F. J. Gil, M. P. Ginebra, F. C. M. Driessens, J. A. Planell, and S. M. Best, “Calcium phosphate bone cements for clinical applications. Part II: Precipitate formation during setting reactions,” *J. Mater. Sci. Mater. Med.*, vol. 10, no. 3, pp. 177–183, Mar. 1999.
- [51] A. J. Ambard and L. Mueninghoff, “Calcium phosphate cement: review of mechanical and biological properties.,” *J. Prosthodont.*, vol. 15, no. 5, pp. 321–8.
- [52] U. Heise, J. F. Osborn, and F. Duwe, “Hydroxyapatite ceramic as a bone substitute,” *Int. Orthop.*, vol. 14, no. 3, Oct. 1990.
- [53] R. Z. LeGeros, “Properties of osteoconductive biomaterials: calcium phosphates.,” *Clin. Orthop. Relat. Res.*, vol. 395, no. 395, pp. 81–98, Feb. 2002.
- [54] S. Joschek, B. Nies, R. Krotz, and A. Göpferich, “Chemical and physicochemical characterization of porous hydroxyapatite ceramics made of natural bone,” *Biomaterials*, vol. 21, no. 16, pp. 1645–1658, Aug. 2000.
- [55] A. Tampieri, “Porosity-graded hydroxyapatite ceramics to replace natural bone,” *Biomaterials*, vol. 22, no. 11, pp. 1365–1370, Jun. 2001.
- [56] M. Valletregi, “Calcium phosphates as substitution of bone tissues,” *Prog. Solid State Chem.*, vol. 32, no. 1–2, pp. 1–31, 2004.
- [57] M. P. Ginebra, E. Fernandez, E. A. P. De Maeyer, R. M. H. Verbeeck, M. G. Boltong, J. Ginebra, F. C. M. Driessens, and J. A. Planell, “Setting Reaction and Hardening of an Apatitic Calcium Phosphate Cement,” *J. Dent. Res.*, vol. 76, no. 4, pp. 905–912, Apr. 1997.
- [58] M. Bohner, “Reactivity of calcium phosphate cements,” *J. Mater. Chem.*, vol. 17, no. 38, p.

3980, 2007.

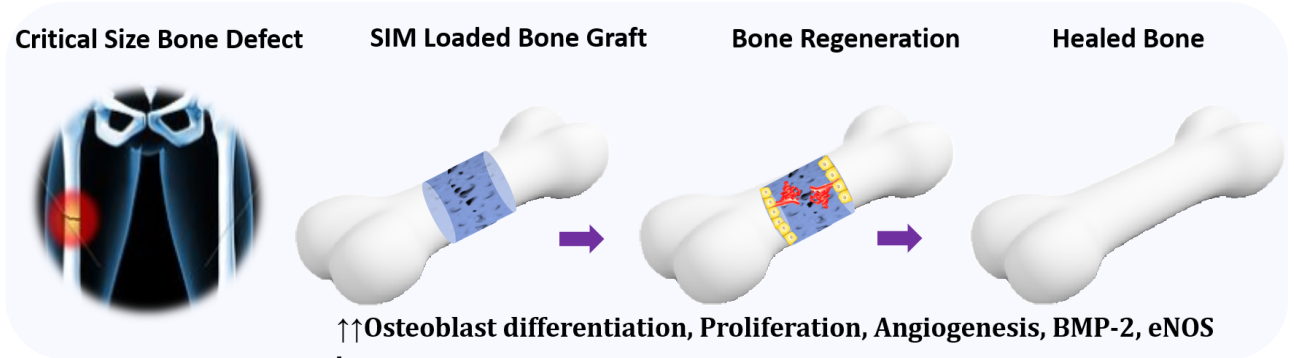
- [59] M. P. Ginebra, M. Espanol, E. B. Montufar, R. A. Perez, and G. Mestres, "New processing approaches in calcium phosphate cements and their applications in regenerative medicine.," *Acta Biomater.*, vol. 6, no. 8, pp. 2863–73, Aug. 2010.
- [60] M. Espanol, R. A. Perez, E. B. Montufar, C. Marichal, A. Sacco, and M. P. Ginebra, "Intrinsic porosity of calcium phosphate cements and its significance for drug delivery and tissue engineering applications.," *Acta Biomater.*, vol. 5, no. 7, pp. 2752–62, Sep. 2009.
- [61] R. P. del Real, J. G. C. Wolke, M. Vallet-Regí, and J. A. Jansen, "A new method to produce macropores in calcium phosphate cements," *Biomaterials*, vol. 23, no. 17, pp. 3673–3680, Sep. 2002.
- [62] K. Ishikawa and K. Asaoka, "Estimation of ideal mechanical strength and critical porosity of calcium phosphate cement.," *J. Biomed. Mater. Res.*, vol. 29, no. 12, pp. 1537–43, Dec. 1995.
- [63] S. Hesaraki, A. Zamanian, and F. Moztarzadeh, "The influence of the acidic component of the gas-foaming porogen used in preparing an injectable porous calcium phosphate cement on its properties: acetic acid versus citric acid.," *J. Biomed. Mater. Res. B. Appl. Biomater.*, vol. 86, no. 1, pp. 208–16, Jul. 2008.
- [64] H. H. K. Xu, M. D. Weir, E. F. Burguera, and A. M. Fraser, "Injectable and macroporous calcium phosphate cement scaffold.," *Biomaterials*, vol. 27, no. 24, pp. 4279–87, Aug. 2006.
- [65] J. E. Barralet, L. Grover, T. Gaunt, A. J. Wright, and I. R. Gibson, "Preparation of macroporous calcium phosphate cement tissue engineering scaffold," *Biomaterials*, vol. 23, no. 15, pp. 3063–3072, Aug. 2002.
- [66] H. H. K. Xu and C. G. Simon, "Fast setting calcium phosphate-chitosan scaffold: mechanical properties and biocompatibility.," *Biomaterials*, vol. 26, no. 12, pp. 1337–48, Apr. 2005.
- [67] A. Almirall, G. Larrecq, J. A. Delgado, S. Martínez, J. A. Planell, and M. P. Ginebra, "Fabrication of low temperature macroporous hydroxyapatite scaffolds by foaming and hydrolysis of an alpha-TCP paste.," *Biomaterials*, vol. 25, no. 17, pp. 3671–80, Aug. 2004.
- [68] R. A. Perez, H.-W. Kim, and M.-P. Ginebra, "Polymeric additives to enhance the functional properties of calcium phosphate cements.," *J. Tissue Eng.*, vol. 3, no. 1, p. 2041731412439555, Jan. 2012.
- [69] C. Canal, D. Pastorino, G. Mestres, P. Schuler, and M.-P. Ginebra, "Relevance of microstructure for the early antibiotic release of fresh and pre-set calcium phosphate cements.," *Acta Biomater.*, vol. 9, no. 9, pp. 8403–12, Sep. 2013.
- [70] Yin et al, "Simvastatin-loaded macroporous calcium phosphate cement: preparation, in vitro characterization, and evaluation of in vivo performance.," *J. Biomed. Mater. Res. A*, vol. 100, no. 11, pp. 2991–3000, Nov. 2012.
- [71] M.-P. Ginebra, T. Traykova, and J. A. Planell, "Calcium phosphate cements: competitive drug carriers for the musculoskeletal system?," *Biomaterials*, vol. 27, no. 10, pp. 2171–7, Apr. 2006.
- [72] M. Nyan, T. Miyahara, K. Noritake, J. Hao, R. Rodriguez, S. Kuroda, and S. Kasugai, "Molecular and tissue responses in the healing of rat calvarial defects after local application of simvastatin combined with alpha tricalcium phosphate.," *J. Biomed. Mater. Res. B. Appl. Biomater.*, vol. 93, no. 1, pp. 65–73, Apr. 2010.
- [73] Y. Zhang and M. Zhang, "Calcium phosphate/chitosan composite scaffolds for controlled in vitro antibiotic drug release.," *J. Biomed. Mater. Res.*, vol. 62, no. 3, pp. 378–86, Dec. 2002.
- [74] E. Verron, I. Khairoun, J. Guicheux, and J.-M. Bouler, "Calcium phosphate biomaterials as bone drug delivery systems: a review.," *Drug Discov. Today*, vol. 15, no. 13–14, pp. 547–52, Jul. 2010.
- [75] D. Wang, S. C. Miller, P. Kopecková, and J. Kopecek, "Bone-targeting macromolecular

- therapeutics.," *Adv. Drug Deliv. Rev.*, vol. 57, no. 7, pp. 1049–76, May 2005.
- [76] M. Otsuka, Y. Matsuda, Y. Suwa, J. L. Fox, and W. I. Higuchi, "A novel skeletal drug delivery system using a self-setting calcium phosphate cement. 5. Drug release behavior from a heterogeneous drug-loaded cement containing an anticancer drug," *J. Pharm. Sci.*, vol. 83, no. 11, pp. 1565–1568, Nov. 1994.
- [77] M. Otsuka, Y. Matsuda, J. L. Fox, and W. I. Higuchi, "A novel skeletal drug delivery system using self-setting calcium phosphate cement. 9: Effects of the mixing solution volume on anticancer drug release from homogeneous drug-loaded cement," *J. Pharm. Sci.*, vol. 84, no. 6, pp. 733–736, Jun. 1995.
- [78] E. Ooms, "Soft-tissue response to injectable calcium phosphate cements," *Biomaterials*, vol. 24, no. 5, pp. 749–757, Feb. 2003.
- [79] E. M. Ooms, J. G. C. Wolke, J. P. C. M. van der Waerden, and J. A. Jansen, "Trabecular bone response to injectable calcium phosphate (Ca-P) cement.," *J. Biomed. Mater. Res.*, vol. 61, no. 1, pp. 9–18, Jul. 2002.
- [80] O. Gauthier, R. Müller, D. von Stechow, B. Lamy, P. Weiss, J.-M. Bouler, E. Aguado, and G. Daculsi, "In vivo bone regeneration with injectable calcium phosphate biomaterial: a three-dimensional micro-computed tomographic, biomechanical and SEM study.," *Biomaterials*, vol. 26, no. 27, pp. 5444–53, Sep. 2005.
- [81] Montazerolghaem et al, "Sustained release of simvastatin from premixed injectable calcium phosphate cement.," *J. Biomed. Mater. Res. A*, pp. 1–8, Mar. 2013.
- [82] D. Apelt, F. Theiss, A. O. El-Warrak, K. Zlinszky, R. Bettschart-Wolfisberger, M. Böhner, S. Matter, J. A. Auer, and B. von Rechenberg, "In vivo behavior of three different injectable hydraulic calcium phosphate cements," *Biomaterials*, vol. 25, no. 7–8, pp. 1439–1451, Mar. 2004.
- [83] P. Kopylov, K. Jonsson, K. Thorngren, and P. Aspenberg, "Injectable calcium phosphate in the treatment of distal radial fractures," *J. Hand Surg. J. Br. Soc. Surg. Hand*, vol. 21, no. 6, pp. 768–771, Dec. 1996.
- [84] S. Larsson and G. Hannink, "Injectable bone-graft substitutes: current products, their characteristics and indications, and new developments.," *Injury*, vol. 42 Suppl 2, pp. S30–4, Sep. 2011.
- [85] J. Fan, J. Lei, C. Yu, B. Tu, and D. Zhao, "Hard-templating synthesis of a novel rod-like nanoporous calcium phosphate bioceramics and their capacity as antibiotic carriers," *Mater. Chem. Phys.*, vol. 103, no. 2–3, pp. 489–493, Jun. 2007.
- [86] M. Böhner, J. Lemaître, P. Van Landuyt, P. Y. Zambelli, H. P. Merkle, and B. Gander, "Gentamicin-loaded hydraulic calcium phosphate bone cement as antibiotic delivery system.," *J. Pharm. Sci.*, vol. 86, no. 5, pp. 565–72, May 1997.
- [87] S. Radin, J. T. Campbell, P. Ducheyne, and J. M. Cuckler, "Calcium phosphate ceramic coatings as carriers of vancomycin," *Biomaterials*, vol. 18, no. 11, pp. 777–782, Jun. 1997.
- [88] T. Luhmann, O. Germershaus, J. Groll, and L. Meinel, "Bone targeting for the treatment of osteoporosis.," *J. Control. Release*, vol. 161, no. 2, pp. 198–213, Jul. 2012.
- [89] J. Zhao, H. Tang, J. Gu, B. Wang, L. Bao, and Q. Wang Bing, "Evaluation of a Novel Osteoporotic Drug Delivery System In Vitro: Alendronate-loaded Calcium Phosphate Cement," *Orthopaedics*, vol. 33, no. 8, Aug. 2010.
- [90] S. Panzavolta, P. Torricelli, B. Bracci, M. Fini, and A. Bigi, "Alendronate and Pamidronate calcium phosphate bone cements: setting properties and in vitro response of osteoblast and osteoclast cells.," *J. Inorg. Biochem.*, vol. 103, no. 1, pp. 101–6, Jan. 2009.
- [91] J. L. Funk, J. Chen, K. J. Downey, and R. A. Clark, "Bone protective effect of simvastatin in experimental arthritis.," *J. Rheumatol.*, vol. 35, no. 6, pp. 1083–1091, Jun. 2008.
- [92] G. Renaudin, P. Laquerrière, Y. Filinchuk, E. Jallot, and J. M. Nedelec, "Structural

- characterization of sol–gel derived Sr-substituted calcium phosphates with anti-osteoporotic and anti-inflammatory properties,” *J. Mater. Chem.*, vol. 18, no. 30, p. 3593, Jul. 2008.
- [93] S. Bose and S. Tarafder, “Calcium phosphate ceramic systems in growth factor and drug delivery for bone tissue engineering: a review.,” *Acta Biomater.*, vol. 8, no. 4, pp. 1401–21, Apr. 2012.
- [94] Y. M. Lee, Y. J. Park, S. J. Lee, Y. Ku, S. B. Han, P. R. Klokkevold, and C. P. Chung, “The bone regenerative effect of platelet-derived growth factor-BB delivered with a chitosan/tricalcium phosphate sponge carrier.,” *J. Periodontol.*, vol. 71, no. 3, pp. 418–24, Mar. 2000.
- [95] E. J. Blom, J. Klein-Nulend, C. P. Klein, K. Kurashina, M. A. van Waas, and E. H. Burger, “Transforming growth factor-beta1 incorporated during setting in calcium phosphate cement stimulates bone cell differentiation in vitro.,” *J. Biomed. Mater. Res.*, vol. 50, no. 1, pp. 67–74, Apr. 2000.
- [96] P. Q. Ruhe, E. L. Hedberg, N. T. Padron, P. H. M. Spauwen, J. A. Jansen, and A. G. Mikos, “rhBMP-2 release from injectable poly(DL-lactic-co-glycolic acid)/calcium-phosphate cement composites.,” *J. Bone Joint Surg. Am.*, vol. 85–A Suppl, no. suppl 3, pp. 75–81, Jan. 2003.
- [97] H. Senta, H. Park, E. Bergeron, O. Drevelle, D. Fong, E. Leblanc, F. Cabana, S. Roux, G. Grenier, and N. Fauchoux, “Cell responses to bone morphogenetic proteins and peptides derived from them: biomedical applications and limitations.,” *Cytokine Growth Factor Rev.*, vol. 20, no. 3, pp. 213–22, Jul. 2009.
- [98] H. K. Yasuda, *Plasma Polymerization*. Academic Press, 2012.
- [99] K. Vasilev, N. Poulter, P. Martinek, and H. J. Griesser, “Controlled release of levofloxacin sandwiched between two plasma polymerized layers on a solid carrier.,” *ACS Appl. Mater. Interfaces*, vol. 3, no. 12, pp. 4831–6, Dec. 2011.
- [100] S. Yoshida, K. Hagiwara, T. Hasebe, and A. Hotta, “Surface modification of polymers by plasma treatments for the enhancement of biocompatibility and controlled drug release,” *Surf. Coatings Technol.*, vol. 233, pp. 99–107, 2013.
- [101] S. Simovic, D. Losic, and K. Vasilev, “Controlled drug release from porous materials by plasma polymer deposition.,” *Chem. Commun. (Camb)*, vol. 46, no. 8, pp. 1317–9, Feb. 2010.
- [102] S. Bhatt, J. Pulpytel, M. Mirshahi, and F. Arefi-Khonsari, “Plasma co-polymerized nano coatings – As a biodegradable solid carrier for tunable drug delivery applications,” *Polymer (Guildf)*, vol. 54, no. 18, pp. 4820–4829, Aug. 2013.

Chapter 2

Simvastatin as an osteogenic drug: facts and future perspectives



Abstract

Simvastatin, a lactone pro-drug is mainly known by its cholesterol-lowering properties, through the inhibition of the enzyme 3-hydroxy-3-methylglutaryl of the mevalonate pathway. However, this pathway is responsible for a number of biochemical molecules, which confers simvastatin pleotropic effects. Particularly, it has been shown that simvastatin can interact with the process of bone remodelling and new bone formation. Several studies including *in vitro* and *in vivo* have been conducted to evaluate its benefits in enhancement of bone formation and inhibiting bone resorption. In this Chapter an overview of the main advances regarding the use of simvastatin in bone regeneration applications is provided, covering both *in vitro* and *in vivo* studies, through local injection or in combination with implantable biomaterials. Overall, the vast amount of research has shown beneficial effects of simvastatin for inducing osteoinduction with increase in number and function of osteoblasts as well as inhibition of osteoclasts activity.

Introduction

Bone defects are a major health issue, result of pathologies like osteoporosis, or incidents such as traumatic accidents or surgical removal. Every year in Europe, one million bone reconstruction surgeries are performed [1]. In 2010, the International Osteoporosis Foundation (IOF) estimated more than 22 million women and 5.5 million men suffering from osteoporosis in the European Union (EU)[2]. This report estimated that approximately one in three women in Europe have excessive bone loss with additional factors leading to osteoporosis. In addition, EU healthcare carries a burden of €37 million derived from fragile fractures due to osteoporosis. These numbers are expected to increase in 23% from 2010 to 2025 with the ageing of population.

Even though bone is a self-repairing tissue, its capacity to self-repair can be affected by the health or disease condition of the bone tissue, but also by extrinsic parameters like the size of the defects. In 1986, Schmitz and Hollinger introduced the term of critical size bone defects referring to the defects that are unable to heal completely during the lifetime of an animal [3]. To heal the critical size defects different options are available: autologous bone grafts, allografts, xenografts or synthetic bone grafts. To further improve the performance of bone grafts, they can be combined with bioactive molecules or

drugs, which can stimulate bone formation and/or inhibit bone resorption. For instance, Bone morphogenetic protein (BMP-2) or Fibroblast growth factors (FGFs) have been evaluated because of their potent role as bone stimulating agents. However, these agents have important drawbacks such as tissue inflammation or initiation of the host immune system, as well as tumorigenic effects [4]–[6]. As an alternative strategy, Bisphosphonates (BPs) have been also employed, based on the finding that BPs prevent osteoclasts activation and survival through inhibition of mevalonate pathway related to osteoclast activity, [7] which inhibits bone resorption.

In the early 90's, statins, a family of drugs was identified as a potent inhibitor of the mevalonate pathway by its inhibiting action over an enzyme, the 3-hydroxy-3-methylglutaryl coenzyme A (HMG -CoA) reductase, which is responsible in this cholesterol production pathway [8]. Statins thus have the ability of reducing serum cholesterol concentrations, which is their main current therapeutic use. However, the mevalonate pathway affects the synthesis of a variety of molecules, which are implicated in the endothelial function, oxidative stress and inflammation and immune system and bone metabolism, among others [9]. Many of these effects have been related to different biological mechanisms including the promotion of osteogenesis and the inhibition of bone resorption.

These findings were confirmed by Mundy et al., who reported new bone formation *in vitro* as well as in rodents by enhancing BMP-2 expression *in vitro* and producing a 50% increase in new bone formation in calvaria defects [10]. After these findings, the interest in SIM for bone regenerative therapies was highly raised. Over the last decade, many studies have been conducted to evaluate the impact of SIM in bone formation, including *in vitro* and *in vivo* studies [11]–[13]. Thereby, this Chapter focuses on the current state of applications of SIM for bone regeneration majorly in osteoporosis and fracture healing among others, summarizing the main findings of *in vitro* and *in vivo* studies.

Mechanism of action of simvastatin and pleiotropic effects

As shown in Figure 1, the molecular structure of SIM has hexahydronaphtalene rings (lactone rings) which are hydrophobic in nature[14] and the metabolism of SIM involves lactone/acid inter-conversion [15]–[17]. SIM is readily distributed in the peripheral tissues and gastrointestinal tract through passive membrane permeability which has been explained by lipophilic factor in other works (Table 1) [18]–[20]. Generally, SIM is metabolized in two

ways: a) hydrolysis through Carboxyl esterase to simvastatin acid (SVA), b) oxidation by P450 isoenzymes into regio- and stereo-selectively metabolized products [21], [22]. The major metabolized product is SVA which inhibits the 3-hydroxy-3-methylglutaryl reductase (HMGR) enzyme by tight binding to it. As this enzyme is responsible for one of the steps of conversion to mevalonate, blocking of this enzyme results in the inhibition of the mevalonate pathway [23], [24]. The mevalonate pathway is involved in many biological pathways (Figure 2-1) other than bone regeneration, so this has led to explore further the pleiotropic effects of the SIM overviewed in further sections.

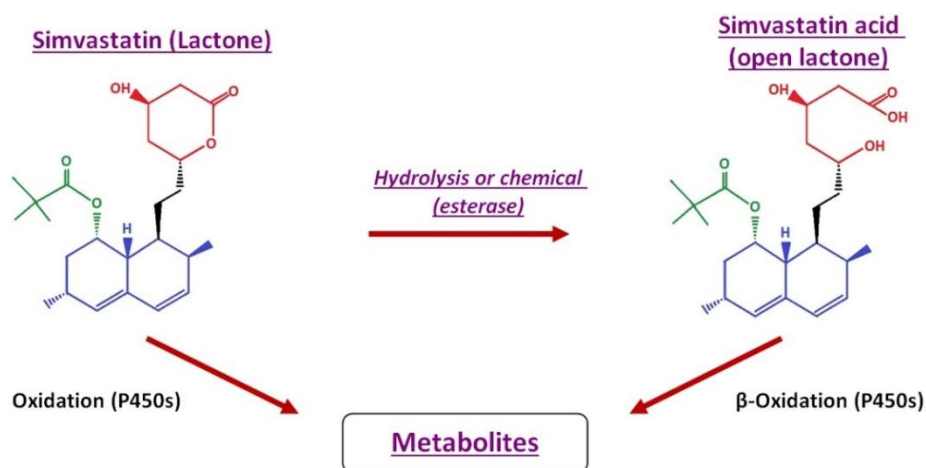


Figure 2-1 Graphic representation of the conversion of simvastatin (SIM) to simvastatin acid (SVA) [16], [17].

As a consequence of its mechanism of action, based in its interference in the synthesis of mevalonic acid (Figure 2-2), SIM has several pleiotropic effects. The mevalonate pathway has many intermediates being involved with inhibition of Guanosine triphosphate (GTP) proteins and isoprenylation. These intermediates and further processes lead to a huge number of pleiotropic effects such as: anti-inflammation, anti-oxidative, angiogenesis or osteogenesis with respective role in bone generating proteins (Figure 2-2) [23], [25]–[28]. It has been seen that inhibition of the mevalonate pathway by statins results in the increase in the endothelial nitric oxide synthase (eNOS) enzyme [29], [30]. While it has been shown that vascular endothelial nitric oxide (NO) plays a major role in the mediation of the anti-inflammatory effects explaining indirect impact of statins[26], [31]–[34][9], [35], [36]. Some other effects of statins have been reported such as enhanced endothelial nitric oxide synthase (eNOS), inhibited apoptosis and accelerated vascular structure formation, *in vitro*

and angiogenesis, *in vivo* [37]. Other studies have reported similar findings with increase in the vascular endothelial growth factor (VEGF) production due to administration of SIM [38]. To summarize, SIM effects on angiogenesis and vascularization have been reported along with osteogenesis among many studies [39]–[41].

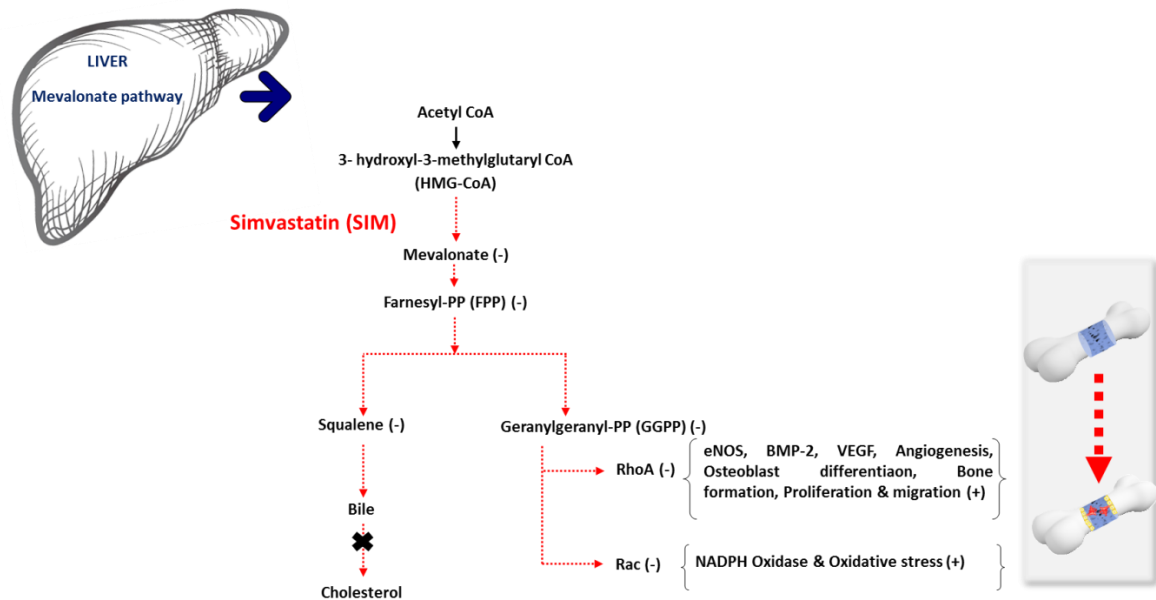


Figure 2-2 Role of Simvastatin (SIM) in the bone regeneration.

Role of simvastatin in bone metabolism and bone regeneration

As mentioned in previous sections, in the last two decades SIM has arisen as a potential alternative drug for enhancing bone regeneration. The research undertaken covers a wide spectrum of approaches, including *in vitro* and *in vivo studies* and different administration routes. This work reviews the most recent publications about the application of SIM in the field of bone regeneration, covering both *in vitro* and *in vivo* models, and the including the administration of SIM either systemically or locally. These are summarized in the following sections focusing in parameters such as drug delivery route, effective drug dosage or selection of animal model among others.

Effects of simvastatin in the cell fate in vitro: cell culture studies

In vitro studies provided the first data on the impact of SIM on the bone regeneration. The majority of the works focus on the effects of SIM on pre-osteoblasts (e.g. MC3T3-E1) or osteoblasts (OBs) (Table 2-2), although other cell lines or primary cells have been

investigated including osteosarcoma cells (MG 63), murine (2T3), human osteosarcoma (hOS), Mesenchymal stem cells (MSCs), human adipose-derived stromal (hADSCs), embryonic cells (mESCs) (Table 2-2). In most cases the administration of SIM in *in vitro* was performed directly in solution in the cell culture medium and only two studies loaded SIM in carriers for further *in vitro* evaluation. The dosage of SIM investigated covered a wide range of concentrations, from 0.1 nM to 1mM and low concentrations of 0.1 and 1 μ M were found to be the most effective.

Table 2-1 Comparison of the lipophilicity of statins, simvastatin being among the most lipophilic. [19], [20].

STATIN	LIPOPHILICITY
Lovastatin	1.70
Cerivastatin	1.69
Simvastatin	1.60
Pitavastatin	1.49
Fluvastatin	1.27
Atorvastatin	1.11
Rosuvastatin	-0.33
Pravastatin	-0.84



The first *in vitro* study was conducted on human osteoblast-like osteosarcoma (MG63) and murine osteoblast cells (2T3) [10]. The study reported the stimulation of BMP-2 gene expression in both types of cells. It was found that in MG63 cells, addition of SIM (2.5 μ M) resulted in an increase of 2.7 fold in the gene expression of BMP-2. Later, Frick *et al.* found that SIM (1–10 μ M) increased VEGF gene expression in human umbilical vein endothelial cells. In contrast, they also reported decreased VEGF production for human vascular smooth muscle cells and microvascular endothelial cells [42]. These differences point out the importance of the cell model chosen, at which we will pay attention in the coming paragraphs.

Zhou *et al.* administering SIM (0.1 μ M) to human adipose-derived stromal cells (hADSCs) showed enhancement of Alkaline phosphatase (ALP) activity at day 14. Alongside, Osteocalcin (OCN) secretion at 24h & 72h, and matrix calcification were significantly

increased [43]. Zhang *et al.* reported a significant increase in the proliferation rate, migration and angiogenesis with mesenchymal stem cells due to SIM [44]. Later, in 2010 Chen *et al.* conducted a study on osteoblast like cells from mice calvaria reporting higher viability in 10^{-6} M SIM-treated cells. BMP-2 and ALP mRNA gene expression increased in the early phase of osteoblast culture at 3 days while SIM-treated group displayed even higher expression indicating increased differentiation [45].

Many studies with pre-osteoblast cells (MC3T3-E1) with SIM observed increase in gene expressions such as BMP-2, ALP, VEGF, OCN, collagen type 1 (COL1) or osteopontin (OP). In 2001, Maeda *et al.*, reported maximal anabolic (bone forming) effects of SIM (10^{-7} M) in mouse osteoblast cells (MC3T3-E1) derived from mouse calvaria. This [46] and other works [47] reported stimulation of BMP-2 which triggered osteoblastic cell differentiation and production of ALP which is responsible for the mineralization process. Apart from direct administration of SIM in cell culture medium of MC3T3-E1, a couple of studies investigated with different drug carriers. A study with SIM-gelatin-polymer scaffolds reported osteogenic differentiation and mineralization with increase in OC gene expression [48]. SIM-PLGA microspheres incorporated in CaP macroporous scaffolds study found higher cell attachment and proliferation with increase in COL-1, OP and OC gene expression [49]. In pre-osteoblast cells, MC3T3-E1, mineralization has been observed in all the studies with increase in gene expressions related to bone regeneration, namely BMP-2 as well as ALP.

In 2013, Montazerolghaem *et al.* loaded β -hydroxy simvastatin acid (0.25, 0.5 & 1mg SVA/g cement) in premixed brushitic calcium phosphate cements observing a diffusion controlled release for over a week. SaOS-2, sarcoma osteogenic cells (human osteoblast like cells) were cultured with extracts from the loaded cements where the highest dose of 1 mg SVA/g employed showed lowest proliferation rate. On the other hand, 0.5 and 0.25 SVA/g cement showed significantly higher ALP activity and mineralization but no significant difference in proliferation [50].

In summary, SIM administration through either cell culture medium or delivered through carrier vehicles has reported efficacy in bone regeneration

Effects of simvastatin in vivo

The effects of SIM have also been evaluated *in vivo*, in models which include heterotopic and orthotopic sites. Heterotopic models avoid a direct contact with the bone tissue to

show the osteoinductive properties of the drug. Thereby, subcutaneous (SC) injection or surgical implantation, intravenous (IV), intraperitoneal (IP) or intramuscular (IM) routes of administration are commonly used in heterotopic models. On the other hand, orthotopic models are used in intraosseous defects evaluating implants and include bone defects such as calvarial, mandibular or trabecular, among others. The models evaluated include bone fractures in either healthy animals or osteoporotic ones.

SIM has been extensively studied in a number of animal models via different routes of administration. In the *in vivo* studies reviewed below, the systemic route is the most studied, mainly by oral (P.O.) or subcutaneous (SC) administration to deliver SIM. A minority of these studies used intravenous (IV), intraperitoneal (IP) and intramuscular (IM) route of administration. On the other hand, local delivery of SIM was performed with either local injections or implantable bone grafts. Thereby, the following sections will review the findings about the effects of SIM, on the basis of route of administration via systemic or local delivery, focusing on osteoporosis or bone defect healing.

Systemic administration

Most of the studies assessed the effect of SIM in osteoporotic animals, ovariectomized (OVX) rats, the most common model for postmenopausal osteoporosis and fracture healing in healthy rats. Most of these studies employed rodents as animal models (rats or mice) and only a few employed medium-sized animals such as rabbits or dogs for particular pathologies. SIM was administered orally, among a range of suitable concentrations generally around 5 - 50 mg kg⁻¹ day⁻¹. Though, in case of spinal fusion model, positive effects were observed with higher SIM concentrations of 120 mg kg⁻¹ day⁻¹ while lower concentrations (20 mg kg⁻¹ day⁻¹) had no effect (Table 2-3). [51], [52].

Osteoporotic animal model

In OVX animal models, the most significant results for bone regeneration were reported at low concentrations of 5, 10 and 20 mg kg⁻¹ day⁻¹.

Junquiera *et al.* reported new bone formation with SIM (20 mg kg⁻¹ day⁻¹) in a mandibular defect in OVX rats at 15 days without any further change [53]. In agreement with these findings, Oxlund *et al.* also reported similar results for the new bone formation in OVX rats [54]. Later, Pytlik *et al.* also reported similar findings for OVX rats with increased bone formation and reduced bone resorption by SIM (3 and 6 mg kg⁻¹ day⁻¹) [55]. In parallel, Ho

et al. also found that SIM (administered orally at 10–20 mg kg⁻¹ day⁻¹) to OVX rats improved their trabecular bone volume/total volume in distal femurs (~25 %) and proximal tibiae (~ 20%) which were significantly higher than OVX- group whereas SIM showed no significant increase in bone volume in SHAM rats [56]. In the same line, Ito *et al.* reported that micelle of deoxycholate containing SIM coated by calcium phosphate (CaP) via IM injection improved bone mineral density and mechanical properties with suppression of inflammation in OVX mice [57].

In contradiction to previous findings, a few studies have reported that SIM has no significant effect on bone healing, new bone formation or bone resorption due to critical dose dependent behavior [58]–[62]. For instance, Maritz *et al.* (2001) reported SIM effect on OVX rats with different dosage of 1, 5, 10 and 20 mg kg⁻¹ day⁻¹ via oral administration (P.O.). Interestingly SIM (20 mg kg⁻¹ day⁻¹) showed increase in both bone formation (osteoid volumes, osteoid surfaces, and osteoblast number) and bone resorption (eroded surfaces occupied by the Osteoclasts). Thereby, globally no net effect was seen neither in bone formation nor in bone resorption [63].

Healthy - fracture animal model

Regarding the effect of SIM in healthy animals, Skoglund *et al.* reported an in vivo study in mice with bone fractures where oral administration of SIM accelerated new bone formation [64]. Later on, Saraf *et al.* conducted an experimental study to investigate the bone healing process by administering SIM orally (120 mg kg⁻¹ of body weight) to rabbits with femur fracture. Bone healing was hastened during the initial 4 to 8 weeks following administration of SIM and the average bending fracture strength and average three point bending stiffness significantly improved at 4 and 8 weeks, in comparison to the control group [51]. The effect of SIM on bone strength in healthy rats was analyzed by Garip *et al.*, who showed a dose dependent effect of SIM (20 & 50 mg kg⁻¹ day⁻¹) in tibiae bone with improved bone strength at the lower dosage [65]. Another study by Oxlund *et al.* (2001), reported that SIM (10 mg kg⁻¹) increased cancellous bone volume by 23%, and this was associated to a 24% increase in its compressive strength in healthy rats [66]. It is important to take into account that an optimum dosage for each animal model is a key point. As reported earlier in fracture healing model for rabbits, bone resorption behavior was observed with SIM (30 mg kg⁻¹ day⁻¹, P.O.) while lower dosage (10 mg kg⁻¹ day⁻¹) did not have any significant effect [67].

Overall, systemic delivery of SIM has been reported as having significant efficacy in

osteoporotic models (i.e. OVX). The majority of studies conducted on OVX rats with SIM reported significant increase in bone formation and inhibition of bone resorption consistently. Moreover, SIM has also been found to be beneficial in other bone pathologies including fracture healing, spinal fusion, osteonecrosis or bone strength in healthy rats. To treat femur fractures and for spinal fusion higher SIM dosages were found to be the most suitable.

Local administration

As discussed in earlier sections, SIM has a very low bioavailability due to high elimination when administered systemically. SIM is known to enhance bone formation through inhibition of mevalonate pathway alone. However, after conversion of SIM to SVA, 20 – 90 % of the hydrophilic SVA is predominantly eliminated by the human bile [68]. Due to such an extensive pre-systemic (first pass) metabolism, SIM has a very low oral bioavailability ($\leq 5\%$) and this justifies the interest for delivering SIM locally to the therapeutic site. In order to maximize the efficiency and have sustained drug release and minimize its side effects, local delivery is a suitable method.

In the following sections, the most relevant results reported in the literature on the effect of locally administered SIM in bone regeneration are discussed, covering both the administration through local injections or by using a biomaterial as a drug delivery vehicle.

-Local injections

Local injections in the overlying tissue of the defect can be applied subcutaneously, intramuscularly or intravenously. The most effective range of dosage to have maximum benefits of SIM has been found to be between 7 and 20 mg kg⁻¹ day⁻¹ for different bone defect models (Table 2-4) which have all been conducted in rodents.

Different studies where SIM was administered subcutaneously in the tissue overlying calvaria defects reported enhanced 50 % increase in new bone formation in OVX rats [10] or increase in bone thickness [69] respectively.

For load bearing locations, bone defects were generated in tibiae and femur. For femoral defect, Skoglund & Aspenberg *et al.*, administered SIM subcutaneously or locally through an osmotic pump. While there was no significant effect with subcutaneous injection, local administration with an osmotic pump resulted in higher force at the fracture site [70]. Another study also reported enhancement of ALP, OCN with local injections of SIM at the

surgical site [71]. Similar findings were reported for tibiae defect, with an increase in BMP-2 and ALP with reduction of osteoclasts via transdermal injections of SIM [72].

Over all, local injections either in calvaria defect or in defects in load bearing locations, both reported significant enhancement in bone regeneration. Even osteoporotic animal models with bone defects reported increase in bone volume. It can be said that SIM efficacy is proven throughout the variation of bone defect models among osteoporotic as well as healthy animal models.

-Administration of SIM using biomaterial carriers

The main body of research dealing with local delivery of SIM has been done with implantable grafts. The major advantage of employing implants for local drug delivery is to allow lower dosage if sustained and controlled, increasing the bioavailability at the therapeutic site and overcoming systemic toxicity.

In the following sections, a summary and brief discussion on the reviewed studies evaluating SIM loaded carriers (Table 2-5) in the different bone defects is provided (calvaria defects, load bearing locations and other models).

Osteoporotic animal model

Yang et al., grafted porous titanium implants coated with SIM-HA in tibiae defect of OVX rat. They reported enhanced bone formation and osteointegration; increased bone implant contact [73]. Similar findings were reported where SIM loaded Biomimetic β -TCP with an apatite coating were employed for OVX rats with a tunable SIM release [74]. They reported increased bone mineral density from 400 to 600 mg/cm³ from week 0 to week 6 respectively. These findings in OVX rats are similar as observed in healthy rat model for tibiae or femur defect discussed ahead [75], [76].

Healthy animal model

Polymeric carriers

Polymer-based drug carriers have been used extensively in last few decades. Major advantages of these carriers include characteristics like biodegradability and biocompatibility. The most common polymer-based implants evaluated as carriers for SIM used polylactic acid (PLA), polyglycolic Acid (PGA) or their co-polymers. Some studies include model of calvaria defect and a majority investigated load bearing location. Among the latter, different models such as tibiae, femur and mandibular defects have been

investigated, usually with very low dosage of SIM (between 5 µg and 1 mg) and reporting significant improvement in treatment of the bone defects.

For defects in rat calvaria, Pişkin *et al.*, reported increased osteointegration and bone restoration by using SIM loaded electrospun PCL scaffolds implanted into calvaria defect [77]. Another study investigated both calvaria and mandibular defects, with SIM loaded (0.1-2.2 mg) methylcellulose gel held by polylactic acid (PLA) membranes [78]. In calvaria, it was able to stimulate gene expression of pro-collagen, fibronectin and matrix metalloproteinase-13 (MMP13) related to collagen synthesis for bone growth. On the other hand, for the mandibular defect, bone area increased by 45% in at the 0.5 mg dosage with reduced inflammation vs. control. In agreement, another study conducted on mandibular defects used SIM-loaded PLA-PGA copolymer [79] and reported improved osteoconduction and inhibited bone resorption.

A few studies employed polymeric grafts combined with hydroxyapatite. For rat calvaria defect, Jiang *et al.*, implanted Poly (lactic-co-glycolic acid)/hydroxyapatite nano-fibrous scaffolds loaded with SIM. They reported increased ALP activity and decrease in the defect size with enhancement of osteoinduction [80]. Another group employed SIM –poly (lactic-co-glycolic acid)/hydroxyapatite (SIM/PLGA/HA) microspheres for tibiae fracture with a necrotic bone gap. They reported neovascularisation with cell ingrowth in grafted bone as well as necrotic bone [81].

Overall, significant bone regeneration enhancement has been reported in the literature when SIM was incorporated in biodegradable polymeric matrices, either in calvaria, mandible or load bearing defects in rodents.

Another option for the local delivery of SIM is the use of hydrogels. Those based on gelatin or collagen are the ones that have been used more often incorporating SIM amounts ranging from 25 µg to 10 mg. In rat calvaria defect, Sukul *et al.* employed a SIM loaded hydrogel scaffold constituted by gelatin-nanofibrillar cellulose and β-Tricalcium phosphate prepared by freeze drying. They reported an increase in the expression of osteoblastic differentiation related genes and showed higher bone formation[82].

For non-union femur defects in rats, fracture union was reported due to enhanced angiogenesis and osteogenesis thanks to SIM-gelatin hydrogel [83]. Moshiri *et al.* employed gelatin cross linked with genipin loaded with SIM in a rabbit femoral bone defect. They reported formation of newly woven ectopic bone. Also, bone maturation and remodeling into cortical bone were found with higher bone volume, mineralization, elastic

modulus, and contact hardness indicated osteogenesis, osteoinduction and osteoconduction [84]. Similarly, another study was conducted on femur cavity with absorbable, hydrolyzed and lyophilized collagen sponges soaked with SIM. They reported enhanced angiogenesis, bone formation and increased number of osteoblasts with an increase in the OCN and VEGF gene expression [85].

SIM-loaded collagen grafts were implanted in a parietal bone defect in rats, and SIM loaded photocured hyaluronic acid hydrogels were used in the same defect in rabbits. SIM-collagen grafts reported a significant increase in new bone formation in comparison to unloaded collagen grafts [86]. Similar findings were reported in a rabbit animal model with new bone formation and enhanced osteogenesis [87].

Tibiae defects were investigated with SIM loaded hydroxypropyl methyl cellulose granules by Rushinek *et al.* They reported increase in osteoid thickness, volume, mineral apposition rate and calcein labeling though trabecular surface had no significant effect on osteoblasts in static histomorphometric analysis [88]. Whether rat calvaria defect or load bearing location defect, different hydrogels and animal model have reported significant bone formation thanks to the presence of SIM.

Inorganic carriers

Inorganic grafts, such as apatites and salts of calcium phosphates with similar composition to bone are increasingly studied as carriers for SIM. Calcium Phosphates are considered excellent bone substitutes due to their bioactivity, osteoconductive behavior, biocompatibility, direct bonding with the bone and resorbability [89], [90]. Although the range of SIM concentrations vary depending on the material used as carrier, a range from 0.1 to 5 mg was incorporated per scaffold or per defect depending on the defect model.

Most studies are conducted with particles of α -TCP, β -TCP or hydroxyapatite, alone or combined with hydrogels, as described in the previous section.

For rat calvaria defect, Nyan *et al.* implanted calcium sulphate powder loaded with SIM showing evident bone formation in 8 weeks, although the early resorption of calcium sulphate resulted in burst release of SIM followed by intense soft tissue inflammation. For the first 5 weeks, inflammation hindered bone formation which improved significantly by 8 weeks [91]. Later, Nyan *et al.* conducted another study with a similar model with SIM loaded in α -TCP particles. They reported soft tissue inflammation at 0.25 and 0.5 mg dosage. Conversely, 0.1 mg of SIM resulted in maximum bone regeneration with higher

bone volume over 8 weeks without any sign of inflammation. Gap bridging was seen between the defect border and the inserted α -TCP particles, so histological imaging suggested this SIM dosage led to maximum stimulation of local cells [92].

Some studies employed different grafts of inorganic bovine bone graft (BOS), combined with calcium sulphate (HACS), and collagen sponge (COS) [75]. They reported an increase in new bone formation which was significant higher at 8 weeks with HACS-SIM ($44.31 \pm 9.89 \text{ mm}^2$) vs. other grafts. On the other hand, at 4 weeks BOS-SIM ($43.22 \pm 8.82 \text{ mm}^2$) showed higher values than other grafts [75].

Calcium Phosphate Cements (CPCs) are considered excellent bone substitutes due to their injectability, ability to harden in-vivo and close composition to the bone's inorganic phase [93]. In addition, CPCs are considered excellent vehicles for delivery of drugs [94], so in the past years progress has been made towards combining SIM with CPCs.

In 2012, Yin *et al.* conducted studies with CPC scaffolds implanted intramuscularly (into back muscles) or endosteally (in the femoral condyle) rabbits. They prepared macroporous apatitic CPCs with SIM (1, 5 and 10 wt %) blended to its solid phase. The highest SIM concentration (10 wt %) resulted into inflammation, muscular necrosis and lowered compressive strength of the graft. Whereas, lowest concentration of 1 wt% was found to prove the osteogenic potential of macroporous CPCs without any inflammation [95].

To modulate the release of SIM from macroporous scaffolds (either from hydroxyapatite or β -TCP), Polycaprolactone – Polyethylene glycol like (PCL-co-PEG) dry coatings were produced by cold plasma [96]. The thickness of the coatings essentially depended on the specific surface area and on the plasma treatment conditions and allowed blocking, delaying or reducing the release rate depending on the with varying thickness of the polymer coatings and treatment conditions [96].

To summarize, different grafts from polymers to inorganic such as CaP or CPCs, SIM has consistently proven its anabolic effects.

Conclusions

Simvastatin is known for its beneficial effects on bone metabolism through a) enhancement of bone formation by fostering osteoinduction and osteoblastic activity and b) inhibition of bone resorption through reduced osteoclastogenesis and osteoclastic

activity.

SIM effects have been widely investigated both *in vitro* and *in vivo*, using different administration routes. *In vivo* studies have provided evidence of the effect of SIM on the gene expression of bone formation related proteins: BMP-2 or ALP. On the other hand, *in vivo* studies have demonstrated the effectiveness of SIM, especially in two major bone pathologies: osteoporosis and bone fractures. The local delivery route has been found to maximize its efficiency.

Local drug delivery carriers evaluated in combination with SIM include polymers and inorganic matrices, such as CaPs. Despite the variety of grafts evaluated in literature, SIM consistently proved its anabolic effects. Bone regeneration was reported throughout the reviewed studies with new bone formation or increase in bone volume *in vivo*, associated to the over-expression of some genes relevant for bone regeneration such as BMP-2, ALP or OCN, as well as suppression of osteoclasts *in vitro*.

To conclude, SIM has proven to be beneficial for bone regeneration from a wide spectrum of investigations, including *in vitro* and *in vivo*, being the choice of the most suitable concentration a critical parameter. Moreover, there is a need to extend the studies to big animal models to gather more conclusive information before going to clinical trials.

Table 2-2 In vitro studies conducted to study the effect of the simvastatin on bone formation.

Year & Author	Study	Dosage of SIM	Main Findings
Via Cell culture medium			
Mundy <i>et al.</i> , 1999 [97]	Human (MG63), Murine (2T3) bone cells	1 -5 μ M	2.7 fold \uparrow BMP-2 with SIM at 2.5 μ M
Ruiz-Gaspa <i>et al.</i> 2007 [98]	Primary human osteoblast (hOB) and MG-63	10^{-6} M to 10^{-9} M	In hOB, a significant \uparrow in COL1A1, OCN, and BMP-2 gene expression and slightly lower values in MG-63 with arrest of proliferation.
Chen <i>et al.</i> , 2010 [45]	Osteoblast-like cells from calvaria bone, mice	10^{-3} - 10^{-9} M	At 10^{-6} M SIM showed the highest cell viability; 3days: \uparrow BMP-2 and ALP gene expression indicating enhancement of differentiation.
Sugiyama <i>et al.</i> , 2000 [99]	Human osteosarcoma (HOS) cells	0.1-10 μ M	BMP-2 RNA expression with 10 μ M of SIM showed ~4.5 fold induction in luciferase activity compared with solvent control.
Maeda <i>et al.</i> 2003 [100]	MC3T3-E1 cells, mouse stromal cells (ST2), and rat osteosarcoma cells (UMR-106)	1 nM - 100 μ M	At 10^{-6} M \uparrow x2 of VEGF expression in MC3T3-E1, \uparrow x7 in ST2 cells at 3h by 7 fold and \uparrow in UMR-106 at short times (<12h).
Maeda <i>et al.</i> 2001 [46]	MC3T3-E1 and rat bone marrow cells	10^{-7} - 10^{-8} M	MC3T3-E1 showed increased ALP activity and mineralization vs. control at 10^{-7} M. Rat bone marrow cells showed significant \uparrow in mineralization (10^{-6} to 10^{-8} M) vs. control.
Montazerolghaem <i>et al.</i> , 2015 [47]	MC3T3-E1 pre-osteoblasts and Primary human monocytes	Zn (10 and 25 μ M) and SVA (0.25 and 0.4 μ M)	Zn (10 μ M) and SVA (0.25 μ M) resulted in significant \uparrow cell differentiation and mineralization without impeding proliferation rate. SVA indicated mineralization with higher ALP activity & secretion of Ca deposits at 22 days.
Ahn KS <i>et al.</i> , 2008 [101]	RAW 264.7 (mouse macrophage), MCF-7 (human breast adenocarcinoma) & U266 (multiple myeloma) Cells	0.1, 0.5 & 1 μ M	Pretreated cells with SIM (1 μ M) for 6 hr suppressed the activation of NF- κ B, I κ Ba kinase, I κ Ba phosphorylation and I κ Ba degradation induced by RANKL & suppression of osteoclastogenesis.
Yamashita <i>et al.</i> , 2008 [102]	C2C12 mouse myoblast cells	1-100 μ M	SIM alone has no effect on Runx2 expression or ALP activity but 24h pretreatment of cells with SIM reverses the effect of TNF- α suppression of BMP-induced Runx2 expression & ALP activity

			significantly at 30 μ M.
Zhou <i>et al.</i> , 2010[43]	human adipose- derived stromal cells (hADSCs)	0.01 μ M-1 μ M	At 0.1 μ M SIM, \uparrow ALP activity at day 14, at \uparrow OCN secretion, and matrix calcification at 24h & 72h.
Pagkalos <i>et al.</i> , 2010 [103]	Murine embryonic stem cells (mESCs)	0.1nM - 100nM	At 0.1 nM, SIM can cause differentiation into osteogenic cells even without osteoinductive supplements. \uparrow OCN and osetrix gene expression.
Carrier			
Valles <i>et al.</i> , 2012 [34]	Saos-2cells; human osteoblasts (hOBs); SIM in the cell culture medium with or without Ti particles	1 μ M	In Saos-2 cells & hOBs, SIM significantly decreased the Ti particle-induced relative <i>IL-6</i> secretion for both. These results showed cytokine-lowering property of SIM.
Montazerolghaem <i>et al.</i> , 2013 [50]	Saos-2 cells; Premixed brushite CPCs	0.25-1 SVA/g cement	4X \uparrow mineralization at lower SVA dosage (0.5 & 0.25mg. Significant increase in ALP for 10^{-6} M and cell viability for 10^{-7} M, 10^{-8} M SVA vs. control.
Park <i>et al.</i> , 2012 [48]	MC3T3-E1 pre-osteoblast cells; Gelatin–poly(ethylene glycol)–tyramine(GPT) hydrogel	1 and 3 mg/ml	Osteogenic differentiation observed with increase in matrix metalloproteinase-13, OC expression levels, and mineralization in 14 days.
Nath <i>et al.</i> , 2013 [104]	MC3T3-E1 pre-osteoblast cells; SIM loaded PLGA microspheres into hydrogel loaded biphasic CaP spongy scaffold	0.2 gm	Biocompatible scaffold resulted in significantly higher cell attachment and proliferation with increase in collagen I (Col-I), OP and OC gene expression.
Jeon <i>et al.</i> , 2007 [105]	MC3T3-E1 cells; Cellulose acetate phthalate/ Pluronic F 127 (PF-127) Microspheres	0-1 μ M (SVA)	Intermittent release (100 pM - 10 nM) of SIM OCN \uparrow , ALP \uparrow and cell number \uparrow depending on the [SIM].
Bae <i>et al.</i> , 2011[87]	MC3T3-E1 cells; Photo-cured hyaluronic acid hydrogels	0.1 and 1 mg	At 1mg, cell proliferation and mineralization were significantly higher than control.

Table 2-3 In vivo systemic administration of simvastatin to study the effect on bone formation. (P.O: Oral administration, IM: Intramuscular, IP: intraperitoneal)

Year & Author	Study	Dosage of SIM	Main Findings
Osteoporotic / Ovariectomized (OVX) rats or mice			
Maritz <i>et al.</i> 2001 [63]	Rats (P.O.)	1, 5, 10 & 20 mg kg ⁻¹ day ⁻¹	SIM (20 mg kg ⁻¹ day ⁻¹) decreased BMD, ↑ 1) bone formation (↑ osteoid volumes, osteoid surfaces, and osteoblast numbers) and 2) bone resorption (↑ eroded surfaces with osteoclasts) = globally no significant difference found.
Junqueira <i>et al.</i> , 2002 [53]	Rats with mandibular defect (P.O.)	20 mg kg ⁻¹ day ⁻¹	Significant ↑ new bone formation in mandibles.
Pytlík <i>et al.</i> , 2003 [55]	Rats (P.O.)	3 and 6 mg kg ⁻¹ day ⁻¹	At higher dosage, strong bone formation and inhibition of bone resorption was observed.
Oxlund & Andreassen <i>et al.</i> , 2004 [66]	Rats (P.O.)	20 mg kg ⁻¹ day ⁻¹	SIM reduced cancellous bone loss due to OVX and new cortical bone formation.
Ho <i>et al.</i> , 2009 [56]	Rats (P.O.)	10–20 mg kg ⁻¹ day ⁻¹	In OVX+20 SIM: ↑ ~10 % Trabecular bone volume/ total volume ↑ ~15% of distal femurs, and ↑ ~15% in proximal tibiae. SHAM rats: No increase in Bone volume.
Yao <i>et al.</i> , 2006 [59]	Rats (P.O.)	0.3 to 10 mg kg ⁻¹ day ⁻¹	No significant changes in bone resorption or new bone formation.
Anbinder <i>et al.</i> , 2007 [58]	Rats (P.O.)	25 mg kg ⁻¹ day ⁻¹	No significant change on bone healing.
Zhibin Du <i>et al.</i> , 2008 [106]	Rats with Ti implants in cancellous bone (P.O.)	5 mg kg ⁻¹ day ⁻¹	OVX +SIM vs. OVX showed improved osteointegration of implants in BIC: 56.06 ± 17.31 vs. 34.92 ± 12.63, BA: 27.03 ± 8.06 vs. 14.45 ± 4.44 and BD: 19.63 ± 7.01 vs. 9.81 ± 4.18 in cancellous region (zone B) with no change in cortical region (zone A)
Du <i>et al.</i> , 2013 [107]	Rats with Ti implants in tibiae (P.O.)	5 mg kg ⁻¹ day ⁻¹	Improved osteointegration & serum had higher bone formations markers such as bone-specific alkaline phosphatase (BALP) and bone Gla protein (BGP) levels.
Von Stechow <i>et</i>	Mice (P.O.)	20 mg kg ⁻¹	No significant change in bone formation.

<i>al.</i> , 2003 [60]		day ⁻¹	
Issa <i>et al.</i> , 2015 [108]	OVX and (SHAM) rats with fractured femur (P.O.)	5 & 20 mg week ⁻¹	Higher dose of 20 mg showed stronger effects with significant bone repair.
Healthy animal model			
Femur Fracture			
Skoglund <i>et al.</i> 2002 [64]	Mice (P.O.)	~120 mg kg ⁻¹ day ⁻¹	At 14 days→ SIM group 53% larger transverse area than controls, 63% greater force required to break the bone, and 150% ↑ energy uptake.
Saraf <i>et al.</i> , 2007 [109]	Rabbits (P.O.)	120 mg kg ⁻¹ day ⁻¹	Bone healing process was hastened during the initial 4 to 8 weeks. ↑ Bending strength, ↑ three point bending stiffness.
Spinal Fusion			
Bostan <i>et al.</i> , 2011 [52]	Rats (P.O.)	120 mg kg ⁻¹ day ⁻¹	SIM group showed no signs of Psuedoarthrosis. Three point bending force showed promotion of fusion in SIM-SF 148.80±39.403 Newtons vs. 123.80±28.479 Newtons in SF.
Yee <i>et al.</i> , 2006 [61]	Rats (P.O.)	20 mg kg ⁻¹ day ⁻¹	No significant effect of SIM on spinal fusion.
Other models			
Chissas <i>et al.</i> , 2010 [110]	Rabbits with ulnar osteotomy (fracture healing) (P.O.)	10 & 30 mg kg ⁻¹ day ⁻¹	Higher dosage leads to significant reduction in BMD, stiffness and after 15 days callus formation whereas lower dosage had no effect even at early stage of fracture remodelling.
Bowers <i>et al.</i> , 2004 [111]	Osteonecrosis in Femoral head of dog (P.O.)	40 mg kg ⁻¹ day ⁻¹	Significant increase in Bone mineral density and volume yet lower values on comparing to alendronate.
Oxlund <i>et al.</i> 2001 [66]	Cortical shell of 5th lumbar vertebra in rats (P.O.)	10 mg kg ⁻¹ day ⁻¹	23% ↑ in cancellous bone volume (52.7 ± 1.6%) against placebo group (42.8 ± 1.7%) and 24% ↑ in compressive strength (31.8 ± 2.7 MPa) compared with the placebo group (24.1 ± 1.9 MPa).
Nakashima & Haneji, 2013 [112]	Female mice (IP)	10 mg kg ⁻¹ day ⁻¹	Reduced osteoclast numbers and reduced bone loss. SIM blocks RANKL induced IRF4 expression involved in osteoclastogenesis.
Ito <i>et al.</i> , 2013 [57]	Deoxycholic acid/SIM in calcium phosphate (CaP-DeCA/SIM) nanocapsules (IM)	150 µg	Reduced cytotoxicity, anti-inflammatory and increase in BMD and bone strength was seen with mechanical testing.

Table 2-4 Local delivery of simvastatin through local injections (INJ) (Subcutaneous (SC), Intradermal (ID) or Intramuscular (IM)) at defect site.

Year & Author	Design	Dosage	Main Findings
Osteoporotic model			
Mundy et al. 1999 [10]	Murine calvaria; OVX Rats (SC INJ)	5 or 10 mg kg ⁻¹	↑39-94% in trabecular bone volume in Rats.
Wang JW et al., 2007 [113]	Tibiae fracture, OVX rats (SC)	10 mg kg ⁻¹ day ⁻¹	↑ Callus cross-section area: 21.3% (1 week; 20.22±3.42 mm ² vs. 16.67±4.02 mm ²) and new woven bone was functional and arranged more tightly and regularly at 2 and 4 weeks; 57.5% ↑ maximal load.
Funk et al., 2008 [114]	Induced rheumatoid arthritis, Osteoporotic rats via Streptococcal cell well (SCW); (SC INJ)	20 mg kg ⁻¹ day ⁻¹ (SVA)	SIM after SCW injection suppressed periarticular bone destruction & osteoclasts, cells/mm ² 33.6 ± 2.4 vs. 43.3 ± 1.9 in SCW alone and SIM reduced the joint inflammation as well.
Healthy animal model			
Thylin et al., 2002 [69]	Murine calvaria; 1) methylcellulose gel (GEL) vs (GEL-SIM) 3) polylactide membrane (MEM-SIM) (SC INJ)	2.2 mg SIM per 50 µl gel and 50 µl of SIM-GEL for injections	MEM-SIM caused a highly significant increase in bone thickness (159% to 172%) and BA (144% to 180%) vs. gel controls. GEL-SIM resulted in more bone (58% to 83%) vs. gel controls.
Anbinder et al., 2006 [115]	Tibiae defect, rat (SC)	7 mg kg ⁻¹ day ⁻¹	Subcutaneously either way no significant bone repair was seen.
Ayukawa et al., 2009 [72]	Tibiae defect, rat (Transdermal INJ)	0.1 mg mL ⁻¹	Local application resulted in bone formation in bone defects with increase in BMP-2 and ALP at the early stage with no effect of OCN. SIM also suppressed osteoclasts with diminution of the RANKL gene expression.
Koçer et al., 2014 [71]	Femoral defect, mice (SC INJ)	10 mg kg ⁻¹ day ⁻¹	Significant increase in ALP, OCN and radiological features of new bone at defect site.
Skoglund & Aspenberg et al., 2007 [116]	Femoral fracture, mice a) SC INJ b) Systematic (implanted in scruff) or local delivery with osmotic mini pump	10 & 20 mg kg ⁻¹ day ⁻¹ or 0.1 mg with osmotic mini-pump	SC INJ showed no effects. Systematic delivery resulted with 160% large force and local delivery with 170% large force at fracture site.
Killeen et al.,	Fenestration defects in Molar	0.5 mg SIM +	ALN after SIM-EtOH injections showed 2-3 fold ↑ in bone width

2012) [117]	roots, rats (SC)	Alendronate (ALN, N-BP; systemically)	around the defect (0.93± 0.12 and 0.78 ± 0.11mm with early and late systemic ALN, respectively) vs. local SIM/ALN-CD preparations (0.32±0.10mm) or short-term SIM-EtOH injections (0.35 ± 0.10 mm).
-------------	------------------	---------------------------------------	---

Table 2-5 Local delivery of simvastatin by incorporating in implantable biomaterial carriers.

Year & Author	Material	Design	Dosage	Main Findings
Osteoporotic model				
Yang <i>et al.</i> , 2012 [73]	Porous titanium implants coated with SIM-HA	Tibiae defect, OVX Rat	10^{-6} & 10^{-7} M	Enhanced bone formation and osteointegration with improved bone-implant contact but no significant changes in between dosage.
Chou <i>et al.</i> , 2016 [74]	SIM -Biomimetic β -TCP with apatite coating	Femoral bone, <u>OVX</u> Mice	20mg in 4 mL of ethanol in scaffold	Significant increase in new bone formation and mechanical strength for SIM- β -TCP-Apatite.
Yang <i>et al.</i> , 2014 [118]	Bovine serum albumin	Femur and caudal vertebrae, <u>OVX</u> Rat	5 or 10 mg	In femur, significantly increased BMD, bone volume fraction (BV/TV), improved bone microstructural parameters and bone strength. In caudal vertebrae, significant increase in BV/TV, bone microstructures, and bone strength.
Healthy animal model				
Polymer-based (Calvaria & load bearing: Mandibular, Tibiae & Femur)				
Pişkin <i>et al.</i> , 2008 [77]	SIM-containing electrospun spiral-wound PCL scaffolds	Rat calvaria defect	20 μ g SIM/scaffold	Implant showed osseous tissue integration and significant mineralized bone restoration in calvaria defect.
Stein <i>et al.</i> , 2006 [78]	Methylcellulose gel/polylactic acid (PLA) membrane	Rat Calvaria & Mandible defect	0.1, 0.5, 1, 1.5 & 2.2 mg day ⁻¹	In calvaria, stimulated gene expression of pro-collagen, fibronectin and matrix metalloproteinase-13 (MMP13) related to collagen synthesis. In mandibular, 0.5 & 2.2 mg SIM \rightarrow 45% \uparrow BA vs. control gel. 0.5 mg \downarrow inflammation as compared to 2.2 mg SIM.

Wu <i>et al.</i> , 2008 [79]	SIM loaded Polylactic acid/polyglycolic acid (PLA/PGA) copolymer carriers	Sockets of right mandibular incisors	1 mg	SIM treated showed osteoinductive and anti-resorption properties. At 12 weeks, Control and SIM treated both healed completely.
Pauly <i>et al.</i> , 2009[119]	Titanium wires coated with or without PLA with SIM	Tibiae fracture, Rat	3 µg/ implant & 50 µg/implant	Study showed osteoconductive behaviour of SIM while high dosage resulted in fracture healing with significant increase in torsional stiffness & maximum load.
Pauly <i>et al.</i> , 2012 [120]	SIM- polymer-only (poly(D,L-lactide)) coatings on the Ti implant	Femur defect, Rat	5.5 & 90 µg	No positive effects rather impaired the osteointegration between implant and defect after 8 weeks.
Zhu <i>et al.</i> , 2010 [121]	SIM loaded PLA scaffold	Radial defect, Rabbit	50, 100 & 200 mg per scaffold	100 mg dosage showed best results with significant bone healing.
Polymer-hydroxyapatite (HA) (Calvaria & Tibiae)				
Jiang <i>et al.</i> , 2013 [80]	poly(lactic-co-glycolic acid)/hydroxyapatite nanofibrous scaffold Poly(lactic-co-glycolic acid)/hydroxyapatite nanofibrous scaffold	Calvaria defect, Rat	8µg per defect	Over 8 weeks ~23.2% i.e. ~116 µg of total loading (500 µg) was released. In PLGA/HA/SIM group, ALP activity was significantly higher and Bone defect was reduced by 10% vs. PLGA/HA group.
Tai <i>et al.</i> , 2013 [81]	SIM –poly(lactic-co-glycolic acid)/hydroxyapatite (SIM/PLGA/HA) microspheres	Tibiae fracture-necrotic bone gap, Mice	3 & 5 mg	Low dosage showed callus formation, 52eovascularisation and cell ingrowth in the grafted bone while high dosage resulted in cell growth in necrotic bone as well.
Hydrogels (Calvaria & load bearing: Tibae, femur, parietal etc.)				
Zhou <i>et al.</i> , 2010[43]	Injectable tissue-engineered bone (ITB) containing hADSCs and platelet-rich plasma gel (hPRP)	Calvaria defect, Mice	0.01,0.1, and 1 µM	SIM group induced bone formation 50% at 4 weeks higher than that of blank control (negative), i.e. no implantation
Sukul <i>et al.</i> , 2015[82]	SIM-Gelatin nanofibrillar cellulose-β TCP scaffolds	Calvaria defect, Rat	0.25, 0.5 and 1 µM	<i>In vitro</i> , GNTS.5 (0.5 µM) showed the highest cell differentiation and maximum amount of bone

				formation. <i>In vivo</i> , release pattern induced osteogenesis at the maximum level and enhanced bone formation.
Rushinek <i>et al.</i> , 2014 [88]	SIM - hydroxypropyl methylcellulose granules	Tibiae defect, Rat	70% w/w SIM per granule (49.4 ± 17.7 mg per defect)	Osteoid thickness, volume, mineral apposition rate and calcein labelling had significant increase yet trabecular bone had no significant effect on osteoblasts.
Fukui <i>et al.</i> , 2012 [83]	SIM-Gelatin hydrogel	Femoral fracture, Rat	25 µg	Significant increase in angiogenesis and osteogenesis leads to bone healing.
Rosselli <i>et al.</i> , 2014 [85]	SIM - hydroxypropyl methylcellulose (HPMC) gel - Collagen sponge	Femur cavity, Rat	0.5 ml of SIM gel (SIM 1 mg / HPMC 0.5 ml)	Significant increase in osteoblasts and fibroblast proliferation and marked bone formation.
Moshiri <i>et al.</i> , 2015 [84]	a) SIM powder b) Gelatin-SIM 3D scaffold	Femur cavity (2 holes), Rabbit	5mg per hole for powder and 169.6mg per scaffold	At 30 days, SIM powder and Gel-SIM scaffold resulted in newly woven ectopic bone. Gel-SIM: maturation and remodelling of new bone into cortical bone with higher bone volume, mineralization, elastic modulus, and contact hardness indicating osteogenesis, osteoinduction and osteoconduction.
Oka <i>et al.</i> , 2013[122]	SIM-Gelatin hydrogel	Anterior cruciate ligament (ACL) reconstruction with tendon graft, Rabbit	125µg SIM loaded in 250µg gelatin hydrogel	Aligned and layered cartilage in area of tendon-bone integration, Neovascularization was significantly increased (capillary density SIM, 112.0±6.9 vs. control, 72.0±5.8/mm ²). Osteogenesis assessed by osteoblast density was significantly enhanced (SIM, 495.3–32.9 vs. control, 272.0–28.3/mm ²).
Wong <i>et al.</i> , 2003 [86]	Fibrillar Collagen sponge	Parietal defect, Rat	10 mg SIM/collagen sponge)	308% ↑ new bone growth with 1.68±0.48 mm ² of area vs. 0.4±0.28 mm ² in the control group.
Bae <i>et al.</i> , 2011[87]	Photo-cured hyalurononic acid hydrogels	Parietal defect, Rabbit	0.1 and 1 mg SIM	Induced osteogenesis with new bone formation.
Inorganic (Calcium sulphate and calcium phosphates) (Calvaria & load bearing: tibiae, femur etc.)				
Nyan <i>et al.</i> , 2007 [91]	Calcium Sulphate (CS)	Calvaria defect, Rat	1 mg SIM: 60 mg CS	After 8 weeks, significant increase in bone growth was seen in BA 1.15 ± 0.01 cm ² and BMC 79.48 ±

				3.23 mg with intense soft tissue inflammation for first 5 weeks.
Nyan <i>et al.</i> , 2009 [92]	α -TCP particles	Calvaria defect, Rat	0.01, 0.1, 0.25 & 0.5 mg / 14 mg of α -TCP	0.1 mg dosage stimulates bone regeneration (266% in 8 weeks). At 8 weeks, defect closure 97.86 ± 1.49 %, BMC 29.07 ± 1.11 mg and BMD 88.07 ± 3.35 mg/cm ² were significantly \uparrow .
Nyan <i>et al.</i> , 2010 [123]	α -TCP particles	Calvaria defect, Rat	0.1 mg / 14 mg of α -TCP	In SIM group, \uparrow proliferation and migration of osteoprogenitor cells from the dura mater, new bone formation, \uparrow BMP-2 expression and upregulation of TGF- β 1 was also observed on day 7-14.
Rojbani <i>et al.</i> , 2011 [124]	Particles of α -TCP, β -TCP, and HA	Calvaria defect, Rat	0.1 mg per defect	α -TCP showed a significant more bone formation and higher rate of degradation than β -TCP and HA.
Ma <i>et al.</i> , 2008 [76]	β -TCP collar	Tibiae defect, Rat	0.1, 0.9 or 1.7 mg per scaffold	At 6 weeks: decrease in mineral apposition At 26 weeks: increase in fibrous tissue area fraction and higher bone area fraction though changes weren't significant.
Papadimitriou <i>et al.</i> , 2015 [75]	Inorganic bovine bone graft (BOS), & hydroxyapatite combined with calcium sulfate (HACS)	Femur defect, Rabbit	2mg	BOS + SIM: At 4 weeks, new bone formation, HACS + SIM: At 8 weeks higher rate of new bone formation
Huang <i>et al.</i> , 2014 [125]	Calcium Sulphate	Ulnar bone defect, Rabbit	0.5 mg per scaffold	Significant new bone formation in ulnar defect due to SIM was comparable to BMP-2.
Calcium Phosphate cements (CPCs)				
Yin <i>et al.</i> , 2012 [95]	Hydroxyapatite (HA) macroporous CPCs	Back muscles & trabecular bone, Rabbit	1, 5 & 10 wt%	At the defect site, new bone formation (1 wt %) with more area ($7.4\% \pm 3.3\%$) vs. control ($3.6\% \pm 1.4\%$); BIC was higher ($78.4\% \pm 23.5\%$) vs. control ($54.3\% \pm 14.6\%$).

References

- [1] E. Gómez-Barrena, P. Rosset, I. Müller, R. Giordano, C. Bunu, P. Layrolle, Y. T. Konttinen, and F. P. Luyten, "Bone regeneration: stem cell therapies and clinical studies in orthopaedics and traumatology.," *J. Cell. Mol. Med.*, vol. 15, no. 6, pp. 1266–86, Jun. 2011.
- [2] E. Hernlund, A. Svedbom, M. Ivergård, J. Compston, C. Cooper, J. Stenmark, E. V McCloskey, B. Jönsson, and J. A. Kanis, "Osteoporosis in the European Union: medical management, epidemiology and economic burden. A report prepared in collaboration with the International Osteoporosis Foundation (IOF) and the European Federation of Pharmaceutical Industry Associations (EFPIA).," *Arch. Osteoporos.*, vol. 8, no. 1–2, p. 136, Jan. 2013.
- [3] J. P. Schmitz and J. O. Hollinger, "The critical size defect as an experimental model for craniomandibulofacial nonunions.," *Clin. Orthop. Relat. Res.*, no. 205, pp. 299–308, Apr. 1986.
- [4] I. Garrett, G. Gutierrez, and G. Mundy, "Statins and Bone Formation.," *Curr. Pharm. Des.*, vol. 7, no. 8, pp. 715–736, May 2001.
- [5] J. R. Lieberman, A. Daluiski, and T. A. Einhorn, "The role of growth factors in the repair of bone. Biology and clinical applications.," *J. Bone Joint Surg. Am.*, vol. 84–A, no. 6, pp. 1032–44, Jun. 2002.
- [6] T. Sakou, "Bone Morphogenetic Proteins: From Basic Studies to Clinical Approaches," *Bone*, vol. 22, no. 6, pp. 591–603, Jun. 1998.
- [7] J. E. Fisher, M. J. Rogers, J. M. Halasy, S. P. Luckman, D. E. Hughes, P. J. Masarachia, G. Wesolowski, R. G. G. Russell, G. A. Rodan, and A. A. Reszka, "Alendronate mechanism of action: geranylgeraniol, an intermediate in the mevalonate pathway, prevents inhibition of osteoclast formation, bone resorption, and kinase activation in vitro," *Proc. Natl. Acad. Sci.*, vol. 96, no. 1, pp. 133–138, Jan. 1999.
- [8] A. W. Alberts, "Lovastatin and Simvastatin - Inhibitors of HMG CoA Reductase and Cholesterol Biosynthesis," *Cardiology*, vol. 77, no. 4, pp. 14–21, 1990.
- [9] I. Buhaescu and H. Izzedine, "Mevalonate pathway: A review of clinical and therapeutical implications," *Clin. Biochem.*, vol. 40, no. 9, pp. 575–584, 2007.
- [10] G. Mundy, "Stimulation of Bone Formation in Vitro and in Rodents by Statins," *Science (80-)*, vol. 286, no. 5446, pp. 1946–1949, Dec. 1999.
- [11] S. R. Shah, C. A. Werlang, F. K. Kasper, and A. G. Mikos, "Novel applications of statins for bone regeneration," *Natl. Sci. Rev.*, vol. 2, no. 1, pp. 85–99, Mar. 2015.
- [12] A. Moshiri, A. M. Sharifi, and A. Oryan, "Role of Simvastatin on fracture healing and osteoporosis: a systematic review on in vivo investigations," *Clin. Exp. Pharmacol. Physiol.*, vol. 43, no. 7, pp. 659–684, Jul. 2016.
- [13] J. Montero, G. Manzano, and A. Albaladejo, "The role of topical simvastatin on bone regeneration: A systematic review," *J. Clin. Exp. Dent.*, vol. 6, no. 3, pp. e286-90, Jul. 2014.
- [14] K.-C. C. Hsieh, C.-L. L. Kao, C.-W. W. Feng, Z.-H. H. Wen, H.-F. F. Chang, S.-C. C. Chuang, G.-J. J. Wang, M.-L. L. Ho, S.-M. M. Wu, J.-K. K. Chang, and H.-T. T. Chen, "A novel anabolic agent: a simvastatin analogue without HMG-CoA reductase inhibitory activity.," *Org. Lett.*, vol. 16, no. 17, pp. 4376–9, Sep. 2014.
- [15] T. R. Pedersen and J. A. Tobert, "Simvastatin: a review," *Expert Opin. Pharmacother.*, vol. 5, no. 12, pp. 2583–2596, Dec. 2004.

- [16] T. Prueksaritanont, B. Ma, X. Fang, R. Subramanian, J. Yu, and J. H. Lin, "beta-Oxidation of simvastatin in mouse liver preparations.," *Drug Metab. Dispos.*, vol. 29, no. 10, pp. 1251–5, Oct. 2001.
- [17] T. Prueksaritanont, R. Subramanian, X. Fang, B. Ma, Y. Qiu, J. H. Lin, P. G. Pearson, and T. A. Baillie, "Glucuronidation of Statins in Animals and Humans: A Novel Mechanism of Statin Lactonization," *Drug Metab. Dispos.*, vol. 30, no. 5, pp. 505–512, May 2002.
- [18] B. A. Hamelin and J. Turgeon, "Hydrophilicity/ lipophilicity: relevance for the pharmacology and clinical effects of HMG-CoA reductase inhibitors," *Trends Pharmacol. Sci.*, vol. 19, no. 1, pp. 26–37, 1998.
- [19] N. Horiuchi and T. Maeda, "Statins and bone metabolism.," *Oral Dis.*, vol. 12, no. 2, pp. 85–101, Mar. 2006.
- [20] R. Y. A. Mukhtar, J. Reid, and J. P. D. Reckless, "Drug focus," *Int. J. Clin. Pract.*, vol. 59, no. February, pp. 239–252, Feb. 2005.
- [21] D. E. Duggan, I. W. Chen, W. F. Bayne, R. A. Halpin, C. A. Duncan, M. S. Schwartz, R. J. Stubbs, and S. Vickers, "The physiological disposition of lovastatin.," *Drug Metab. Dispos.*, vol. 17, no. 2, pp. 166–73, 1989.
- [22] R. Halpin, E. Ulm, A. Till, P. Kari, K. Vyas, D. Hunninghake, and D. Duggan, "Biotransformation of lovastatin. V. Species differences in in vivo metabolite profiles of mouse, rat, dog, and human," *Drug Metab. Dispos.*, vol. 21, no. 6, pp. 1003–1011, Nov. 1993.
- [23] J. K. Liao and U. Laufs, "Pleiotropic effects of statins.," *Annu. Rev. Pharmacol. Toxicol.*, vol. 45, pp. 89–118, Jan. 2005.
- [24] E. S. Istvan, "Structural mechanism for statin inhibition of 3-hydroxy-3-methylglutaryl coenzyme A reductase.," *Am. Heart J.*, vol. 144, no. 6 Suppl, pp. S27–S32, 2002.
- [25] O. Adam and U. Laufs, "Antioxidative effects of statins.," *Arch. Toxicol.*, vol. 82, no. 12, pp. 885–92, Dec. 2008.
- [26] I. Inoue, S. Goto, K. Mizotani, T. Awata, T. Mastunaga, S. Kawai, T. Nakajima, S. Hokari, T. Komoda, and S. Katayama, "Lipophilic HMG-CoA reductase inhibitor has an anti-inflammatory effect," *Life Sci.*, vol. 67, no. 8, pp. 863–876, Jul. 2000.
- [27] K. Koh, "Effects of statins on vascular wall: vasomotor function, inflammation, and plaque stability," *Cardiovasc. Res.*, vol. 47, no. 4, pp. 648–657, Sep. 2000.
- [28] A. Tavridou, A. Efthimiadis, I. Efthimiadis, and H. Paschalidou, "Antioxidant effects of simvastatin in primary and secondary prevention of coronary heart disease.," *Eur. J. Clin. Pharmacol.*, vol. 62, no. 6, pp. 485–9, Jun. 2006.
- [29] D. Pruefer, R. Scalia, and A. M. Lefer, "Simvastatin Inhibits Leukocyte-Endothelial Cell Interactions and Protects Against Inflammatory Processes in Normocholesterolemic Rats," *Arterioscler. Thromb. Vasc. Biol.*, vol. 19, no. 12, pp. 2894–2900, Dec. 1999.
- [30] J. L. Wallace, "Nitric oxide as a regulator of inflammatory processes," *Mem. Inst. Oswaldo Cruz*, vol. 100, pp. 5–9, Mar. 2005.
- [31] U. Ikeda, T. Ito, and K. Shimada, "Interleukin-6 and acute coronary syndrome," *Clin. Cardiol.*, vol. 24, no. 11, pp. 701–704, Nov. 2001.
- [32] P. M. Ridker, "High-Sensitivity C-Reactive Protein : Potential Adjunct for Global Risk Assessment in the Primary Prevention of Cardiovascular Disease," *Circulation*, vol. 103, no. 13, pp. 1813–1818, Apr. 2001.
- [33] C. Arnaud, F. Burger, S. Steffens, N. R. Veillard, T. H. Nguyen, D. Trono, and F. Mach, "Statins

- reduce interleukin-6-induced C-reactive protein in human hepatocytes: new evidence for direct antiinflammatory effects of statins.," *Arterioscler. Thromb. Vasc. Biol.*, vol. 25, no. 6, pp. 1231–6, Jun. 2005.
- [34] G. Vallés, C. Pérez, A. Boré, F. Martín-Saavedra, L. Saldaña, and N. Vilaboa, "Simvastatin prevents the induction of interleukin-6 gene expression by titanium particles in human osteoblastic cells.," *Acta Biomater.*, vol. 9, no. 1, pp. 4916–25, Jan. 2013.
- [35] A. Rezaie-Majd, T. Maca, R. A. Bucek, P. Valent, M. R. Müller, P. Husslein, A. Kashanipour, E. Minar, and M. Baghestanian, "Simvastatin Reduces Expression of Cytokines Interleukin-6, Interleukin-8, and Monocyte Chemoattractant Protein-1 in Circulating Monocytes From Hypercholesterolemic Patients," *Arterioscler. Thromb. Vasc. Biol.*, vol. 22, no. 7, 2002.
- [36] H. Loppnow, L. Zhang, M. Buerke, M. Lautenschläger, L. Chen, A. Frister, A. Schlitt, T. Luther, N. Song, B. Hofmann, S. Rose-John, R.-E. Silber, U. Müller-Werdan, and K. Werdan, "Statins potently reduce the cytokine-mediated IL-6 release in SMC/MNC cocultures," *J. Cell. Mol. Med.*, vol. 15, no. 4, pp. 994–1004, Apr. 2011.
- [37] Y. Kureishi, Z. Luo, I. Shiojima, A. Bialik, D. Fulton, D. J. Lefer, W. C. Sessa, and K. Walsh, "The HMG-CoA reductase inhibitor simvastatin activates the protein kinase Akt and promotes angiogenesis in normocholesterolemic animals.," *Nat. Med.*, vol. 6, no. 9, pp. 1004–10, Sep. 2000.
- [38] S. Dimmeler, A. Aicher, M. Vasa, C. Mildner-Rihm, K. Adler, M. Tiemann, H. Rütten, S. Fichtlscherer, H. Martin, and A. M. Zeiher, "HMG-CoA reductase inhibitors (statins) increase endothelial progenitor cells via the PI 3-kinase/Akt pathway.," *J. Clin. Invest.*, vol. 108, no. 3, pp. 391–7, Aug. 2001.
- [39] I. Shiojima and K. Walsh, "Role of Akt Signaling in Vascular Homeostasis and Angiogenesis," *Circ. Res.*, vol. 90, no. 12, 2002.
- [40] A. R. Chade, X. Zhu, O. P. Mushin, C. Napoli, A. Lerman, and L. O. Lerman, "Simvastatin promotes angiogenesis and prevents microvascular remodeling in chronic renal ischemia.," *FASEB J.*, vol. 20, no. 10, pp. 1706–8, Aug. 2006.
- [41] C. J. Edwards and T. D. Spector, "Statins as modulators of bone formation.," *Arthritis Res.*, vol. 4, no. 3, pp. 151–3, Jan. 2002.
- [42] M. Frick, J. Dulak, J. Cisowski, A. Józkowicz, R. Zwick, H. Alber, W. Dichtl, S. P. Schwarzacher, O. Pachinger, and F. Weidinger, "Statins differentially regulate vascular endothelial growth factor synthesis in endothelial and vascular smooth muscle cells," *Atherosclerosis*, vol. 170, no. 2, pp. 229–236, 2003.
- [43] Y. Zhou, Y. Ni, Y. Liu, B. Zeng, Y. Xu, and W. Ge, "The role of simvastatin in the osteogenesis of injectable tissue-engineered bone based on human adipose-derived stromal cells and platelet-rich plasma.," *Biomaterials*, vol. 31, no. 20, pp. 5325–35, Jul. 2010.
- [44] Y. Zhang, R. Zhang, Y. Li, G. He, D. Zhang, and F. Zhang, "Simvastatin augments the efficacy of therapeutic angiogenesis induced by bone marrow-derived mesenchymal stem cells in a murine model of hindlimb ischemia," *Mol. Biol. Rep.*, vol. 39, no. 1, pp. 285–293, Jan. 2012.
- [45] P.-Y. Chen, J.-S. Sun, Y.-H. Tsuang, M.-H. Chen, P.-W. Weng, and F.-H. Lin, "Simvastatin promotes osteoblast viability and differentiation via Ras/Smad/Erk/BMP-2 signaling pathway.," *Nutr. Res.*, vol. 30, no. 3, pp. 191–9, Mar. 2010.
- [46] T. Maeda, a Matsunuma, T. Kawane, and N. Horiuchi, "Simvastatin promotes osteoblast differentiation and mineralization in MC3T3-E1 cells.," *Biochem. Biophys. Res. Commun.*, vol. 280, no. 3, pp. 874–7, Jan. 2001.
- [47] M. Montazerolghaem, Y. Ning, H. Engqvist, M. Karlsson Ott, M. Tenje, and G. Mestres, "Simvastatin and zinc synergistically enhance osteoblasts activity and decrease the acute

- response of inflammatory cells," *J. Mater. Sci. Mater. Med.*, vol. 27, no. 2, p. 23, Feb. 2016.
- [48] Y. S. Park, A. E. David, K. M. Park, C.-Y. Lin, K. D. Than, K. Lee, J. B. Park, I. Jo, K. D. Park, and V. C. Yang, "Controlled release of simvastatin from in situ forming hydrogel triggers bone formation in MC3T3-E1 cells.," *AAPS J.*, vol. 15, no. 2, pp. 367–76, Apr. 2013.
- [49] S. D. Nath, N. T. Linh, A. Sadiasa, and B. T. Lee, "Encapsulation of simvastatin in PLGA microspheres loaded into hydrogel loaded BCP porous spongy scaffold as a controlled drug delivery system for bone tissue regeneration," *J. Biomater. Appl.*, vol. 28, no. 8, pp. 1151–1163, Apr. 2014.
- [50] M. Montazerolghaem, K. Ott, and Montazerolghaem et al, "Sustained release of Simvastatin from premixed injectable Calcium Phosphate Cement," *J. Biomed. Mater. Res. A*, pp. 1–8, Mar. 2013.
- [51] S. K. Saraf, A. Singh, R. S. Garbyal, and V. Singh, "Effect of simvastatin on fracture healing—An experimental study," 2007. [Online]. Available: <http://nopr.niscair.res.in/handle/123456789/5526>. [Accessed: 10-Jul-2014].
- [52] B. Bostan, T. Güneş, M. Aşçı, C. Sen, M. H. Keleştemur, M. Erdem, R. D. Köseoğlu, and U. Erkorkmaz, "Simvastatin improves spinal fusion in rats.," *Acta Orthop. Traumatol. Turc.*, vol. 45, no. 4, pp. 270–5, 2011.
- [53] J. C. Junqueira, M. N. G. Mancini, Y. R. Carvalho, A. L. Anbinder, I. Balducci, and R. F. Rocha, "Effects of simvastatin on bone regeneration in the mandibles of ovariectomized rats and on blood cholesterol levels.," *J. Oral Sci.*, vol. 44, no. 3–4, pp. 117–24, Dec. 2002.
- [54] H. Oxlund and T. T. Andreassen, "Simvastatin treatment partially prevents ovariectomy-induced bone loss while increasing cortical bone formation," *Bone*, vol. 34, no. 4, pp. 609–618, Apr. 2004.
- [55] M. Pytlik, W. Janiec, M. Misiarz-Myrta, and I. Gubała, "Effects of simvastatin on the development of osteopenia caused by ovariectomy in rats.," *Pol. J. Pharmacol.*, vol. 55, no. 1, pp. 63–71.
- [56] M.-L. Ho, Y.-H. Chen, H.-J. Liao, C.-H. Chen, S.-H. Hung, M.-J. Lee, Y.-C. Fu, Y.-H. Wang, G.-J. Wang, and J.-K. Chang, "Simvastatin increases osteoblasts and osteogenic proteins in ovariectomized rats.," *Eur. J. Clin. Invest.*, vol. 39, no. 4, pp. 296–303, Apr. 2009.
- [57] T. Ito, M. Takemasa, K. Makino, and M. Otsuka, "Preparation of calcium phosphate nanocapsules including simvastatin/deoxycholic acid assembly, and their therapeutic effect in osteoporosis model mice," *J. Pharm. Pharmacol.*, vol. 65, no. 4, pp. 494–502, Apr. 2013.
- [58] A. L. Anbinder, F. de A. Prado, M. de A. Prado, I. Balducci, and R. F. da Rocha, "The influence of ovariectomy, simvastatin and sodium alendronate on alveolar bone in rats.," *Braz. Oral Res.*, vol. 21, no. 3, pp. 247–52.
- [59] W. Yao, R. Farmer, R. Cooper, P. A. Chmielewski, X. Y. Tian, R. B. Setterberg, W. S. S. Jee, and M. W. Lundy, "Simvastatin did not prevent nor restore ovariectomy-induced bone loss in adult rats.," *J. Musculoskelet. Neuronal Interact.*, vol. 6, no. 3, pp. 277–83, 2006.
- [60] D. von Stechow, S. Fish, D. Yahalom, I. Bab, M. Chorev, R. Müller, and J. M. Alexander, "Does simvastatin stimulate bone formation in vivo?," *BMC Musculoskelet. Disord.*, vol. 4, no. 1, p. 8, Dec. 2003.
- [61] A. J. M. Yee, H. W. Bae, D. Friess, S. M. Roth, C. Whyne, M. Robbin, B. Johnstone, and J. U. Yoo, "The use of simvastatin in rabbit posterolateral lumbar intertransverse process spine fusion," *Spine J.*, vol. 6, no. 4, pp. 391–396, Jul. 2006.
- [62] A. L. Anbinder, F. de A. Prado, M. de A. Prado, I. Balducci, and R. F. da Rocha, "The influence of ovariectomy, simvastatin and sodium alendronate on alveolar bone in rats," *Braz. Oral Res.*, vol. 21, no. 3, pp. 247–252, Sep. 2007.
- [63] F. J. Maritz, M. M. Conradie, P. A. Hulley, R. Gopal, and S. Hough, "Effect of Statins on Bone

- Mineral Density and Bone Histomorphometry in Rodents,” *Arterioscler. Thromb. Vasc. Biol.*, vol. 21, no. 10, pp. 1636–1641, Oct. 2001.
- [64] B. Skoglund, C. Forslund, and P. Aspenberg, “Simvastatin improves fracture healing in mice,” *J. Bone Miner. Res.*, vol. 17, no. 11, pp. 2004–8, Nov. 2002.
- [65] S. Garip and F. Severcan, “Determination of simvastatin-induced changes in bone composition and structure by Fourier transform infrared spectroscopy in rat animal model,” *J. Pharm. Biomed. Anal.*, vol. 52, no. 4, pp. 580–588, Aug. 2010.
- [66] H. Oxlund, M. Dalstra, and T. T. Andreassen, “Statin given perorally to adult rats increases cancellous bone mass and compressive strength,” *Calcif. Tissue Int.*, vol. 69, no. 5, pp. 299–304, Nov. 2001.
- [67] D. Chissas, G. Stamatopoulos, D. Verettas, K. Kazakos, A. Papalois, G. Agrogiannis, A. Papaeliou, E. Agapitos, A. Balanika, E. Papadopoulou, G. Anastopoulos, P. G. Ntagiopoulos, and A. Asimakopoulos, “Can low doses of simvastatin enhance fracture healing? An experimental study in rabbits,” *Injury*, vol. 41, no. 7, pp. 687–692, 2010.
- [68] S. Vickers, C. A. Duncan, I. W. Chen, A. Rosegay, and D. E. Duggan, “Metabolic disposition studies on simvastatin, a cholesterol-lowering prodrug,” *Drug Metab. Dispos.*, vol. 18, no. 2, pp. 138–45, 1990.
- [69] M. R. Thylin, J. C. McConnell, M. J. Schmid, R. R. Reckling, J. Ojha, I. Bhattacharyya, D. B. Marx, and R. A. Reinhardt, “Effects of Simvastatin Gels on Murine Calvarial Bone,” *J. Periodontol.*, vol. 73, no. 10, pp. 1141–1148, Oct. 2002.
- [70] B. Skoglund and P. Aspenberg, “Locally applied Simvastatin improves fracture healing in mice,” *BMC Musculoskelet. Disord.*, vol. 8, no. 1, p. 98, Dec. 2007.
- [71] A. Koçer, M. Öner, İ. Karaman, D. Koçer, İ. H. Kafadar, A. Güney, and Z. F. Karaman, “The effects of locally applied simvastatin on an experimental mouse femur nonunion model,” *Acta Orthop. Traumatol. Turc.*, vol. 48, no. 6, pp. 679–84, 2014.
- [72] Y. Ayukawa, E. Yasukawa, Y. Moriyama, Y. Ogino, H. Wada, I. Atsuta, and K. Koyano, “Local application of statin promotes bone repair through the suppression of osteoclasts and the enhancement of osteoblasts at bone-healing sites in rats,” *Oral Surg. Oral Med. Oral Pathol. Oral Radiol. Endod.*, vol. 107, no. 3, pp. 336–42, Mar. 2009.
- [73] G. Yang, L. Song, C. Guo, S. Zhao, L. Liu, and F. He, “Bone responses to simvastatin-loaded porous implant surfaces in an ovariectomized model,” *Int. J. Oral Maxillofac. Implants*, vol. 27, no. 2, pp. 369–74.
- [74] J. Chou, T. Ito, M. Otsuka, B. Ben-Nissan, and B. Milthorpe, “The effectiveness of the controlled release of simvastatin from β -TCP macrosphere in the treatment of OVX mice,” *J. Tissue Eng. Regen. Med.*, vol. 10, no. 3, pp. E195–E203, Mar. 2016.
- [75] K. Papadimitriou, G. Karkavelas, I. Vouros, E. Kessopoulou, and A. Konstantinidis, “Effects of local application of simvastatin on bone regeneration in femoral bone defects in rabbit,” *J. Cranio-Maxillofacial Surg.*, vol. 43, no. 2, pp. 232–237, Mar. 2015.
- [76] B. Ma, S. A. Clarke, R. A. Brooks, and N. Rushton, “The effect of simvastatin on bone formation and ceramic resorption in a peri-implant defect model,” *Acta Biomater.*, vol. 4, no. 1, pp. 149–155, Jan. 2008.
- [77] E. Pişkin, I. A. İşoğlu, N. Bölgen, I. Vargel, S. Griffiths, T. Çavuşoğlu, P. Korkusuz, E. Güzel, and S. Cartmell, “*In vivo* performance of simvastatin-loaded electrospun spiral-wound polycaprolactone scaffolds in reconstruction of cranial bone defects in the rat model,” *J. Biomed. Mater. Res. Part A*, vol. 90A, no. 4, pp. 1137–1151, Sep. 2009.

- [78] D. Stein, Y. Lee, M. J. Schmid, B. Killpack, M. A. Genrich, N. Narayana, D. B. Marx, D. M. Cullen, and R. A. Reinhardt, "Local Simvastatin Effects on Mandibular Bone Growth and Inflammation," *J. Periodontol.*, vol. 76, no. 11, pp. 1861–1870, Nov. 2005.
- [79] Z. Wu, C. Liu, G. Zang, and H. Sun, "The effect of simvastatin on remodelling of the alveolar bone following tooth extraction.," *Int. J. Oral Maxillofac. Surg.*, vol. 37, no. 2, pp. 170–6, Feb. 2008.
- [80] L. Jiang, H. Sun, A. Yuan, K. Zhang, D. Li, C. Li, C. Shi, X. Li, K. Gao, C. Zheng, B. Yang, and H. Sun, "Enhancement of Osteoinduction by Continual Simvastatin Release from Poly(lactic-co-glycolic acid)-Hydroxyapatite-Simvastatin Nano-Fibrous Scaffold," *J. Biomed. Nanotechnol.*, vol. 9, no. 11, pp. 1921–1928, Sep. 2013.
- [81] M.-L. Ho, Tai, Fu, Wang, and Chang, "Local delivery of controlled-release simvastatin/PLGA/HAP microspheres enhances bone repair," *Int. J. Nanomedicine*, vol. Volume 8, no. 1, p. 3895, Oct. 2013.
- [82] M. Sukul, Y.-K. Min, S.-Y. Lee, and B.-T. Lee, "Osteogenic potential of simvastatin loaded gelatin-nanofibrillar cellulose- β tricalcium phosphate hydrogel scaffold in critical-sized rat calvarial defect," *Eur. Polym. J.*, vol. 73, pp. 308–323, 2015.
- [83] T. Fukui, M. Ii, T. Shoji, T. Matsumoto, Y. Mifune, Y. Kawakami, H. Akimaru, A. Kawamoto, T. Kuroda, T. Saito, Y. Tabata, R. Kuroda, M. Kurosaka, and T. Asahara, "Therapeutic effect of local administration of low-dose simvastatin-conjugated gelatin hydrogel for fracture healing," *J. Bone Miner. Res.*, vol. 27, no. 5, pp. 1118–1131, May 2012.
- [84] A. Moshiri, M. Shahrezaee, B. Shekarchi, A. Oryan, and K. Azma, "Three-Dimensional Porous Gelatin-Simvastatin Scaffolds Promoted Bone Defect Healing in Rabbits," *Calcif. Tissue Int.*, vol. 96, no. 6, pp. 552–564, Jun. 2015.
- [85] J. E. G. C. Rosselli, D. M. F. S. Martins, J. L. Martins, C. R. G. C. M. Oliveira, D. J. Fagundes, M. O. Taha, J. E. G. C. Rosselli, D. M. F. S. Martins, J. L. Martins, C. R. G. C. M. de Oliveira, D. J. Fagundes, and M. O. Taha, "The effect of simvastatin on the regeneration of surgical cavities in the femurs of rabbits," *Acta Cir. Bras.*, vol. 29, no. 2, pp. 87–92, Feb. 2014.
- [86] R. W. . Wong and a. B. . Rabie, "Statin collagen grafts used to repair defects in the parietal bone of rabbits," *Br. J. Oral Maxillofac. Surg.*, vol. 41, no. 4, pp. 244–248, Aug. 2003.
- [87] M. S. Bae, D. H. Yang, J. B. Lee, D. N. Heo, Y.-D. Kwon, I. C. Youn, K. Choi, J. H. Hong, G. T. Kim, Y. S. Choi, E. H. Hwang, and I. K. Kwon, "Photo-cured hyaluronic acid-based hydrogels containing simvastatin as a bone tissue regeneration scaffold," *Biomaterials*, vol. 32, no. 32, pp. 8161–8171, Nov. 2011.
- [88] H. Rushinek, M. Alterman, A. Laviv, E. I. Weiss, M. Friedman, and N. Casap, "Topical application of slow-release simvastatin as a bone substitute in bone defects in the rat tibia: a pilot study.," *Int. J. Oral Maxillofac. Implants*, vol. 29, no. 2, pp. e241-6.
- [89] C. G. Finkemeier, "Bone-grafting and bone-graft substitutes.," *J. Bone Joint Surg. Am.*, vol. 84–A, no. 3, pp. 454–64, Mar. 2002.
- [90] R. Z. LeGeros, "Properties of osteoconductive biomaterials: calcium phosphates.," *Clin. Orthop. Relat. Res.*, vol. 395, no. 395, pp. 81–98, Feb. 2002.
- [91] M. Nyan, D. Sato, M. Oda, T. Machida, H. Kobayashi, T. Nakamura, and S. Kasugai, "Bone Formation With the Combination of Simvastatin and Calcium Sulfate in Critical-Sized Rat Calvarial Defect," *J. Pharmacol. Sci.*, vol. 104, no. 4, pp. 384–386, 2007.
- [92] M. Nyan, D. Sato, H. Kihara, T. Machida, K. Ohya, and S. Kasugai, "Effects of the combination with alpha-tricalcium phosphate and simvastatin on bone regeneration.," *Clin. Oral Implants Res.*, vol. 20, no. 3, pp. 280–7, Mar. 2009.

- [93] M.-P. Ginebra, T. Traykova, and J. A. Planell, "Calcium phosphate cements: competitive drug carriers for the musculoskeletal system?," *Biomaterials*, vol. 27, no. 10, pp. 2171–7, Apr. 2006.
- [94] M.-P. Ginebra, C. Canal, M. Espanol, D. Pastorino, and E. B. Montufar, "Calcium phosphate cements as drug delivery materials.," *Adv. Drug Deliv. Rev.*, vol. 64, no. 12, pp. 1090–110, Sep. 2012.
- [95] Yin et al, "Simvastatin-loaded macroporous calcium phosphate cement: preparation, in vitro characterization, and evaluation of in vivo performance.," *J. Biomed. Mater. Res. A*, vol. 100, no. 11, pp. 2991–3000, Nov. 2012.
- [96] C. Canal, K. Khurana, S. Gallinetti, S. Bhatt, J. Pulpytel, F. Arefi-Khonsari, and M.-P. Ginebra, "Design of calcium phosphate scaffolds with controlled simvastatin release by plasma polymerisation," *Polymer (Guildf)*, vol. 92, pp. 170–178, Jun. 2016.
- [97] S. E. Harris, L. F. Bonewald, M. A. Harris, M. Sabatini, S. Dallas, J. Q. Feng, N. Ghosh-Choudhury, J. Wozney, and G. R. Mundy, "Effects of transforming growth factor beta on bone nodule formation and expression of bone morphogenetic protein 2, osteocalcin, osteopontin, alkaline phosphatase, and type I collagen mRNA in long-term cultures of fetal rat calvarial osteoblasts.," *J. Bone Miner. Res.*, vol. 9, no. 6, pp. 855–63, Jun. 1994.
- [98] S. Ruiz-Gaspa, X. Nogues, A. Enjuanes, J. C. Monllau, J. Blanch, R. Carreras, L. Mellibovsky, D. Grinberg, S. Balcells, A. Díez-Perez, and J. Pedro-Botet, "Simvastatin and atorvastatin enhance gene expression of collagen type 1 and osteocalcin in primary human osteoblasts and MG-63 cultures.," *J. Cell. Biochem.*, vol. 101, no. 6, pp. 1430–8, Aug. 2007.
- [99] M. Sugiyama, T. Kodama, K. Konishi, K. Abe, S. Asami, and S. Oikawa, "Compactin and simvastatin, but not pravastatin, induce bone morphogenetic protein-2 in human osteosarcoma cells.," *Biochem. Biophys. Res. Commun.*, vol. 271, no. 3, pp. 688–92, May 2000.
- [100] T. Maeda, T. Kawane, and N. Horiuchi, "Statins augment vascular endothelial growth factor expression in osteoblastic cells via inhibition of protein prenylation.," *Endocrinology*, vol. 144, no. 2, pp. 681–92, Feb. 2003.
- [101] K. S. Ahn, G. Sethi, M. M. Chaturvedi, and B. B. Aggarwal, "Simvastatin, 3-hydroxy-3-methylglutaryl coenzyme A reductase inhibitor, suppresses osteoclastogenesis induced by receptor activator of nuclear factor-kappaB ligand through modulation of NF-kappaB pathway.," *Int. J. Cancer*, vol. 123, no. 8, pp. 1733–40, Oct. 2008.
- [102] M. Yamashita, F. Otsuka, T. Mukai, H. Otani, K. Inagaki, T. Miyoshi, J. Goto, M. Yamamura, and H. Makino, "Simvastatin antagonizes tumor necrosis factor-alpha inhibition of bone morphogenetic proteins-2-induced osteoblast differentiation by regulating Smad signaling and Ras/Rho-mitogen-activated protein kinase pathway.," *J. Endocrinol.*, vol. 196, no. 3, pp. 601–13, Mar. 2008.
- [103] J. Pagkalos, J. M. Cha, Y. Kang, M. Heliotis, E. Tsiroidis, and A. Mantalaris, "Simvastatin induces osteogenic differentiation of murine embryonic stem cells.," *J. Bone Miner. Res.*, vol. 25, no. 11, pp. 2470–8, Nov. 2010.
- [104] S. D. Nath, N. T. Linh, A. Sadiasa, and B. T. Lee, "Encapsulation of simvastatin in PLGA microspheres loaded into hydrogel loaded BCP porous spongy scaffold as a controlled drug delivery system for bone tissue regeneration," *J. Biomater. Appl.*, vol. 28, no. 8, pp. 1151–1163, Apr. 2014.
- [105] J. H. Jeon, M. V. Thomas, and D. A. Puleo, "Bioerodible devices for intermittent release of simvastatin acid.," *Int. J. Pharm.*, vol. 340, no. 1–2, pp. 6–12, Aug. 2007.
- [106] Z. Du, J. Chen, F. Yan, and Y. Xiao, "Effects of Simvastatin on bone healing around titanium implants in osteoporotic rats.," *Clin. Oral Implants Res.*, vol. 20, no. 2, pp. 145–50, Feb. 2009.
- [107] Z. Du, J. Chen, F. Yan, N. Doan, S. Ivanovski, and Y. Xiao, "Serum bone formation marker

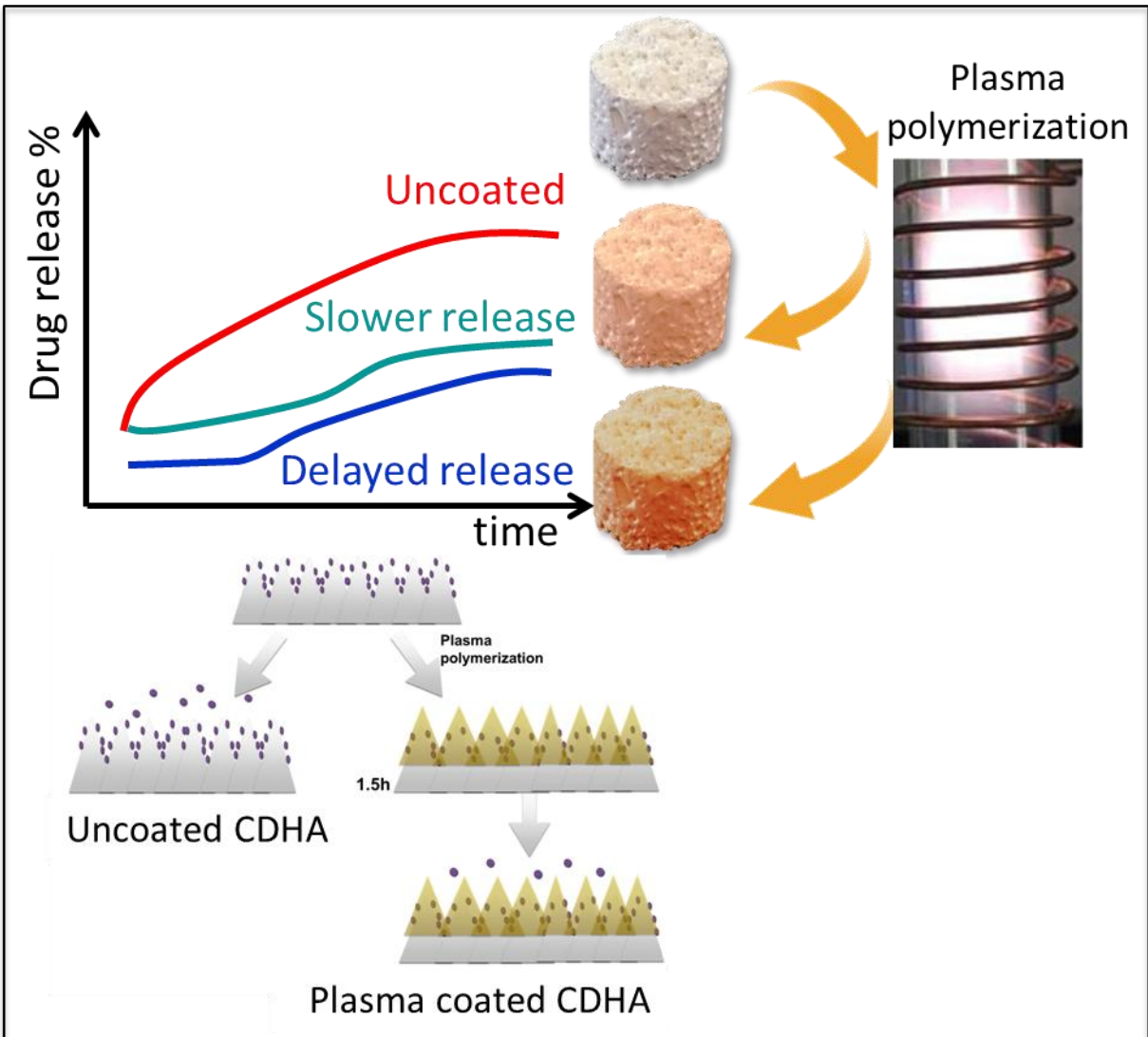
- correlation with improved osseointegration in osteoporotic rats treated with simvastatin," *Clin. Oral Implants Res.*, vol. 24, no. 4, pp. 422–427, Apr. 2013.
- [108] J. P. M. Issa, C. Ingraci de Lucia, B. G. dos Santos Kotake, M. Gonçalves Gonzaga, F. A. Tocchini de Figueiredo, D. Mizusaki Iyomasa, A. P. Macedo, and E. Ervolino, "The effect of simvastatin treatment on bone repair of femoral fracture in animal model," *Growth Factors*, vol. 33, no. 2, pp. 139–148, Mar. 2015.
- [109] S. K. Saraf, A. Singh, R. S. Garbyal, and V. Singh, "Effect of simvastatin on fracture healing--an experimental study.," *Indian J. Exp. Biol.*, vol. 45, no. 5, pp. 444–449, 2007.
- [110] D. Chissas, G. Stamatopoulos, D. Verettas, K. Kazakos, A. Papalois, G. Agrogiannis, A. Papaeliou, E. Agapitos, A. Balanika, E. Papadopoulou, G. Anastopoulos, P. G. Ntagiopoulos, and A. Asimakopoulos, "Can low doses of simvastatin enhance fracture healing? An experimental study in rabbits," *Injury*, vol. 41, no. 7, pp. 687–692, Jul. 2010.
- [111] J. R. Bowers, Z. H. Dailiana, E. F. McCarthy, and J. R. Urbaniak, "Drug therapy increases bone density in osteonecrosis of the femoral head in canines.," *J. Surg. Orthop. Adv.*, vol. 13, no. 4, pp. 210–6, 2004.
- [112] Y. Nakashima and T. Haneji, "Stimulation of Osteoclast Formation by RANKL Requires Interferon Regulatory Factor-4 and Is Inhibited by Simvastatin in a Mouse Model of Bone Loss," *PLoS One*, vol. 8, no. 9, p. e72033, Sep. 2013.
- [113] J. W. Wang, S. W. Xu, D. S. Yang, and R. K. Lv, "Locally applied simvastatin promotes fracture healing in ovariectomized rat.," *Osteoporos. Int.*, vol. 18, no. 12, pp. 1641–50, Dec. 2007.
- [114] J. L. Funk, J. Chen, K. J. Downey, and R. A. Clark, "Bone protective effect of simvastatin in experimental arthritis.," *J. Rheumatol.*, vol. 35, no. 6, pp. 1083–1091, Jun. 2008.
- [115] A. L. Anbinder, J. C. Junqueira, M. N. G. Mancini, I. Balducci, R. F. da Rocha, and Y. R. Carvalho, "Influence of simvastatin on bone regeneration of tibial defects and blood cholesterol level in rats.," *Braz. Dent. J.*, vol. 17, no. 4, pp. 267–73, 2006.
- [116] B. Skoglund and P. Aspenberg, "Locally applied Simvastatin improves fracture healing in mice.," *BMC Musculoskelet. Disord.*, vol. 8, p. 98, Jan. 2007.
- [117] A. C. Killeen, P. a Rakes, M. J. Schmid, Y. Zhang, N. Narayana, D. B. Marx, J. B. Payne, D. Wang, and R. a Reinhardt, "Impact of local and systemic alendronate on simvastatin-induced new bone around periodontal defects.," *J. Periodontol.*, vol. 83, no. 12, pp. 1463–71, Dec. 2012.
- [118] N. Yang, Y. Cui, J. Tan, X. Fu, X. Han, H. Leng, and C. Song, "Local injection of a single dose of simvastatin augments osteoporotic bone mass in ovariectomized rats," *J. Bone Miner. Metab.*, vol. 32, no. 3, pp. 252–260, May 2014.
- [119] S. Pauly, F. Luttosch, M. Morawski, N. P. Haas, G. Schmidmaier, and B. Wildemann, "Simvastatin locally applied from a biodegradable coating of osteosynthetic implants improves fracture healing comparable to BMP-2 application.," *Bone*, vol. 45, no. 3, pp. 505–11, Sep. 2009.
- [120] S. Pauly, D. A. Back, K. Kaeppler, N. P. Haas, G. Schmidmaier, and B. Wildemann, "Influence of statins locally applied from orthopedic implants on osseous integration.," *BMC Musculoskelet. Disord.*, vol. 13, p. 208, Oct. 2012.
- [121] J. Zhu, Q. Song, J. Wang, X. Han, Y. Yang, J. Liao, and C. Song, "[Study on local implantation of simvastatin for repairing rabbit radial critical size defects].," *Zhongguo Xiu Fu Chong Jian Wai Ke Za Zhi*, vol. 24, no. 4, pp. 465–71, Apr. 2010.
- [122] S. Oka, T. Matsumoto, S. Kubo, T. Matsushita, H. Sasaki, Y. Nishizawa, T. Matsuzaki, T. Saito, K. Nishida, Y. Tabata, M. Kurosaka, and R. Kuroda, "Local administration of low-dose simvastatin-conjugated gelatin hydrogel for tendon-bone healing in anterior cruciate ligament reconstruction.,"

Tissue Eng. Part A, vol. 19, no. 9–10, pp. 1233–43, May 2013.

- [123] M. Nyan, T. Miyahara, K. Noritake, J. Hao, R. Rodriguez, S. Kuroda, and S. Kasugai, “Molecular and tissue responses in the healing of rat calvarial defects after local application of simvastatin combined with alpha tricalcium phosphate.,” *J. Biomed. Mater. Res. B. Appl. Biomater.*, vol. 93, no. 1, pp. 65–73, Apr. 2010.
- [124] H. Rojbani, M. Nyan, K. Ohya, and S. Kasugai, “Evaluation of the osteoconductivity of α -tricalcium phosphate, β -tricalcium phosphate, and hydroxyapatite combined with or without simvastatin in rat calvarial defect,” *J. Biomed. Mater. Res. Part A*, vol. 98A, no. 4, pp. 488–498, Sep. 2011.
- [125] X. Huang, Z. Huang, and W. Li, “Highly efficient release of simvastatin from simvastatin-loaded calcium sulphate scaffolds enhances segmental bone regeneration in rabbits,” *Mol. Med. Rep.*, vol. 9, no. 6, pp. 2152–8, Apr. 2014.

Chapter 3

Design of calcium phosphate scaffolds with controlled simvastatin release by plasma polymerization



Abstract

Calcium Phosphates (CaPs) have excellent bone regeneration capacity, and their combination with specific drugs is of interest because it allows adding new functionalities. In CaPs, drug release is mainly driven by diffusion, which is strongly affected by the porosity of the matrix and the drug-material interaction. Therefore, it is very difficult to tune their drug release properties beyond their intrinsic properties. Furthermore, when the CaPs are designed as scaffolds, the increased complexity of the macrostructure further complicates the issue.

In this chapter we investigate the use of biocompatible plasma-polymers to provide a tool to control drug release from drug-loaded CaP scaffolds with complex surfaces and intricate 3D structure. Two different CaPs were selected displaying great differences in microstructure: low-temperature CaPs (Calcium-deficient hydroxyapatite cements, CDHA) and sintered CaP ceramics (β -Tricalcium Phosphate, β -TCP). The deposition of PCL-co-PEG (1:4) copolymers on CaPs was achieved by a low pressure plasma process, which allowed coating the inner regions of the scaffolds up to a certain depth. The coating covered the micro and nanopores of the CaPs surface and produced complex geometries presenting a nano and micro rough morphology which lead to low wettability despite the hydrophilicity of the copolymer. Plasma coating with PCL-co-PEG on scaffolds loaded with Simvastatin acid (potentially osteogenic and angiogenic) allowed delaying and modulating the drug release from the bone scaffolds depending on the thickness of the layer deposited, which, in turn depends on the initial specific surface area of the CaP.

Introduction

Calcium Phosphates (CaP) are excellent candidates in bone replacement due to their similarity to the mineral phase of bone and potential resorbability [1, 2]. Their combination with different types of drugs allows providing them with additional functionalities, in addition to their excellent osteoconductivity and osteogenicity. However, in CaPs a part of the loaded drug often remains trapped in the matrix [3, 4]. This could be partly solved by introduction of macroporosity to the material, by production of different kinds of scaffolds [5, 6]. In any case – both in bulk materials as in scaffolds - the performance of these ceramic matrices as drug delivery systems is tightly linked to their inherent porosity and pore size distribution features, which is dependent on the fabrication method followed [3]. Thus,

whereas biomimetic calcium phosphate cements exhibit a high porosity, ranging from the nanometric to the micrometric scale, the porosity in sintered CaP ceramics tends to be micrometric in size.

Thus, a common problem is that drug release cannot be tuned beyond their intrinsic capacity, which is related with their porosity. Therein, adapting the release profile to specific pathologies requiring a certain rate of delivery poses a problem. Coating of the material's surface could be a solution. However, once the ceramic matrices are loaded with drugs, coating by conventional wet methods can lead to loss of drug from the material to the coating media.

In those cases, a promising novel approach to tune the drug release kinetics can be found in low temperature plasma technologies. Low temperature plasma, herein plasma, can be defined as a particular state of a gas or mixture of gases containing a mixture of ions, free radicals, electrons, excited molecules, UV and visible radiation that preserves electrical neutrality. This reactive medium can modify the first nanometers of the surface of the material without altering its bulk properties. Roughly, the three main effects of plasmas on the surface of a material are: i) functionalization or grafting (covalent bonding of new chemical species); ii) etching (removal of surface material); and iii) thin film deposition (deposition of thin layers).

These effects may be employed to tailor drug release; Recent works [7,8] have shown that surface functionalization of polyamide 6.6 fibers can improve the amount of anti-inflammatories and lipolitic agents released due to improved interaction of the materials with the surrounding media.

Another approach which can be used to slow down the drug release profile is by creation of thin films by plasma polymerisation on the surface of the materials, acting as barrier for its release. Coating by plasma polymerization refers to the deposition of polymer films due to the excitation of an organic monomer in the gas state and subsequent deposition and polymerization of the excited species on the surface of a substrate [9].

Few works have investigated plasma polymerization to produce an overlayer to control the release kinetics of drugs placed on the surface of solid carrier surfaces. Vasilev et al. have coated Vancomycin contained in nanoporous anodic aluminium oxide with allylamine plasma layers [10]. In another work, quartz surfaces were employed as supports for a first n-heptylamine plasma polymer layer, to allow suitable wettability of Levofloxacin which was subsequently coated with a second n-heptylamine layer [11]. Similarly, quartz surfaces were

employed as supports for model dye molecules (Methylene Blue) or anticancer agents (Cisplatin) and were plasma coated with multilayered biodegradable Poly caprolactone-co-polyethyleneglycol (PCL-co-PEG) coatings [12]. Both authors have shown that by gradually increasing the barrier layer thickness with plasma polymerization deposition time, the amount of drug released diminished. In all cases, simple model surfaces have been employed.

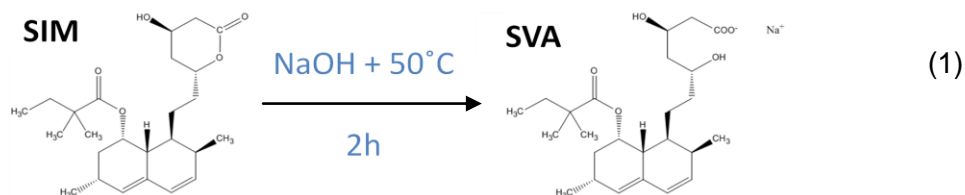
However, coating of complex surfaces in 3D scaffold structures and being able to fine tune drug release from them is far from being obvious. Therefore, it is the main aim of this chapter to show the potential of plasma polymerization in drug modulation from complex ceramic scaffolds for bone regenerative applications. These scaffolds were obtained by foaming of a calcium phosphate cement, and contained different levels of micro and nanoporosity, depending on the subsequent treatment applied, namely low-temperature setting to yield Calcium Deficient Hydroxyapatite (CDHA) or high-temperature sintering to produce β -Tricalcium Phosphate (β -TCP). Given the great differences on the surface texture of both ceramic materials, in the first stage, we investigated the deposition of biocompatible PCL-co-PEG polymer layers on 2D discs. Subsequently, the level of complexity was increased introducing 3D scaffolds, and the coating of the surface and the penetration of the plasma-polymers within the scaffolds was ascertained. To evaluate the possibilities of these layers on drug release, Simvastatin acid (SVA), was incorporated to the CaP scaffolds. In local drug delivery to the bone site from CaPs, different drugs are of interest [3]. SVA has shown potential action on bone and blood vessel formation [13-14], which is of clear interest in views of improving bone healing. Thus, to tailor the SVA release from the scaffolds plasma polymerisation of a biocompatible and biodegradable copolymer of PCL-co-PEG was evaluated as barrier layer in different conditions, and its potential effect on modulating the drug release kinetics was assessed.

Experimental

Materials

ϵ -Caprolactone (ϵ -CL, Purity: 97%, MW: 114, Empirical formula: $C_6H_{10}O_2$), and the cyclic ester monomer Diethylene glycol dimethyl ether (DEGME, Purity: 99.5%, MW: 134.17, linear formula: $(CH_3OCH_2CH_2)_2O$) were purchased from Sigma Aldrich, France and used in this study without further purifications. Simvastatin ($\geq 97\%$, MW: 418.57, Sigma-Aldrich) was used as the precursor of Simvastatin acid (SVA) (1), which was prepared according to [15].

α -TCP was used as starting material for the preparation of the powder phase of the cement, and was obtained by heating in a furnace (Hobersal CNR-58) in air, an appropriate mixture of calcium hydrogen phosphate (CaHPO_4 , Sigma Aldrich) and calcium carbonate (CaCO_3 , Sigma-Aldrich) at 1400°C for 15 h followed by quenching in air. α -TCP powder was milled in an agate ball mill (Pulverisette 6, Fritsch GmbH) with 10 balls ($d=30\text{mm}$) for 15 min at 450 rpm and blended with 2%wt of precipitated hydroxyapatite (PHA) (HA; BP-E341, Merck, Germany), which was added as a seed. The liquid phase employed in the preparation of cements consisted of a 2.5% solution of Na_2HPO_4 (Panreac) in MilliQ water, while the liquid phase used to prepare scaffolds was a solution of 1 wt% of Polysorbate 80, herein Tween80 (Polysorbate 80, Sigma Aldrich, USA) in distilled water. 10 wt% Pluronic F-127 (Sigma Aldrich, USA) was blended with the solid phase in the preparation of the scaffolds.



Preparation of low temperature and sintered CaP ceramic discs and scaffolds

CaP discs were used for the characterization of the polymer layer obtained. In the first place, CaP cements were prepared with a liquid-to-powder (L/P) ratio of 0.35 mL/g. The powder phase was mixed with the liquid phase in a mortar for about 1 min and then transferred into disc moulds of 2 x 15 mm. Samples were allowed to set in Ringer's solution (0.9 % NaCl) for 7 days to obtain Calcium-Deficient Hydroxyapatite (CDHA) discs.

To obtain β -Tricalcium Phosphate (β -TCP) ceramic discs, the CDHA samples were sintered in an oven (Hobersal), in air, by heating for 2.5 h up to 400°C , and then for 2.20h up to 110°C where samples were maintained for 9 h. Cooling was achieved naturally.

Calcium phosphate scaffolds were prepared by foaming, using a L/P ratio of 0.55 mL/g. The powder phase was a mixture of α -TCP containing 2 wt% of PHA and 10 wt% Pluronic F-127. The liquid phase was a solution of 1%wt of Tween80 in water. The foams were injected into moulds (6 mm diameter x 12 mm height) and allowed to set as described. To obtain β -TCP scaffolds, the CDHA scaffolds were sintered applying the same protocol used for the β -TCP ceramic discs.

Methods

Plasma polymerization of PCL-co-PEG coatings

PCL-co-PEG coatings were fabricated in a low pressure inductively excited radio frequency-tubular quartz plasma reactor system (5 cm diameter, 40 cm length, base pressure of 3×10^{-2} mbar). The schematics of plasma deposition setup and technical details of the process have been provided in earlier works [12, 16 - 17]. Briefly, the partial pressure ratio of the two monomers fed in the reactor was controlled by the flow rate of carrier gas (i.e. Ar, Air liquide, France), which was regulated and measured by electronic mass flow controllers (MKS instruments). The partial pressure in the reactor of ϵ -CL and DEGME exhibited linear correlations with the flow rate of argon gas and were comparable with each other [12]. Plasma co-polymerization of organic monomers was carried out on CDHA and β -TCP discs for the preliminary study on the layer characteristics, as well as on SVA-loaded macroporous CDHA and β -TCP scaffolds. For the current study, the total flow rate was varied from 20 to 25 standard cubic centimeter per minute (SCCM) by keeping the operating pressure constant at 0.5 mbar. Two operating modes were investigated to deposit the plasma coatings: Continuous Wave (CW) or Pulse Wave (PW).

Copolymer coatings were deposited at 20W CW plasma for 20 min or 90 min followed by deposition of a copolymer at 1W PW plasma for 5 min to improve the surface wettability. The pulsed plasma discharge coatings were performed for 20 min, the peak power (Ppk) was 25W and the duty cycle ($DC = (t_{on} / (t_{on} + t_{off}))$, where t_{on} and t_{off} were the 'plasma ON' and 'plasma OFF' times respectively) was 4% to obtain the effective plasma power (Peff) which was 1W PW ($t_{on} = 4$ ms and $t_{off} = 96$ ms). After polymer deposition, the reactor was again evacuated to base pressure before the plasma polymerization system was vented to atmospheric pressure with air.

Characterization of Plasma Polymerized Coatings

X-ray Photoelectron Spectroscopy

The chemical composition was analyzed by XPS with a SPECS (Germany) using an Al non monochromatic source XR50 (200W and 14 kV) with an analyzer Phoibos 150 MCD-9 with pass energy of 25eV, high resolution steps of 0.1eV, chamber pressure of $5 \cdot 10^{-9}$ mbar and using a Flood gun FG15/40. Peak deconvolution was performed with CasaXPS software.

Surface Wettability Measurements

Sessile drop contact angle values were measured using a video capture apparatus (Digidrop GBX-3S system, France). For each measurement, 6 μL of DI water droplets were dispensed onto the coated surfaces. Four measurements were carried out on each coating and resulting values were averaged.

Scanning Electron Microscopy

Surface topography of CDHA and β -TCP discs was studied by Field-Emission Scanning Electron Microscopy using a Jeol JSM-5000/5610 SEM. Samples were Pd-Pt-coated before SEM observation. Observations were carried out at 10 kV working voltage.

Focus Ion Beam

To ascertain the thickness of the plasma polymer layer deposited on the CDHA and β -TCP surface, Focus Ion Beam tomography (FIB, Zeiss Neon40) was performed. A 30 x 30 x 25 μm parallelepiped was coated with Pt, cut in slices and FE-SEM pictures were taken.

BET

The Specific Surface Area (SSA) of the CaPs was measured by Nitrogen adsorption according to the Brunauer-Emmet-Teller (BET) method, (BET) in an ASAP 2020 (Micromeritics).

Mercury intrusion porosimetry

Mercury Intrusion Porosimetry (MIP, AutoPore IV, Micromeritics, USA) was performed to determine the porosity and pore entrance size distribution within the materials.

Drug incorporation

CaP scaffolds were loaded with SVA by immersion in 200 μg SVA/ml solution (1 mL/cylinder) during 2 h in the case of CDHA or 24 h in the case of β -TCP to achieve equilibration maximum impregnation. The CaP scaffolds were subsequently freeze-dried.

Drug release experiments

CDHA and β -TCP scaffolds loaded with SVA and plasma-coated as described were immersed in 3 ml of Phosphate Buffer Saline (PBS, pH=7.4) at 37°C with continuous stirring. 350 μL of sample was withdrawn at different time points and replaced by 350 μL of fresh PBS.

The amount of drug released was obtained by measuring the release media collected at each time point by High performance liquid chromatography (HPLC) in a Shimadzu HPLC system. A mobile phase of Acetonitrile: 0.1% Phosphoric acid at a ratio of 50:50 (v/v), at a flow rate of 0.8 ml/min was passed through a C8 column (Shim-pack, Shimadzu). An injection volume of 10 μ l of the release sample was measured by photodiode array (PDA) at $\lambda_{\text{max}} = 238$ nm.

Results

Characterization of the plasma polymer layer

In this work two CaP materials were employed: CDHA obtained by low-temperature setting of a calcium phosphate cement, and β -TCP ceramic, obtained by sintering the former at high temperature. Both kinds of materials were subjected to low temperature plasma polymerization of a biocompatible and biodegradable copolymer mixture of PCL-co-PEG 1:4. As shown in Figure 3-1 a) and b) the microstructure of the two substrates was significantly different, just as the SSA, which was much higher for CDHA ($\text{SSA}_{\text{CDHA}} = 20\text{m}^2/\text{g}$) than for β -TCP ($\text{SSA}_{\beta\text{-TCP}} = 0.60\text{m}^2/\text{g}$). The scanning electron micrographs obtained on the surface of the materials (Figure 3-1) revealed the typical microporous structure of β -TCP with its sintering grains, while CDHA consisted of entangled platelet-like crystals derived from the dissolution-precipitation responsible for cement hardening.

In the first place it was of interest to characterize the plasma polymer layer deposited with CW discharge on the two materials at the longest time evaluated of 90 min.

FTIR measurements were performed on material obtained from the top surface of the CaPs. All materials tested display phosphate vibrations (Supplementary material 1), where the wide, strong bands correspond to ν_3 stretching ($944\text{--}1122\text{ cm}^{-1}$) and ν_4 bending ($545\text{--}640\text{ cm}^{-1}$) typical of calcium phosphates or apatites [18, 19]. On the plasma coated materials, β -TCP-90CW and CDHA-90CW, different bands indicated the presence of the coating, which were more evident in β -TCP-90CW. In particular, bands were recorded at 1716 cm^{-1} , which were attributed to the C=O stretching vibrations of the ester carbonyl group from PCL; C-H stretching bonds were centered at 2950 and 2870 cm^{-1} . The C-H bending was observed at 1380 and 1460 cm^{-1} . The weak absorption band at 3430 cm^{-1} was assigned to terminal -OH groups in the coatings which indicated the presence of polar groups incorporated into the

copolymer structures [12], as -OH groups from hydroxyapatite usually appear at higher bending energies 3567 cm^{-1} [20].

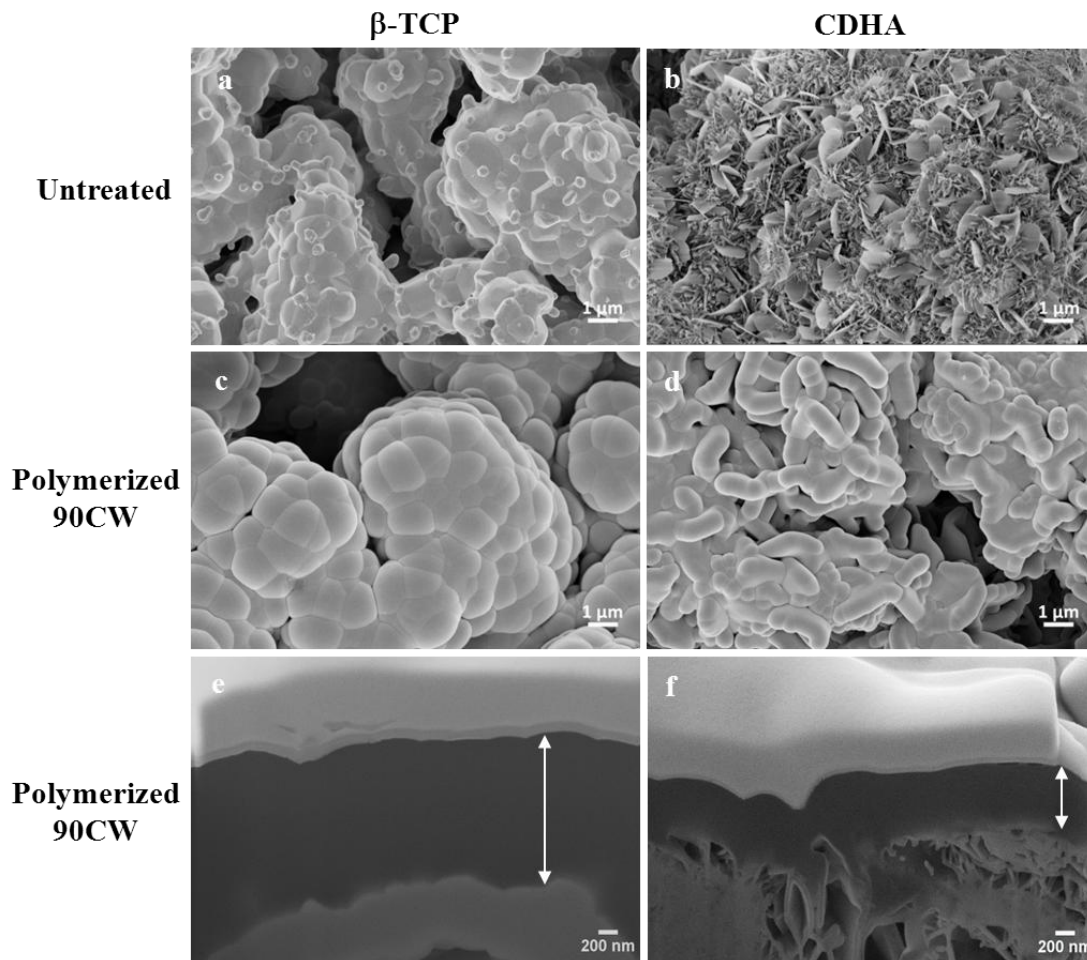


Figure 3-1 SEM images of the different materials before (top images) and after plasma polymerization with PCL-PEG (4:1). β -TCP (a), CDHA (b), β -TCP-90CW (c), and CDHA-90CW (d). FIB-SEM cross-section of the surface of both polymerized materials β -TCP-90CW (e) and CDHA-90CW (f).

Modifications on the surface energy and surface chemistry were recorded by means of static contact angle and XPS measurements, respectively (Table 3-1). Both untreated materials were very hydrophilic and due to their inherent porosity absorbed water very fast, not allowing contact angle measurement. However, after plasma polymerization water was no longer absorbed and the contact angle rose to hydrophobic values above 110° in both materials, showing the highest values for β -TCP-90CW.

The surface chemistry of the untreated CaPs as measured by XPS correlated adequately with their nominal composition. The polymerization treatment with PCL-co-PEG led to a decrease in the O/C ratio, showing the presence of polymer on the surface. The layer deposited in the case of β -TCP-90CW was thicker than the detection limit of the XPS (10 nm), as Ca and P species were no longer detected by the technique. In the case of CDHA-90CW both Ca and P were detected but in very small quantities which could indicate that the CDHA is not completely covered by the plasma polymer. However, such low values measured can be also ascribed to background noise, so these particular Ca and P values presented in Table 3-1 should be taken with precaution.

Table 3-1 Static contact angle and X-ray photoelectron spectroscopy (atomic concentration and atomic ratio) of the different CaP discs either untreated or after plasma polymerization.

	θ_s (°)	Atomic concentration %				Atomic ratio	
		C1s	O1s	Ca2p	P2p	O/C	Ca/P
β -TCP	*	14.83	53.61	19.54	11.98	3.61	1.63
β -TCP-90CW	121 ± 2	76.99	23.01	--	--	0.29	--
CDHA	*	10.51	57.81	19.05	12.62	5.50	1.51
CDHA-90CW	115 ± 1	76.09	23.75	0.12**	0.04**	0.30	--**

*Not possible to measure contact angle due to too fast water absorption.

** Too small quantities to be taken with precaution.

Decomposition of C1s core level spectra of the plasma polymerized samples (Table 3-2, Figure 3-2) showed a profile clearly including 3 peaks corresponding to: C-C and/or C-H 285.00 eV, which were the most abundant groups, followed by C-O at 286.63 eV (in ether groups) and C=O 288.63 eV (probably carboxylic/ester groups). The presence of these bonds reflected the presence of the copolymer PCL: PEG 1:4. The contribution of the C=O peaks was slightly lower in β -TCP than in CDHA, in both cases up to around 6%.

Table 3-2 C1s peak deconvolution.

	Atomic percentage		
	C1s		
	285.00 eV	286.63 eV	288.64 eV
	C-C,C-H	C-O	C=O
β -TCP-90CW	55.7	37.9	6.4
CDHA-90CW	51.5	42.4	6.1

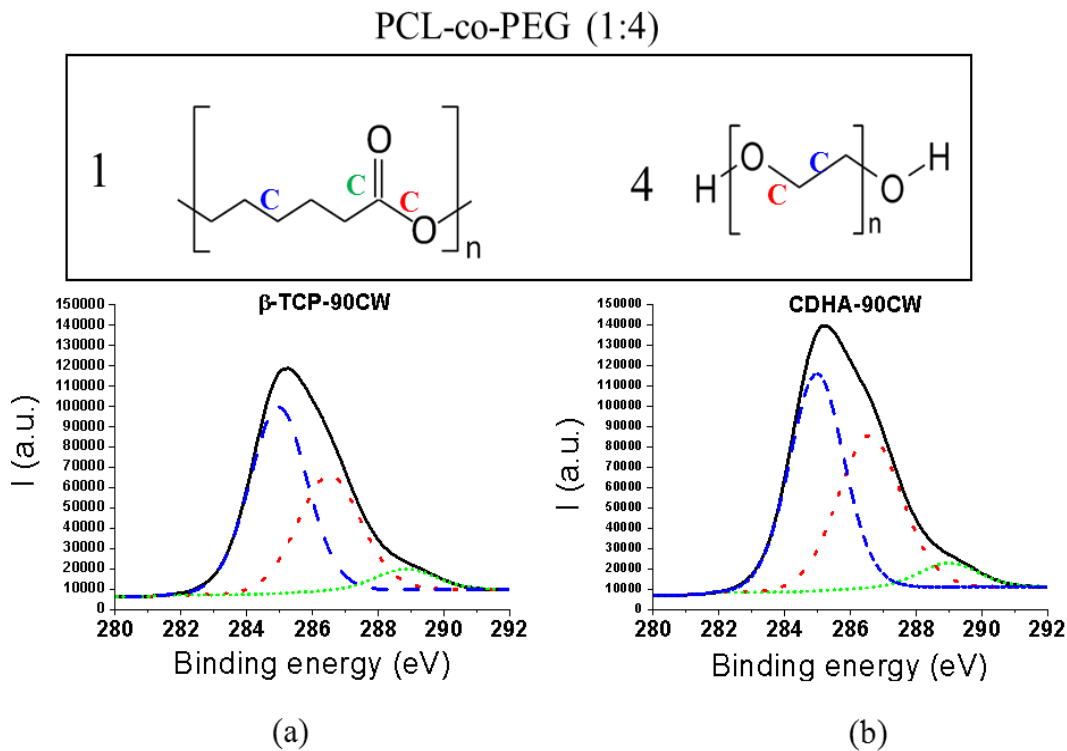


Figure 3-2 X-ray Photoelectron Spectroscopy C1s peak deconvolution, of (a) β -TCP and (b) CDHA with PCL-co-PEG (1:4) plasma coating 90CW.

As displayed in the SEM images (Figure 3-1), after plasma polymerization with PCL-co-PEG the structure of the CaPs was covered by a layer following the original patterns of the materials, forming bush-like structures on β -TCP-90CW and worm-like structures for CDHA-90CW.

Transversal sections obtained by FIB revealed that, as anticipated by XPS measurements, the plasma polymer deposited on β -TCP-90CW was thicker (1496 ± 162 nm) than that deposited on CDHA-90CW (628 ± 61 nm), in the same experimental conditions.

Once demonstrated that it was possible to produce PCL-co-PEG coatings on the surface of flat CDHA and β -TCP discs, the possibility to obtain polymer layers on the surface of 3D macroporous samples, herein designated as CaP scaffolds, was assessed. As shown in the transversal section of a CaP scaffold (Figure 3-3 left), both β -TCP and CDHA scaffolds contained macropores of 80 μ m of pore entrance size (Figure 3-4), with a smaller volume of pores around 2 μ m corresponding to the distance between sintering necks / crystal aggregates.

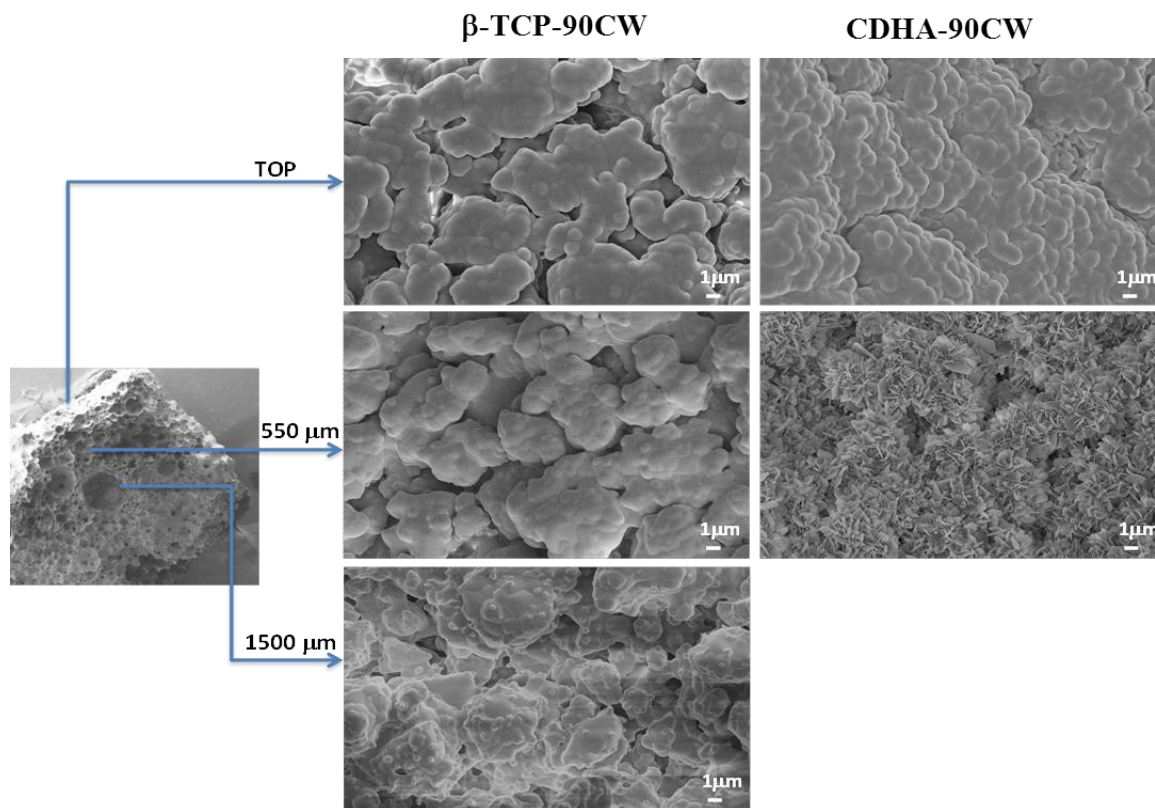


Figure 3-3 Scanning electron micrographs of transversal sections of β -TCP and CDHA scaffolds after 90 min CW plasma polymerization at different depths. Views of the surface of pores found on the top surface layer (top image), at a depth of 550 μ m, and at 1500 μ m (lower image).

The plateau at the nanoscale range is only present in CDHA scaffolds and corresponds to intercrystal distance. The total porosity was of 81.5% for β -TCP and of 82.2% for CDHA. Plasma polymerization for 90CW min showed the same bush-like and worm-like structures in the pores located at the top surface of the samples (Figure 3-3, right). In addition, it was observed that for β -TCP, the plasma process evaluated here was capable of depositing PCL-co-PEG coatings up to a depth of 550 μ m by diffusion through the interconnected macropores of the material. This was not visible for CDHA samples, where the coating was restricted to the outer surface.

Drug loading and release

CaP Scaffolds were drug-loaded by immersion in a solution containing SVA. SVA showed high affinity for CDHA as high loadings of 168 μ g/scaffold were obtained in only two hours

(Table 3-3), which accounts for $84 \pm 6\%$ loading efficiency. As β -TCP scaffolds displayed lower affinity they were allowed 24 h to equilibrate in the SVA solutions. Anyhow, the loading efficiency was much lower ($9 \pm 2\%$) so the quantity of drug loaded in β -TCP was of $18.78 \mu\text{g}$.

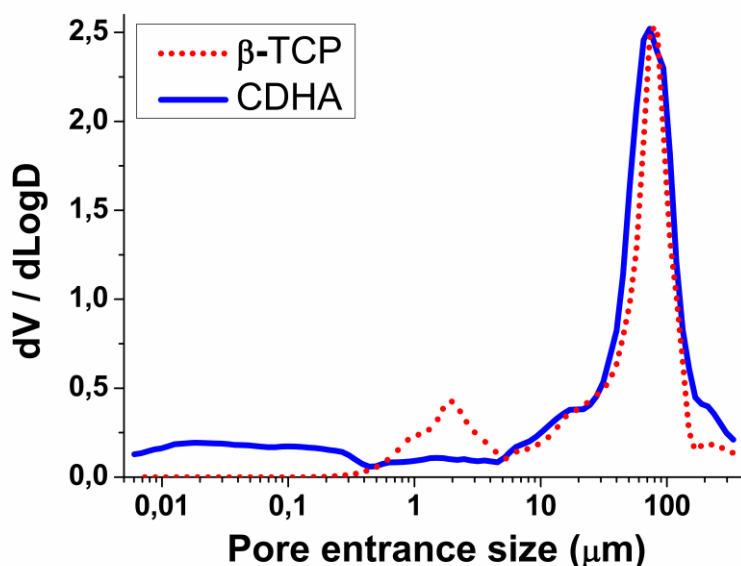


Figure 3-4 Pore entrance size distribution of β -TCP and CDHA obtained by Mercury Intrusion Porosimetry.

Table 3-3 Simvastatin acid loaded and final amount released (11 days) from CDHA and β -TCP scaffolds with different plasma polymerization times.

Samples	$Q_{\text{loaded}} (\mu\text{g})$	$Q_{\text{released}} (\mu\text{g})$
β -TCP-SVA	18.8 ± 3.7	18.4 ± 0.4
β -TCP-SVA-20CW	18.8 ± 3.7	0.0 ± 0.0
β -TCP-SVA-90CW	18.8 ± 3.7	0.1 ± 0.1
β -TCP-SVA-20PW	18.8 ± 3.7	1.3 ± 0.1
CDHA-SVA	168.1 ± 12.9	27.6 ± 11.7
CDHA-SVA-20CW	168.1 ± 12.9	2.5 ± 2.5
CDHA-SVA-90CW	168.1 ± 12.9	4.7 ± 0.7
CDHA-SVA-20PW	168.1 ± 12.9	2.6 ± 2.6

The drug release pattern for the SVA-loaded β -TCP and CDHA either untreated or after 90 min of CW plasma coating is shown in Figure 3-5. Despite these loading differences, the amount of drug released was very similar between the untreated β -TCP and CDHA scaffolds. Over nearly 2 weeks (284 h) both untreated materials showed a progressive release, while the coated samples displayed different behavior: β -TCP-SVA-90CW did not show any drug release along 2 weeks of experiment, while in the case of CDHA release was initially blocked, delayed for the first 2 h, and release progressed slowly afterwards.

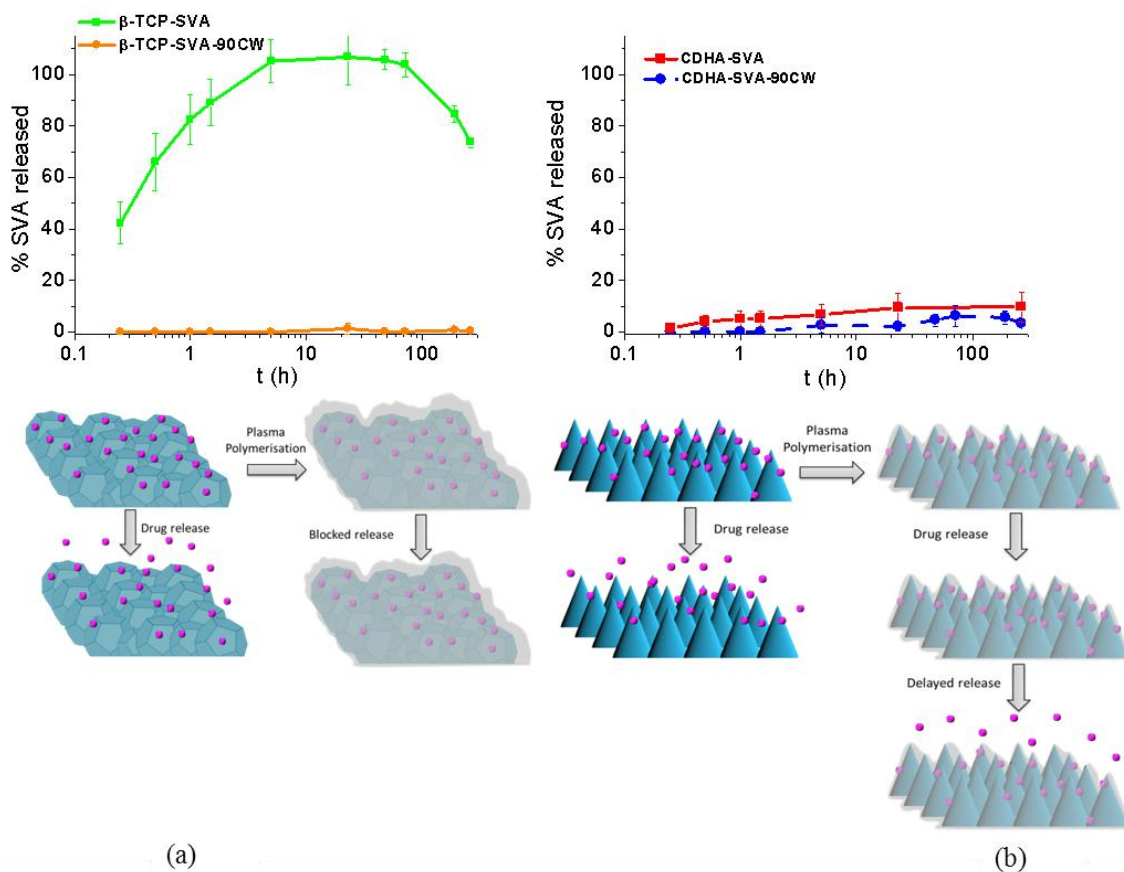


Figure 3-5 Cumulative release of SVA in (%) from β -TCP (a) or CDHA (b) scaffolds either untreated or after 90 min coating in continuous wave mode with hypothesis on the possible phenomena taking place (below).

Once it was established that the plasma coatings were effective in blocking drug release, shorter treatment times and pulsed mode depositions were evaluated. All conditions evaluated completely blocked SVA release from β -TCP scaffolds. On the contrary, CDHA scaffolds coated with shorter

polymerization times of 20 min in continuous wave mode (Figure 3-6 a) displayed controlled release properties over the course of the experiment. Plasma polymers produced in pulsed wave mode showed to be more efficiently blocking the surface in 20 min than CW polymers (Figure 3-6 b), as release was delayed for 5 h and progressed slowly afterwards.

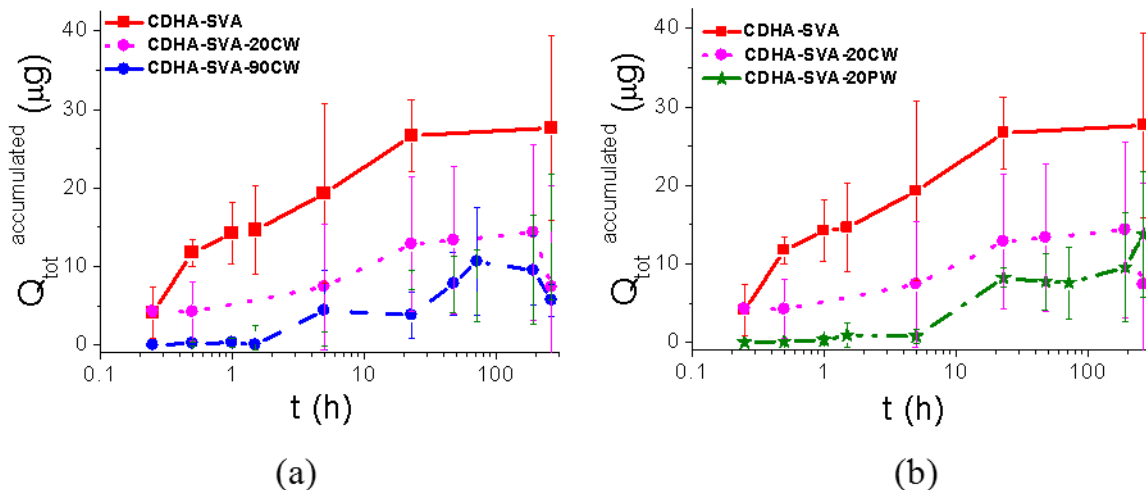


Figure 3-6 Release pattern for SVA from CDHA scaffolds at (a) different treatment times with continuous wave mode (CW) or (b) different power supply mode being either continuous (CW) or pulsed (PW).

Discussion

To overcome the intrinsic limitations of CaPs to regulate drug release, this paper focuses on the use of biocompatible plasma-polymers to provide a tool to control drug release from drug-loaded CaP scaffolds with very complex surfaces and intricate 3D structures. One advantage of using a dry method such as plasma lies in avoiding, for instance, any ion dissolution of the calcium phosphates and thus conserving intact their initial properties. If the material has already been loaded with drugs, coating them is a complicated issue, as any contact with processing solutions would lead to dissolution/diffusion of the drugs and thus loss active principle from the biomaterial.

In this work, it has been shown that plasma polymers (PCL-co-PEG) can be deposited on the surface of CaP cements and ceramics with very different surface features. As shown by the IR spectra (Figure 3-1), the bands corresponding to C-H, C-O and OH confirm the formation of a polymer layer on the surface of the ceramics. The thickness of this polymer layer is variable depending on the material used, i.e. β -TCP ceramics or CDHA cements

which have different morphologies and specific surface area (SSA). This was confirmed both by XPS (Table 3-1), in which the Ca and P species were not detected – or hardly - after the CW plasma polymerization treatment for 90 min, and also by SEM-FIB (Figure 3-2), which allowed measuring the thickness of the layers. Thus, β -TCP showed a layer which was two times thicker than the one deposited on CDHA in the same conditions. This can be attributed to the great differences in SSA between both materials (CDHA has 33 times higher SSA than β -TCP), which is related to their structure, consisting in CDHA platelet-like crystals in one case, and flat porous structures typical of sintered materials in β -TCP. The thickness of the layer obtained by CW plasma discharge for 90 min was much larger than that recorded in previous works [12], mainly due to the longer treatment times employed. The thickness of the coating (1.49 ± 0.16 and 0.63 ± 0.06 μm on β -TCP and CDHA respectively) led to important changes in the surface topography of the CaP materials, leading to the formation of bush or worm-like structures. This change in surface morphology, together with the change in the chemical nature of the surface is expected to result in significant changes in the in vitro and in vivo biological performance of the material [9], which will have to be further investigated.

The chemical structure of β -TCP and CDHA is $\text{Ca}_3(\text{PO}_4)_2$, and $\text{Ca}_9(\text{HPO}_4)(\text{PO}_4)_5(\text{OH})_2$ respectively, with a theoretical Ca/P ratio of 1.5 for both compounds [21]. None of the materials itself contains carbon, so its presence on the surface of the samples (Table 3-1) indicates an alteration of the surface chemistry, which could be ascribed to contamination by adsorbed hydrocarbons. The PCL-co- PEG 1:4 plasma coatings (90 CW) deposited on the surface had a 0.3 O/C ratio in both β -TCP and CDHA, which was close to that of Bhatt et al. [102] (0.36 O/C), who employed different deposition conditions (mainly treatment time and substrates employed) (Table 3-1). Moreover, the coatings led to a significant change in the wetting properties of the materials; both CaPs were initially hydrophilic, with fast water absorption through the pores of the materials. After plasma polymerization these relatively low O/C ratios, together with blocking of the surface porosity, raised the surface hydrophobicity of the materials, which displayed contact angles between 115° and 121° . The high roughness of the materials, generated in the growth of the plasma polymer on the intricate crystalline structures of the CaPs must also be related to these considerable differences in the wettability measurements.

In the second part of the work, 3D CaP scaffolds made of β -TCP or CDHA were studied. These are the macroporous counterparts of the β -TCP and CDHA evaluated in the first part

of the work, thus preserving their microstructure (Figure 3-1a and b) but with additional interconnected macroporosity (Figure 3-3 left). The advantage of introducing macroporosity to CaPs is envisaged as a method to facilitate bone ingrowth not only from the external surface but throughout the bulk of the material [22]. This would accelerate its resorption and transformation into newly formed bone tissue [23]. It has also been shown that macroporosity is relevant for drug delivery, as it allows improving fluid flow throughout the material [5].

In the 3D treatment of the macroporous CaP scaffolds it was shown here that the plasma polymer coating can be performed successfully on the materials, and that the interconnections between the macropores allow the penetration of the plasma polymer inside the scaffold (Figure 3-3). This is particularly evident in the case of β -TCP, where the characteristic bush-like structures can be observed both on the surface, and inside pores of the scaffold down to a depth of 550 μm (Figure 3-3). The higher SSA of CDHA was probably related to the fact that the coating layer was restricted to the top surface of the CaP scaffolds, and no penetration was observed by SEM, as possibly all available monomer was already consumed in the coating of the wider surface.

In the subsequent steps, the drug release of the plasma-coated scaffolds was evaluated. Simvastatin acid (SVA) was incorporated to the CaP scaffolds. Simvastatin is a commonly used cholesterol-lowering drug which has been shown to stimulate osteogenesis locally through an up-regulation of BMP-2 expression [24] and it has also been related to dose-dependent improved angiogenesis [25]. Enhancing blood vessel growth within the scaffolds is of interest with views on promoting scaffold resorption and bone regeneration.

The adsorption of SVA, which is a hydrophilic drug (eq. 1), was much favoured in CDHA scaffolds than in β -TCP (Table 3-3). This is reflected in drug loading of β -TCP being only 11% of that of CDHA – even after β -TCP samples allowed to equilibrate with the loading solution for 24 h in comparison to 2 h for CDHA scaffolds. As both kinds of scaffolds have very close porosity around 82%, this difference can probably be attributed to the higher SSA of CDHA but also to its different chemistry, which can probably allow for the creation of hydrogen bonds with SVA.

Drug release patterns were significantly modified by the PCL-co-PEG plasma coatings deposited (Figures 3-5 and 3-6). On the one hand, uncoated β -TCP scaffolds showed a continuous progressive release for the first 5 h where 98% of the initial drug loads was released. After 3 days the drug in the media started degrading (shown by a decrease of the

measured drug in the media) (Figure 3-5a). None of the β -TCP scaffolds plasma coated with the PCL-co-PEG in different conditions showed any SVA release in the evaluated timeframe of 11 days (Data not shown - Scheme shown in Figure 3-5a). This is indicative of the lack of diffusion of SVA through the thick plasma layer deposited on the β -TCP, shown to be much thicker than that of CDHA in the 90 CW coated samples. It is important to recall that the amount of SVA loaded into β -TCP is an order of magnitude lower than that of CDHA, so even thinner coatings of 20CW (Supplementary material 2) are able to block release from β -TCP.

In contrast, untreated CDHA scaffolds showed continuous release for more than 10 days, although the amount released was only around 16 % of the initial SVA loading (Figure 3-5b). The 90 CW PCL-co-PEG layer on the drug-loaded CDHA scaffolds was three times thinner than that of β -TCP. Initially (first 1.5h) it blocked SVA release and subsequently allowed its slow diffusion along the timeframe of the experiment. Shorter treatment times of 20 min (CDHA-SVA-20CW) presented the same profile (Figure 3-6a), and though release started from the beginning of the experiment, the rate of release was slowed down with respect to the untreated CDHA scaffolds. This is in agreement with a previous work, where Bhatt et al. [12] showed that by gradually increasing the barrier layer thickness with longer plasma deposition times, the amount of a dye released was reduced.

In parallel, the mode of deposition clearly affected the drug release, as only 20 min of treatment in pulsed mode (CDHA-SVA-20PW) were able to block the release for the initial 5 h, allowing afterwards for sustained release (Figure 3-6b). This is most probably related to a lower extent of monomer fragmentation achieved by pulsed discharges, with higher retention of ether functional groups [26, 27]. Plasma phase fragmentation plays an important role in determining the deposition rate and surface chemistry of the deposited film and depends on the kind of monomer [28].

The drug delivery matrices developed in this work constitute complex structures, which combine: i) a highly porous (macro, micro and nanoporous) non-degrading bulk [3] which was shown to release drugs (i.e. antibiotics) through complex mechanisms following non-Fickian diffusion [5] with ii) a biodegradable plasma polymer coating. The mechanisms involved in drug release from this kind of coatings on flat surfaces were shown to range from zero-order to non-Fickian diffusion as the coating thickness increased [12]. Thus, the drug release in the developed dosage forms is expected to be ruled by the coating until it is completely degraded, followed by diffusion from the CaP matrix afterwards.

Conclusions

This work has allowed demonstrating that it is possible to fine-tune drug release from 3D ceramic scaffolds (CDHA & β -TCP) with different and very complex surface textures by a dry plasma polymerization process by employing biocompatible plasma polymers, depending on the treatment conditions. The thickness and structure of the PCL-co-PEG (1:4) polymer layer obtained is highly dependent on the texture of the materials, in particular on its SSA. Thicknesses of up to 1.4 μm were obtained on β -TCP, and the plasma polymers were able to penetrate the macroporous structure of 3D calcium phosphate foams, up to a certain depth. The topography and chemistry of the materials were significantly modified by the coatings which led to nano-rough structures which could explain the low wettability measured on the materials.

Simvastatin acid (SVA) was incorporated to the calcium phosphate scaffolds of β -TCP and CDHA as osteogenic and angiogenic drug, and the plasma coatings were useful to modulate the drug release: thicker PCL-co-PEG layers acted as barriers on β -TCP foams impairing SVA release throughout the whole release experiment (11 days), while on CDHA the presence of thinner polymer layers – due to its much higher SSA - allowed for the diffusion of the drug, leading to progressive and controlled drug release with respect to the uncoated biomaterial. On CDHA, longer treatment times (90 min in continuous wave plasma discharges) implied initially blocking of release followed by a slow release pattern, while shorter times (20 min) allowed a slow, controlled release. Pulsed wave plasma discharges allowed efficiently depositing plasma polymer layers which could initially block the release, in shorter times (20 min). Thus, the plasma coatings evaluated have shown to be useful tools for the tuning of drug release from bone biomaterials, allowing to produce ceramic dosage forms combining delayed release, followed by controlled delivery of drugs.

REFERENCES

- [1] Ginebra M. P., Espanol M., Montufar E. B., Perez R. A., Mestres G., New processing approaches in calcium phosphate cements and their applications in regenerative medicine, *Acta Biomater.* 6 (8) (2010) 2863–2873.
- [2] LeGeros R. Z., Calcium phosphate-based osteoinductive materials, *Chem. Rev.*, 108 (11) (2008) 4742–4753.
- [3] Ginebra M.P., Canal C., Espanol M., Pastorino D., Montufar E. B., Calcium phosphate cements as drug delivery materials, *Adv. Drug Deliv. Rev.*, 64(12) (2012) 1090–1110.
- [4] Canal C., Pastorino D., Mestres G., Schuler P., Ginebra M.P. Relevance of microstructure for the early antibiotic release of fresh and pre-set calcium phosphate cements. *Acta Biomater.* 9 (2013) 8403–12.
- [5] Pastorino D., Canal C., Ginebra M.P., Drug delivery from injectable calcium phosphate foams by tailoring the macroporosity-drug interaction, *Acta Biomater.*, 12 (2015) 250–259.
- [6] Maazouz Y., Montufar E. B., Guillem-Marti J., Fleps I., Ohman C., Persson C., Ginebra M. P., Robocasting of biomimetic hydroxyapatite scaffolds using self-setting inks, *J. Mater. Chem. B*, 2 (2014) 5378-5386.
- [7] Labay C., Canal C., García-Celma M. J., Influence of Corona Plasma Treatment on Polypropylene and Polyamide 6.6 on the Release of a Model Drug, *Plasma Chem. Plasma Process.*, 30 (6) (2010) 885–896.
- [8] Labay C., Canal J. M., Canal C., Relevance of Surface Modification of Polyamide 6.6 Fibers by Air Plasma Treatment on the Release of Caffeine, *Plasma Process. Polym.*, 9(2) (2012) 165–173.
- [9] Szili E.J., Short R.D., Steele D.A., Bradley J.W., Surface modification of biomaterials by Plasma Polymerization, in: *Surface Modification of Biomaterials; Methods, Analysis and Applications*, First ed. Woodhead Publishing Limited, 2011, pp. 3–39.
- [10] Simovic S., Losic D., Vasilev K., Controlled drug release from porous materials by plasma polymer deposition, *Chem. Commun.*, 46(8) (2010) 1317–1319.
- [11] Vasilev K., Poulter N., Martinek P., Griesser H.J., Controlled release of levofloxacin sandwiched between two plasma polymerized layers on a solid carrier, *ACS Appl. Mater. Interfaces*, 3 (12) (2011) 4831–4836.
- [12] Bhatt S., Pulpytel J., Mirshahi M., Arefi-Khonsari F., Plasma co-polymerized nano coatings – As a biodegradable solid carrier for tunable drug delivery applications, *Polymer*, 54(18) (2013) 4820–4829.
- [13] Montazerolghaem M., Enqvist H., Karlson Ott M., Sustained release of simvastatin from premixed injectable calcium phosphate cement, *J. Biomed. Mater. Res. A*, 102 (2014) 304-307.
- [14] Yin H., Li Y.G., Si M., Li J.M., Simvastatin-loaded macroporous calcium phosphate cement: preparation, in vitro characterization, and evaluation of in vivo performance, *J. Biomed. Mater. Res. A*, 100 (2012) 2991–3000.
- [15] Kaesemeyer W.H., Caldwell R.B., Huang J., Caldwell R.W., Pravastatin sodium activates endothelial nitric oxide synthase independent of its cholesterol-lowering actions, *J. Am. Coll. Cardiol.*, 33(1) (1999) 234–241.
- [16] Bhatt S., Pulpytel J., Mirshahi M., Arefi-Khonsari F., Catalyst-Free Plasma-Assisted Copolymerization of Poly(ϵ -caprolactone)-poly(ethylene glycol) for Biomedical Applications, *ACS Macro Lett.*, 1(6) (2012) 764–767.
- [17] Bhatt S., Pulpytel J., Mirshahi M., Arefi-Khonsari F., Nano thick poly(ϵ -caprolactone)-poly(ethylene glycol) coatings developed by catalyst-free plasma assisted copolymerization process for biomedical applications, *RSC Adv.*, 2 (2012) 9114-9123.

- [18] Mestres G., Le Van C., Ginebra M.P., Silicon-stabilized α -tricalcium phosphate and its use in a calcium phosphate cement: characterization and cell response, *Acta Biomater.*, 8 (2012) 1169–1179.
- [19] Radin S. R., Ducheyne P., The effect of calcium phosphate ceramic composition and structure on in vitro behavior. II. Precipitation., *J. Biomed. Mater. Res.*, 27 (1993) 35–45.
- [20] Antonakos A., Liarokapis E., Leventouri T., Micro-Raman and FTIR studies of synthetic and natural apatites., *Biomaterials*, 28 (2007) 3043–3054.
- [21] Ginebra M.P., Fernandez E., De Maeyer E.A.P., Verbeeck R.M.H., Boltong M.G., Ginebra J., Driessens F.C.M., Planell J.A., Setting Reaction and Hardening of an Apatitic Calcium Phosphate Cement, *J. Dent. Res.*, 76 (1997) 905–912.
- [22] Montufar E.B., Traykova T., Gil C., Harr I., Almirall A., Aguirre A., Engel E., Planell J.A., Ginebra M.P., Foamed surfactant solution as a template for self-setting injectable hydroxyapatite scaffolds for bone regeneration, *Acta Biomater.*, 6 (2010) 876–885.
- [23] Karageorgiou V., Kaplan D., Porosity of 3D biomaterial scaffolds and osteogenesis, *Biomaterials*, 26 (2005) 5474–5491.
- [24] Mundy G., Stimulation of Bone Formation in Vitro and in Rodents by Statins, *Science*, 286(5446) (1999) 1946–1949.
- [25] Weis M., Statins Have Biphasic Effects on Angiogenesis, *Circulation*, 105 (2002) 739–745.
- [26] Buxadera-Palomero J., Canal C., Torrent-Camarero S., Garrido B., Gil F.J., Rodríguez D., Antifouling coatings for dental implants: Polyethylene glycol-like coatings on titanium by plasma polymerization, *Biointerphases*, 10(2) (2015) 029505.
- [27] Labay C., Canal J.M., Modic M., Cvelbar U., Quiles M., Armengol M., Arbos M.A., Gil F.J., Canal C., Antibiotic-loaded polypropylene surgical meshes with suitable biological behaviour by plasma functionalization and polymerization, *Biomaterials*, 71 (2015) 132–144.
- [28] Michelmore A., Gross-Kosche P., Al-Bataineh S.A., Whittle J.D., Short R.D., On the effect of monomer chemistry on growth mechanisms of nonfouling PEG-like plasma polymers, *Langmuir*, 29 (2013) 2595–2601.

Supplementary material 1

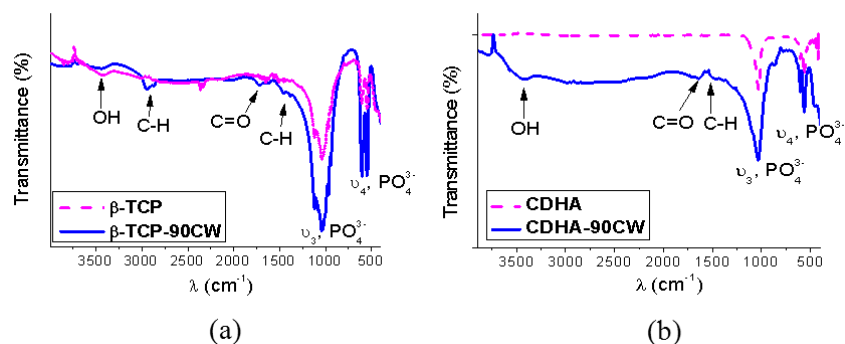


Figure 3-S1. IR-ATR spectra of the CaP materials without and with 90CW polymer layer (a) β -TCP and (b) CDHA.

Supplementary material 2

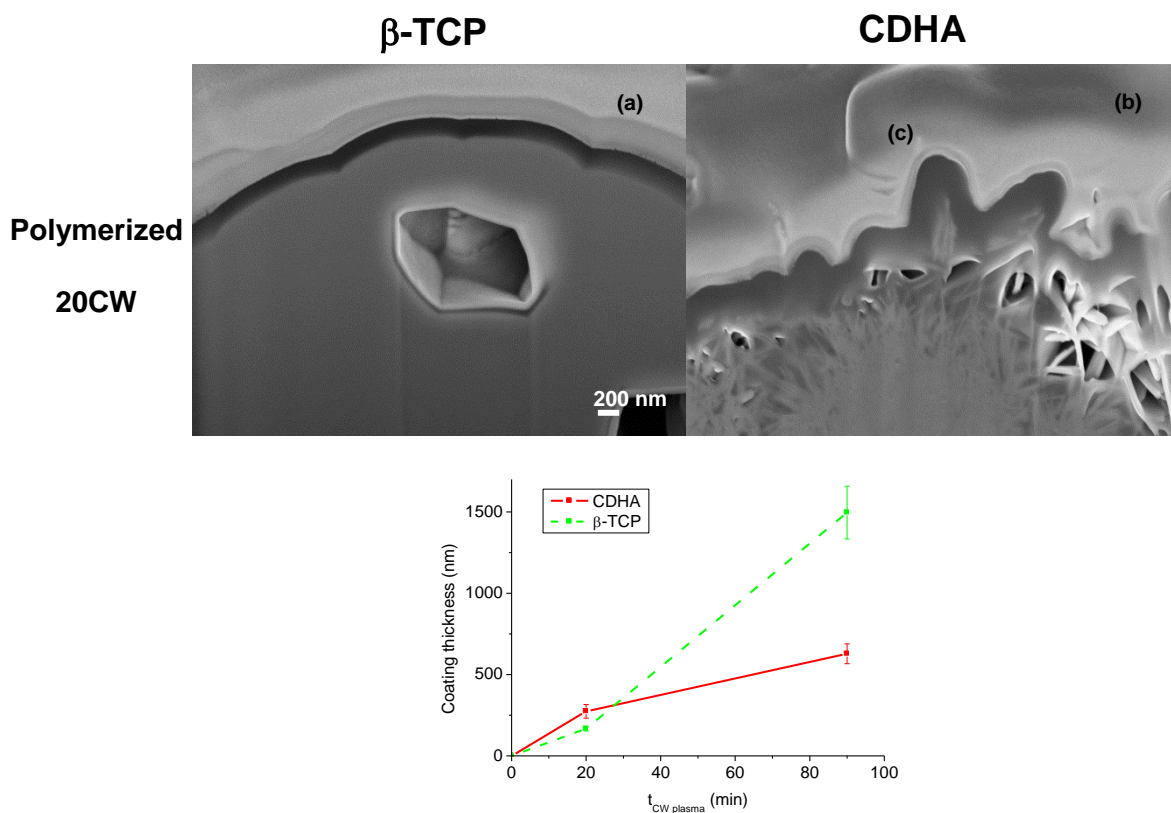
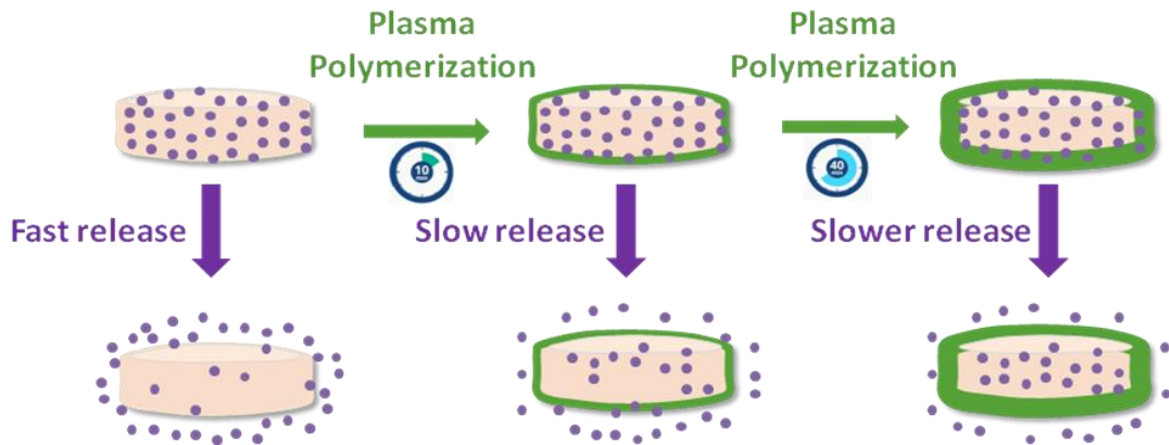


Figure 3-S2. FIB-SEM cross-section of the surface of both PCL-co-PEG (4:1) polymerized materials (a) β -TCP-20CW and (b) CDHA-20CW, and (c) evolution of the coating thickness in nm depending on the polymerization time.

Chapter 4

Effect of plasma polymerization coating of tricalcium phosphate ceramics on antibiotic delivery and biological performance



Abstract

One of the treatments for recurrent or complicated osteomyelitis is by local antibiotherapy mediated by suitable bone grafts. β -Tricalcium Phosphate (β -TCP) bioceramic is a resorbable osteogenic bone graft. Its microporosity allows for incorporation of drugs, but a too fast release is often obtained. Complex strategies have been explored to obtain controlled drug release. In this chapter, plasma polymerization of a biocompatible polymer was investigated on β -TCP. PEG-like polymer coatings of different thickness were deposited on microporous β -TCP loaded with antibiotics. A highly hydrophobic surface was obtained despite the hydrophilicity of the PEG-like layer, which was associated to the roughness of the β -TCP substrate. The bioceramics nevertheless retained their suitable biological behavior with regard to human osteoblast cells. The microbiological activity of the antibiotics was preserved, and the coatings reduced the total amount of drug released as a function of the increasing plasma treatment time.

Introduction

Osteomyelitis is a bone infection. It can spring from different causes: i) from spreading of bacteria originating from an infection elsewhere in the body, ii) through an open wound over a bone or iii) after the exposure of bone to bacteria during a surgery or an injection around a bone. The most usual treatments involve administration of antibiotics, but sometimes surgery may be necessary, and whenever bone is damaged it requires removal and replacement with a bone graft [1]. Systemic antibiotic regimes are used for four to eight weeks depending on the pathogenic bacteria and the response of the patient. But with long delays in diagnosis or treatment, significant bone damage, or if the initial treatment is not effective, patients are more prone to reoccurrence and the condition can become chronic and difficult to eradicate [2], [3].

The delivery and maintenance of therapeutic levels of antibiotic at the site of infection can be achieved by using implants or carriers that release antibiotics locally; these have significantly improved the treatment of osteomyelitis [4]. Many local antibiotic releasing systems have been developed in recent years, and several are available for clinical use, such as polymethylmethacrylate (PMMA) beads, collagen, apatite-wollastonite glass ceramic blocks, hydroxyapatite blocks, polylactide/polyglycolide implants, and polylactate polymers [3], [5]–[7]. Among these PMMA rosary beads impregnated with gentamicin have been often employed in the clinics, but they have several disadvantages, especially the

need to remove the foreign material surgically under general anesthesia [5], [6], [8]–[10].

An ideal local carrier should be biocompatible and biodegradable, and in applications requiring bone substitution, it should be resorbable and able to promote bone formation. Many calcium phosphates (CaPs) have been widely employed as bone grafts and many of them are in the market. Among them, β -Tricalcium Phosphate (β -TCP) is an interesting bioceramic obtained at high temperatures with higher solubility than i.e. Hydroxyapatite and that has been widely employed in reconstructive surgery [11] due to its resorbability and ability to promote new bone formation [12]–[14].

β -TCP has been evaluated as drug delivery system of different drugs. For example in the release of gentamicin, fast release was obtained in the first day and different strategies, more or less complex were evaluated to control this release [15]. Different works have relied in producing composite materials from β -TCP or other CaPs and biocompatible polymers (such as chitosan, gelatin, etc.) [16], [17], to improve different features of the material, among which to modulate drug release from the matrices. However, this approach usually involves complex processing stages. Plasma polymerization is a versatile technique for the deposition of films with functional properties suitable for a wide range of applications [18], [19]. Although plasma polymerization is a well-studied field, its application to bioceramics is rather recent. In a recent work, we proposed plasma polymerization of a hydrophilic PEG-like layer as a dry method allowing treating β -TCP and slowing down the release kinetics of an antibiotic [20]. However, the coatings produced by plasma polymerization led to very hydrophobic surfaces. This change in wettability could have a critical impact on the biological behavior of these bioceramics.

In this chapter, we aim at investigating in-depth the origins of this unexpected hydrophobicity, with a particular focus on its effects on biological behavior. Therein, β -TCP has been subjected to plasma polymerization to obtain PEG-like coatings, by using single and multi-step coatings, and the modified surfaces have been characterized. To ascertain the barrier effect of the coatings developed, the release of two different antibiotics (gentamicin and ampicillin) has been evaluated from these bioceramics, and their microbiological behavior has been studied after the plasma polymerization process undergone by the samples.

Experimental

Materials

Calcium hydrogen phosphate (CaHPO_4 , *Sigma-Aldrich* C7263) and calcium carbonate (CaCO_3 , *Sigma-Aldrich* C4830) were used as raw materials for the synthesis of β -Tricalcium Phosphate ($\beta\text{-Ca}_3(\text{PO}_4)_2$, $\beta\text{-TCP}$). Sodium phosphate dibasic (Na_2HPO_4 , *Sigma-Aldrich*) was used in solution as accelerant in the synthesis of calcium deficient hydroxyapatite (CDHA) used as a precursor of $\beta\text{-TCP}$. Ampicillin sodium salt (371.39 g/mol; 50mg/ml in water), and Gentamicin sulphate (477.6 g/mol, 50mg/ml in water) provided by Sigma-Aldrich were selected as antibiotics for loading $\beta\text{-TCP}$ ceramics (Figure 4-1).

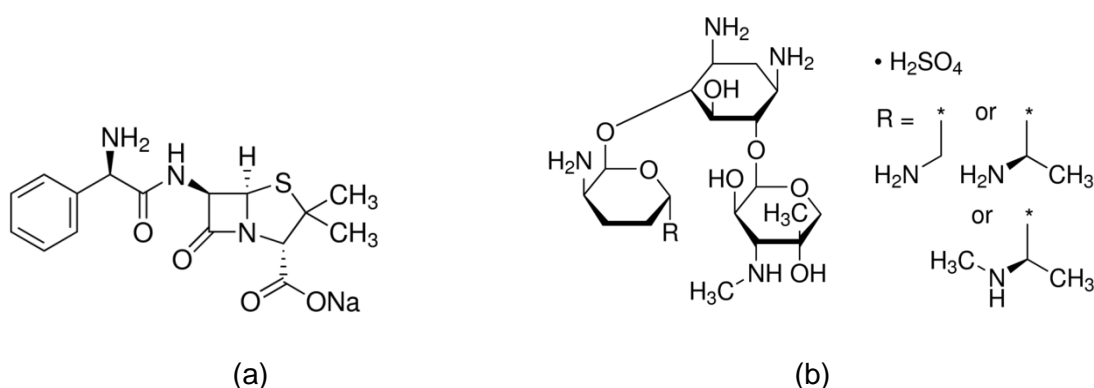


Figure 4-1 Chemical structure of ampicillin sodium salt (a) and gentamicin sulphate (b).

Diethylene glycol dimethyl ether (Diglyme, anhydrous, 99.5%, Sigma Aldrich) ($\text{CH}_3\text{OCH}_2\text{CH}_2$)₂O was used as precursor for plasma polymerization. Phosphate buffer saline (PBS), pH 7.4, was prepared from PBS Tablets (Gibco, LifetechnologiesTM, UK) and Milli-Q[®] deionized water. Agar bacteriological (Scharlau S.A., Spain) and Brain Heart Infusion Broth (BHI Broth) (Scharlau S.A., 02-599, Spain) were used to prepare the bacteriological culture media of *Staphylococcus aureus* (*S. aureus*), (Culture Collection University of Göteborg (CCUG 15915), Sweden).

$\beta\text{-TCP}$ synthesis

Microporous $\beta\text{-TCP}$ discs were obtained by thermal treatment of calcium deficient hydroxyapatite (CDHA), which was in turn obtained through the setting reaction of an α -

TCP calcium phosphate cement. α -TCP was obtained by solid state reaction of a 1:2 molar mixture of calcium hydrogen phosphate and calcium carbonate at 1400 °C. A cement was produced by blending α -TCP with a solution of sodium phosphate dibasic at 2.5% (w:w) at liquid to powder ratio of 0.65. The mixture was put in a disc-shaped mold and allowed to set immersed in water for 7 days to obtain CDHA, as described in [21]. The former discs were sintered at 1100 °C to obtain microporous β -TCP discs of 2 mm thickness \times 12 mm \varnothing . This allowed obtaining a 100% β -TCP material, according to DRX (not shown).

Plasma polymerization

Plasma polymerization of β -TCP discs was performed using low-pressure radio-frequency plasma (13.56 MHz) (Standard Femto Plasma System, Diener, Germany) with a cylindrical glass chamber. Diethylene glycol dimethyl ether (Diglyme, anhydrous, 99.5%, Sigma Aldrich) was used as source of ethylene oxide monomers to obtain a PEG-like coating on β -TCP [22]. Unloaded or antibiotic-loaded β -TCP discs were placed in the center of the reactor. To enhance the polymerization process a short surface activation step with O₂ (5.0 sccm, 0.40 mbar, 150 W) was performed for 60 s. The subsequent polymerization process consists in introducing Diglyme in the plasma reactor by bubbling a carrier gas (Ar) through the liquid monomer. The polymerization treatment performed in continuous mode (15 sccm, 1.70 mbar, 150 W) for 10 min is labeled as single polymerization (SP10). Repetition of the polymerization cycle in the same conditions described, without removing the samples from the reactor was named designed double (DP), triple (TP) or quadruple (QP) polymerizations were performed on each side of the β -TCP materials, and the corresponding samples were referenced as DP10, TP10 and QP10 respectively (Figure 4-2).

Surface topography

Topography of untreated and plasma polymerized β -TCP discs were studied by Scanning Electron Microscopy using a Zeiss Neon 40 cross-beam workstation with Gemini SEM column for sample observation. Samples were C-coated before SEM observation. Observations were carried out at 5.0 kV working voltage. Coupled-Energy-Dispersive X-ray spectroscopy (EDX) equipment (INCAPentaFETx3 detector, 30 mm², ATW2 window) was also used for *in situ* elemental analysis of the surface of a cross-section of plasma-polymerized β -TCP to determine the depth of the effects of plasma treatment on the surface of the bioceramic materials.

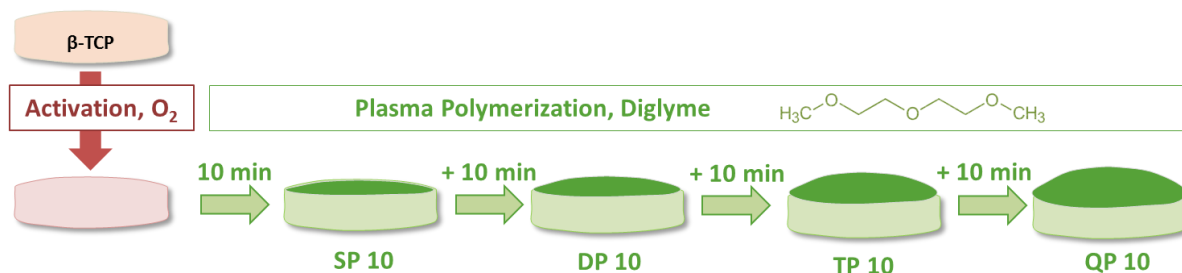


Figure 4-2 Scheme of the experimental layout employed to obtain PEG-like coatings on β -TCP discs. Low pressure plasma: 1st activation of the surface by O_2 plasma and 2nd plasma polymerization Ar as carrier with Diglyme monomer, with 10 min sequential treatments named as single polymerization (SP10), double polymerization (DP10), triple polymerization (TP10) and quadruple polymerization (QP10).

Wetting properties

Determination of the wettability of the β -TCP surfaces, to compare the untreated with the PEG-coated ceramics by plasma polymerization was done by static and dynamic contact angle measurements. A Contact Angle System OCA15 (*Dataphysics*, Germany) was used with the SCA20 Software (*Dataphysics*, Germany) to analyze the images acquired with a CCD. In static, 10 μ L water droplet were deposited on the β -TCP surface and in dynamic, volume changes continuously. Measurements were carried out on the plasma-polymerized side of the samples. In this study, a minimum of 5 replicates of each kind of treatment were carried out.

Dynamic contact angles were calculated as follows: Advancing contact angles were measured by increasing the volume of the water drop, until the contact angle remained constant. Receding contact angles were measured by decreasing the volume of the drop until the contact angle value remained constant and the solid/liquid interface started to decrease. Values reported result from the average of at least 6 replicates measured in independent samples.

The contact angle hysteresis was calculated as the difference between dynamic advancing and receding contact angles, according to eq. 1:

$$\Delta\theta = \theta_{adv} - \theta_{rec} \quad (\text{eq.1})$$

Chemical characterization

To determine the chemical composition of the surface of bare and treated β -TCP samples and assess the influence of plasma polymerization, XPS experiments were performed with

a ESCALab MKII spectrometer by Vacuum Generators using non-monochromatic Al-K α (photon energy 1486.6 eV) in normal emission mode (i.e. photoelectrons were detected along the surface normal of the samples). Survey spectra were recorded at reduced energy resolution at a pass energy of 50 eV, while the detail spectra of C $_{1s}$, Ca $_{2p}$, Ca $_{2s}$, P $_{2p}$, P $_{2s}$ and O $_{1s}$ were recorded at a pass energy of 10 eV. For estimating the distribution of elements in terms of at-% the intensity of the photoemission (as obtained after background correction) were weighted with the photoemission cross sections. The relative error associated to the XPS measurements is about 0.5%.

Fourier Transformed Infrared Spectra were recorded using a FTIR Nicolet 6700 in the transmittance mode, (128 scans and resolution 1 with data spacing 0.482cm $^{-1}$). Si wafer were used as the substrate instead of β -TCP disc for the FTIR measurement.

Ampicillin and Gentamicin loading of β -TCP

Loading of ampicillin and gentamicin was done prior to plasma polymerization, by soaking the β -TCP discs in 1.0 mL of 4.0% aqueous drug solution at 100 r.p.m. and 24 - 27 °C during 30 min, by complete immersion of the sample. Samples were dried at 37 °C for 24 h prior to release studies.

Drug release experiments

Ampicillin and gentamicin release experiments were performed using untreated and plasma-polymerized β -TCP discs previously loaded with the 4.0% solution of drugs respectively. For the drug release study, an USP equipment (TDT-08L Dissolution Tester (USP), *Pharma Alliance Group*, U.S.A.) with 8 thermo-jacketed opaque cells of 300 mL was used, each one filled with 150 mL of PBS at pH 7.4 as receptor media. Temperature and rotation were maintained constant at 37 °C and 100 r.p.m. respectively. 1 mL samples were withdrawn from the receptor liquid media for release concentration analysis from the untreated and plasma-polymerized β -TCP discs. After each sample withdrawn, the same volume of PBS was added to the receptor media. Release experiments were performed with four replicates of each plasma polymerization condition.

For the quantification of the ampicillin release, an UV-visible-NIR spectrophotometer *UV-3600 Shimadzu* was used at $\lambda = 204$ nm, corresponding to the wavelength of maximum absorbance of ampicillin in PBS solution. The concentration of ampicillin was below 10% saturation concentration (SINK conditions) in the receptor solution during the experiment. Stability of ampicillin after plasma polymerization on the ampicillin-loaded β -TCP was also

checked by UV- spectroscopy after release of ampicillin in PBS through comparison of the general spectra. The amount of gentamicin released was obtained by measuring the release media collected at each time point by High performance liquid chromatography (HPLC) in a Shimadzu HPLC system. Mobile phase consisted of methanol–water–ammonium acetate buffer (0.02M, adjusted with concentrate ammonia to pH = 9): 35:60:5 (v/v/v), at a flow rate of 0.3 ml/min was passed through a C8 column (Shim-pack, Shimadzu). An injection volume of 20 µl of the release sample was measured by photodiode array (PDA) at $\lambda_{\text{max}} = 238$ nm corresponding to the wavelength of maximum absorbance of gentamicin in PBS solution. Stability of gentamicin after plasma polymerization on the gentamicin-loaded β -TCP was also checked by HPLC after release of gentamicin in PBS through comparison of the control spectra.

The kinetic models used were Zero order equation ($Q_t = Q_0 - K_0t$) and Kopcha kinetics ($Q_t = At_{1/2} + Bt$) [Q_0 is the initial amount of drug in the solution $Q_0 = 0$, K_0 is the zero order release constant and Q_t is the amount of drug released at time t , A = diffusional constant and B = erosion constant].

Antibacterial assay

The antibacterial activity of the ampicillin and gentamicin loaded plasma polymerized β -TCP discs were tested in suspension against *Staphylococcus aureus* (*S. aureus*) in BHI Broth at [BHI] = 37.0 g.L⁻¹. After incubation for 24 h at 37 °C, 1 mL of the inoculate media was put in each well of a 48-well Falcon™ culture well-plates, previously prepared by connecting two adjacent wells. The optical density of bacterial suspension was adjusted to 0.2 ± 0.01 at 600nm, giving approximately 1 x 10⁸ colony-forming units (CFU)/ml. The assay was conducted with samples loaded with drug (D) (ampicillin (AMP) or gentamicin (GENTA): UT-D; SP10-D, DP10-D, TP10-D and QP10-D) and samples without antibiotics that were treated as controls (untreated β -TCP: UT, untreated β -TCP with 40 min polymerization: UT_P40m Samples) apart from controls of *S. aureus* Ctrl+ (with bacteria) and Ctrl- (bacteria growth medium without bacteria). Later, samples were placed in one of the connected wells, while the second was employed to measure absorbance and monitoring the growth of *S. aureus* by means of a Synergy HTX Multimode Reader (BioTek Instruments, Inc.). The antibacterial growth kinetics was monitored for 48 hours at $\lambda=600$ nm absorbance [23]. Measurements were recorded using Gen. 5 software (BioTek Instruments, Inc.) and results are presented in growth curve with standard deviation.

Cell Biocompatibility

The effect of the plasma coating on β -TCP discs on the interaction with osteoblastic cells was evaluated using a human osteosarcoma cell line (Saos-2, ATCC, USA), with three replicates for each condition. The coated or uncoated β -TCP discs were sterilized by UV treatment for 15 min and placed in 24-well tissue polystyrene (TCPS) plates. Saos-2 cells (80,000 cells/well) were seeded on the surface of the discs in McCoy's cell culture medium (Invitrogen, Carlsbad, CA, USA) and incubated at 37 °C for a week. Cell culture media was replaced at every 24 h. At 6 h, 24 h, 3 days and 7 days' time point, cells were lysed with 300 μ L of M-PER® (Mammalian Protein Extraction Reagent, Thermo Scientific, Waltham, MA, USA). The cell number was evaluated using the Cytotoxicity Detection Kit LDH (Roche Applied Science, Penzberg, Germany), according to the manufacturer's instructions. The LDH activity was measured spectrophotometrically at 492 nm with PowerWave HT microplate reader (Bio-Tek Instruments, Inc.) [24]. The results were expressed as a relative fold change compared to the cell number obtained on TCPS at 6 hours (SaOS-2 cells). The cell viability was calculated following Eq. (2), where Abs is the measured absorbance for the samples (Abs sample) and the positive (AbsC+) and negative control (AbsC-), all the results have been normalized with respect to surface area of TCPS.

$$\text{Cell viability} = \text{Abs sample} - \frac{\text{AbsC} -}{(\text{AbsC}+) - (\text{AbsC}-)} \text{ (eq. 2)}$$

Specimens were prepared for SEM observation by fixing the cells with 4% paraformaldehyde in PBS, and a sequence for dehydrating the cells was performed by immersing the samples in 50%, 70%, 90%, 96%, and 100% (v/v) ethanol during 15 min each step. As the final step, samples were immersed in HDMS overnight and carbon coated.

Statistical Analysis

The data were analyzed using Student's t-tests and one-way ANOVA Tables with Tukey's multiple comparison tests in order to evaluate statistically significant differences between sample groups. The differences were considered to be statistically significant when $p < 0.05$. All statistical analysis was performed with Minitab 16™ software (Minitab, Inc., State College, PA).

Results

Characterization of the plasma coatings on β -TCP

Plasma polymer coatings were produced on β -TCP, based on the polymerization of Diglyme at low pressure. To assess the kind of polymer produced by the low temperature plasma process evaluated, FTIR was performed on a model Si flat surface (Figure 4-3). The hump observed at 3600 cm^{-1} can be attributed to adsorbed water, the other peaks found were characteristic of polymers: Two weak bands at 2952 cm^{-1} and 2888 cm^{-1} which can be attributed to hydrocarbon stretching $\nu(\text{C-H})$ in alkanes. A medium peak at 1655 cm^{-1} and another at 1533 cm^{-1} may correspond to $\nu(\text{C=O})$, and the shoulder at 1464 cm^{-1} can probably be attributed to $\nu(\text{C-O})$. The intense bands at 1218 cm^{-1} and 1055 cm^{-1} can probably be assigned to $\nu_{\text{as}}(\text{C-O})$ and $\nu_{\text{s}}(\text{C-O})$, respectively.

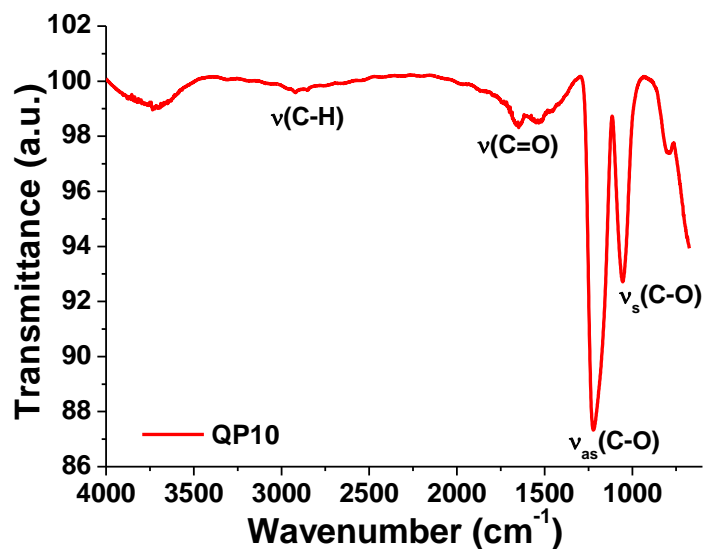


Figure 4-3 FTIR spectra of the plasma polymer (QP10) obtained on Si wafer as model surface.

Uncoated β -TCP is a hydrophilic and porous material, and therefore it quickly absorbs water, not allowing contact angle measurement (Table 4-1). Furthermore, PEG being a hydrophilic polymer, its coatings should display contact angles below 90° , as recorded here for some selected plasma treatments on a Silicon wafer employed as flat model surface (Figure 4-3). Surprisingly, this was not the case for the different plasma treatments evaluated on β -TCP (Table 4-1) which displayed contact angle values above 120° , except for the SP10 sample that still absorbed water (although more slowly than the pristine material). It is remarkable that with DP10, TP10 or QP10 the droplet was strongly pinned to

the surface, not rolling off even if the sample was held vertical (photographs on Figure 4-4).

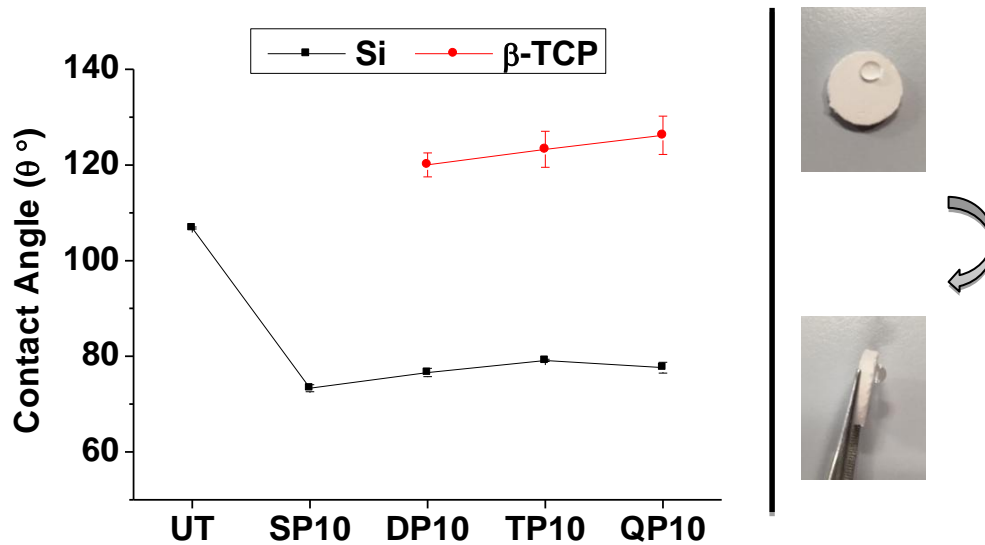


Figure 4-4 Wettability of two plasma-polymerized substrates: silicon wafer (employed as flat model surface) and β -TCP samples (UT and SP10 were not measurable due to hydrophilicity). Images of the droplet on the surface of QP10 with the sample lying flat, or held vertical.

Dynamic contact angles were also measured (Table 4-1), and allowed calculating hysteresis, which was high and similar in the three plasma coated samples.

Table 4-1 Polymerization conditions evaluated on β -TCP, static contact angle and Dynamic advancing and receding contact angles and contact angle hysteresis of β -TCP samples untreated (UT) or with different plasma treatments.

Description	$t_{\text{plasma}}^{\text{tot}}$ (min)	θ_s (°)	θ_{adv} (°)	θ_{rec} (°)	$\Delta\theta$ (°)
UT	--	0	*	*	-
SP10	Single, 10 min	10	*	*	-
DP 10	Double, 10 min	20	120.03 ± 2.51	128.92 ± 1.04	± 65.61 ± 4.18
TP 10	Triple, 10 min	30	123.27 ± 3.76	125.32 ± 3.42	± 59.97 ± 6.17
QP 10	Quadruple, 10min	40	126.20 ± 3.99	119.45 ± 1.83	± 57.08 ± 5.67

* Quick water absorption did not allow static contact angle measurement

The modification in surface chemistry indicated by contact angles was confirmed by XPS, by measuring the elemental composition of the untreated and plasma-polymerized β -TCP (Table 4-2). The composition of untreated β -TCP copes very well with its theoretical concentration, with a Ca/P ratio of 1.48, and the presence of some C can be attributed to adsorbed ambient contamination or surface carbonates. The increase in C/O ratio following all plasma polymerization treatments indicates the presence of a polymer, and the fact that Ca or P were not detected pointed out thickness of the polymer layer above 10 nm (the depth of detection of XPS). Figure 4-5 shows the C1s spectra of the QP10 PEG-like coatings, with three peaks corresponding to C-C or C-H, C-O, being the latter the most abundant, and C=O. SP10, DP10 and TP10 showed very similar C1s spectra.

Table 4-2 Elemental composition obtained by XPS.

Codes	C _{1s}	O _{1s}	Ca _{2p}	P _{2p}	C/O
UT	12.4	56.1	18.8	12.7	0.22
SP10	77.5	22.5	-	-	3.44
DP10	77.3	22.7	-	-	3.41
TP10	78.2	21.8	-	-	3.59
QP10	77.7	22.3	-	-	3.47

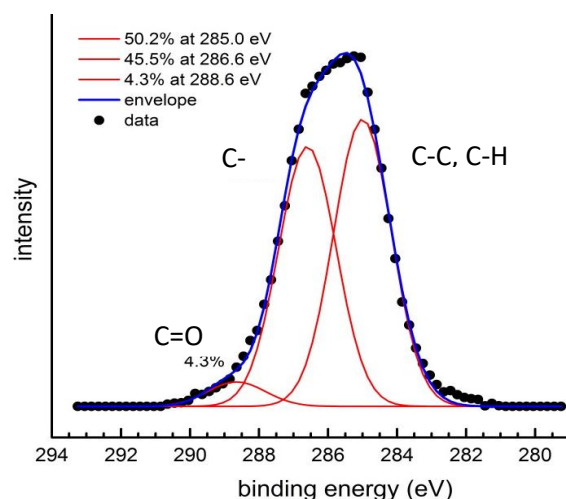


Figure 4-5 C1s spectra of the PEG-like plasma polymer coating on β -TCP for QP10.

Scanning electron micrographs (Figure 4-6, left) reflect the roughness and porosity of β -TCP. Moreover, following plasma polymerization SEM images clearly show that the coating itself is very thin, not masking any topographic features of β -TCP. At the same time, Focused ion beam (FIB-SEM) transversal sections allowed visualizing (Figure 4-6, right) and measuring (Figure 4-7) the thickness of the coating as a function of the total treatment time of the plasma polymerization process. Thickness ranged between 10 nm for SP10 to close to 38 nm for QP10, revealing increasing thickness with longer total plasma treatment times but not following a completely linear behavior.

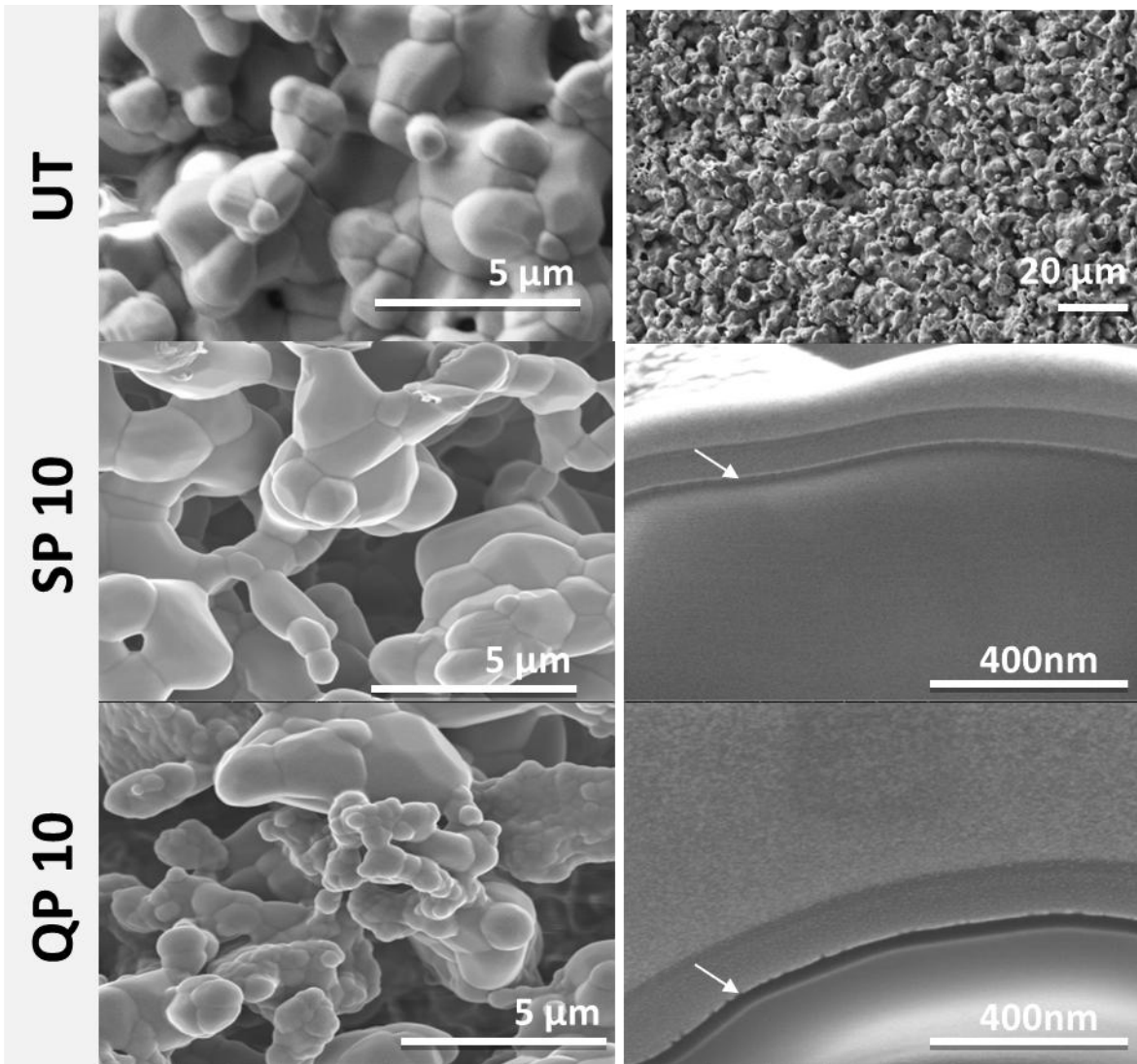


Figure 4-6 Scanning Electron Micrographs of β -TCP untreated at two different magnifications (top) surfaces and of the surface of β -TCP at different polymerization conditions (left) with their corresponding transversal sections obtained by FIB. Arrows indicate the polymer coatings. (Other plasma polymer coatings: DP10, TP10 not shown).

Biological response

The changes in the wettability of the samples might affect the biological response of the material. Therefore, the cytocompatibility of the samples was evaluated through adhesion and proliferation assays (Figure 4-8). All PEG-like plasma-coated β -TCP samples displayed the same cell adhesion and proliferation than β -TCP for all conditions evaluated, with the sole exception of QP10, which showed slightly lower proliferation values at 1 and 7 days.

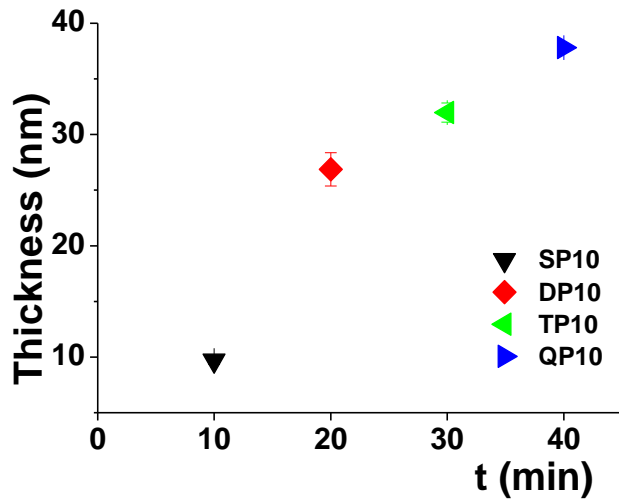


Figure 4-7 Thickness of the PEG-like layer obtained by different plasma polymerization treatments on the surface of β -TCP as a function of the total treatment time.

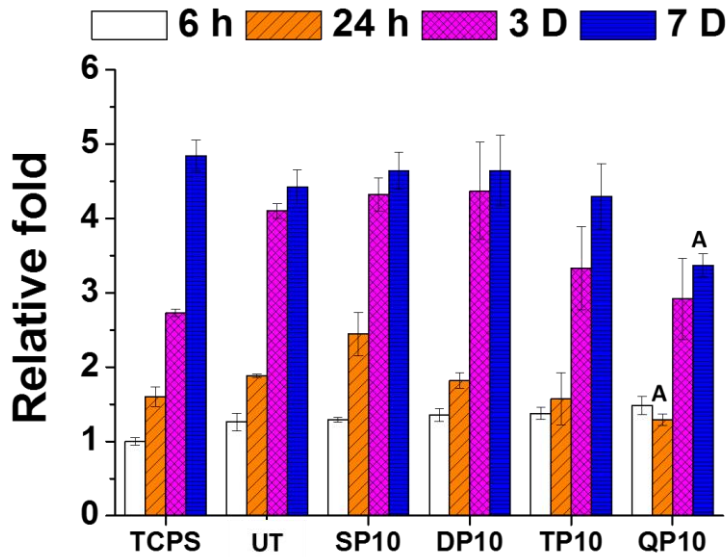


Figure 4-8 SaOS-2 cells relative fold growth on untreated β -TCP and plasma-polymerized β -TCP at different cell culture times. (A indicates significant differences with respect to β -TCP, $P > 0.05$). TCPS accounts for "Tissue culture polystyrene" which is taken as a positive control.

Scanning electron micrographs (Figure 4-9) show cells attached on the surface of β -TCP at different time points (6 h & 3 days). The morphology of the cells on all bioceramics showed extended cells, with visible filopodia, disregard of the presence or absence of the coating.

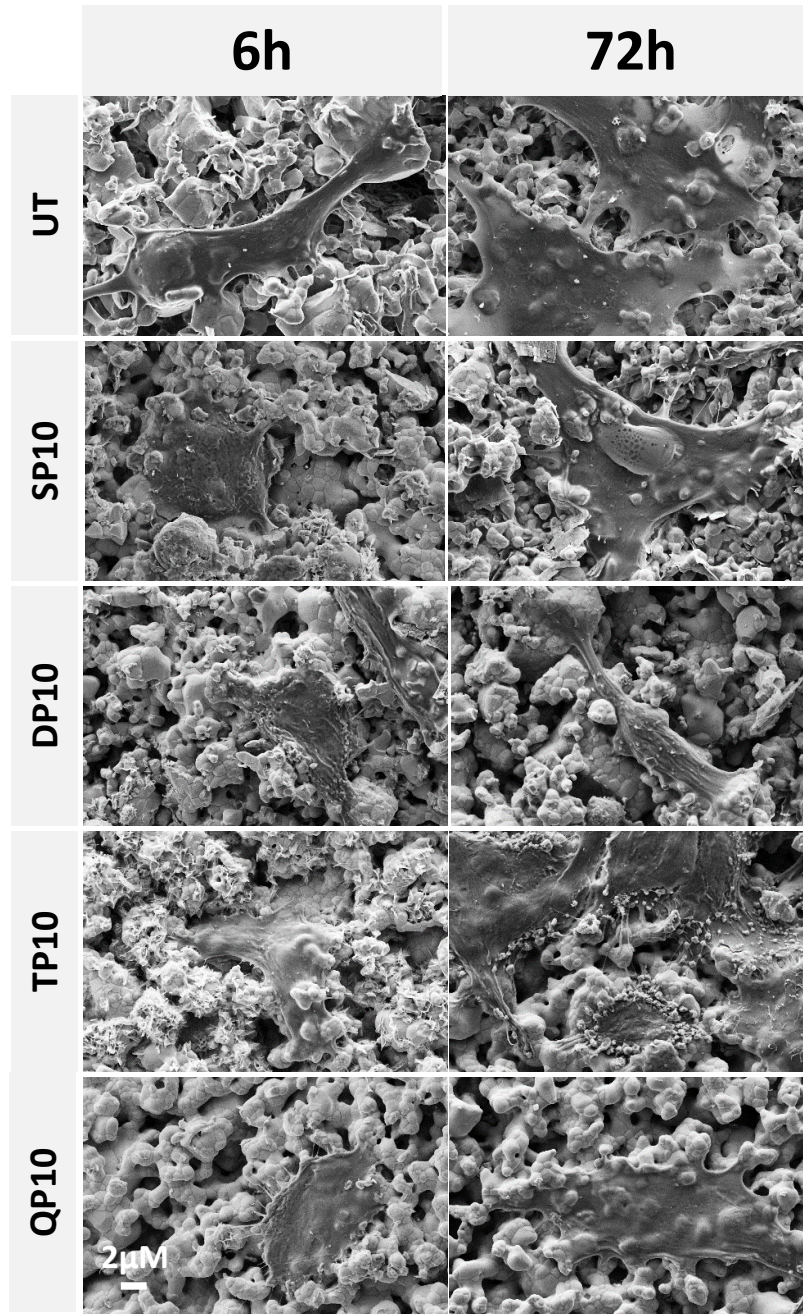


Figure 4-9 Scanning electron micrographs of untreated and plasma-coated β -TCP seeded with SaOS-2 cells for either 6 h (left) or 72 h (right).

Drug Release

Two different antibiotics were incorporated to the β -TCP ceramics prior to plasma coating: ampicillin (AMP) and gentamicin (GENTA). Their release kinetics was investigated following USP pharmacopoeia protocols for 24 h (Figure 4-10) and it can be observed that each drug follows a different release profile. On the one hand, ampicillin follows a burst release within

the first 2 h in which most of the drug loaded is released (Figure 4-10a). On the other hand, gentamicin follows a more progressive release during 24 h (Figure 4-10b). Regarding the plasma coatings, it can be underlined that while for GENTA the total amount released decreases with the thicker plasma coating, the profile of release remains unaltered, for AMP slightly different profile is observed for the samples DP10-D, TP10-D and QP10-D, as shown in Figure 4-10c.

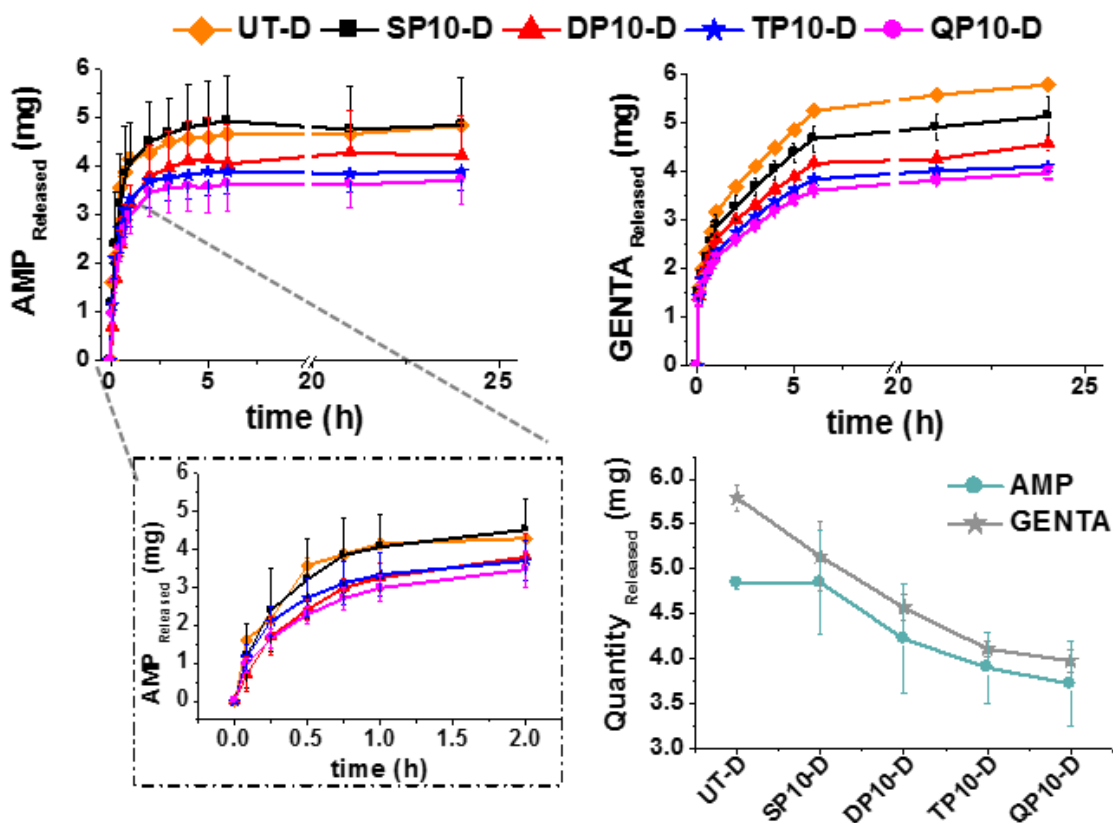


Figure 4-10 Evaluation of release kinetics of ampicillin and gentamicin (top) for 24 hours, total quantity released for both ampicillin and gentamicin (labeled with "D" for drug) for untreated and different treatments (bottom).

The final release percentage of both drugs was close to 100 % for the untreated β -TCP samples, while as plasma polymerization times were longer, the total release % progressively decreased by close to 20% (Table 4-3). The release kinetics were fitted to different models, being Kopcha's model the one showing best fitting. Fitting of the release data to Kopcha's model showed that the release kinetics are governed by diffusion phenomena, A/B being >1.

Table 4-3 Ampicillin or Gentamicin released percentage β -TCP discs after 24 h and kopcha kinetics for the release kinetics.

	Ampicillin					Gentamicin				
	AMP released (%)	R ²	A	B	A/B (>1)	GENTA released (%)	R ²	A	B	A/B (>1)
UT	99.6 ± 0.5	0.983	0.736	0.022	32.6	99.3±0.9	0.987	0.540	0.015	35.79
SP10	99.8 ± 1.7	0.982	0.586	0.010	55.8	98.7 ± 2.1	0.986	0.512	0.015	33.70
DP10	96.9 ± 1.3	0.994	0.499	0.012	39.0	88.1 ± 4.1	0.975	0.506	0.016	30.53
TP10	96.2 ± 2.2	0.993	0.559	0.016	34.8	80.9 ± 6.7	0.970	0.475	0.016	29.73
QP10	80.7 ± 8.0	0.997	0.458	0.011	39.7	78.9 ± 2.8	0.975	0.442	0.015	30.32

Antibacterial properties

The influence of plasma polymerization on the antibacterial activity of ampicillin and gentamicin was studied in a kinetic growth assay over 26 hours (Figure 4-11).

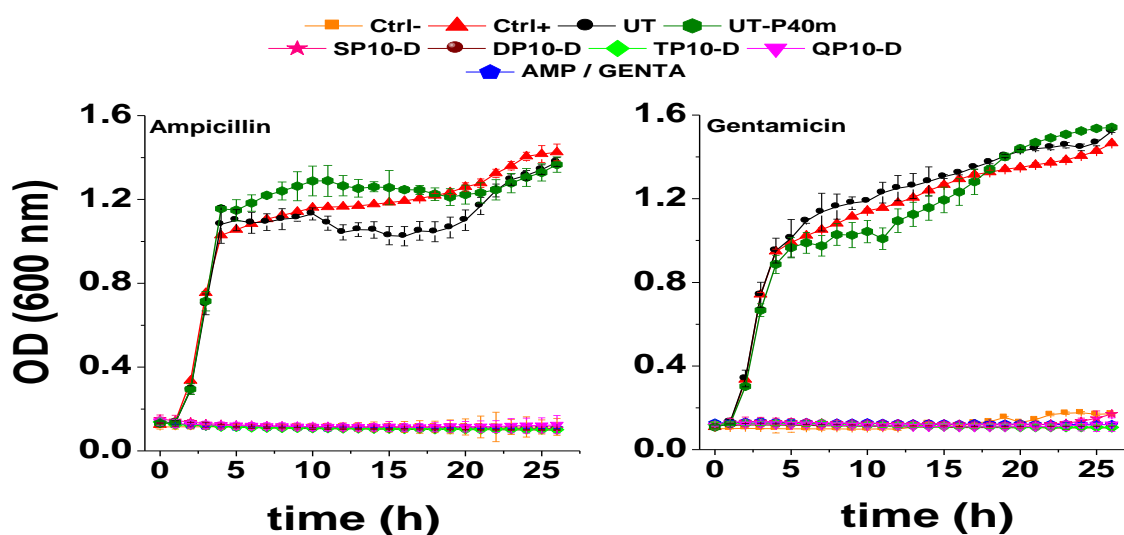


Figure 4-11 Continuous monitoring of the optical density of *Staphylococcus Aureus* bacterial suspensions in contact with ampicillin (AMP) and gentamicin (GENTA) loaded β -TCP ceramics either untreated (UT) or plasma polymerized (UT_P40m, SP10-D, DP10-D, TP10-D and QP10-D) or the suitable controls (in contact with *S. aureus* growth activity during 26 hours).

The growth activity of *S. aureus* was measured for plasma polymerized β -TCP with antibiotics (ampicillin; gentamicin): SP10-D, DP10-D, TP10-D, QP10-D and the bacterial growth in BHI medium was used as a control. It was observed that only the samples without antibiotic (bacterial suspension used as positive control, untreated β -TCP (UT) and 40 mins plasma polymerized β -TCP (UT-P40m) showed bacterial growth. On the contrary, samples loaded with antibiotics either untreated or coated with the plasma polymer coating resulted in the inhibition of bacterial growth.

Discussion

Plasma-polymerization is a versatile technique for the deposition of films with functional properties suitable for a wide range of applications [18] and in this work it was employed to coat β -TCP bioceramics. These biomaterials are excellent bone substitutes, and their intrinsic microporosity allows incorporation of drugs. However, control of drug release is complex and a new strategy has been evaluated.

Plasma polymer coatings deposited on top of polymers have been shown to have excellent barrier properties allowing to delay and control drug release [25], [26]. For biomedical applications, the polymers selected need to be, of course, non-toxic and biocompatible. Conventional polyethylene glycol (PEG) or polyethylene oxide materials (repeating unit: -CH₂CH₂O-) are often defined as non-fouling but when they are synthesized by plasma processes the chemical structure of the polymer obtained might be very different, with a certain degree of cross-linking, and presence of other moieties (i.e. ester, carbonyl, carboxyl and hydrocarbon groups)[27].

The coatings obtained here were produced on β -TCP from Diglyme as precursor at low pressure in sequential treatments ranging from 10 to 40 min of total treatment time (Figure 4-2). The coatings obtained revealed characteristic FTIR peaks of PEG - C-O groups and C-H (Figure 4-3). The C/O surface ratio of the coatings was calculated from XPS data (Table 4-2), being around 3.5 for the four different coatings evaluated. The stoichiometric C/O ratio of Diglyme is of 2, so the values obtained in this work indicate loss of oxygen moieties and increased cross-linking due to high fragmentation in the plasma as also found by E. Sardella et al. for similar plasma coatings obtained at high power on a polymeric substrate [27]. They designated this as “reduced PEG-character” in the plasma coatings contributed by cross-linking and oxygen loss from the Diglyme precursor. This is in agreement with the peak fitting of C1s XPS spectra of QP10 (Figure 4-4) where the C-C, C-

H component at 285.0 eV is the most important component (relative fraction ~50%), closely followed by C-O (~45%) attesting for the high hydrocarbon nature of PEG-like coatings deposited here. Similar results were obtained in [27], [28]

It is not surprising to find this reduced PEG character, as in general, plasma polymers have different properties than those fabricated by conventional polymerization: the plasma-polymerized films are usually branched, highly cross-linked, insoluble, pinhole-free, and adhere well to most substrates [29], [30]. Due to these excellent properties, plasma-polymerized films have been utilized in a wide range of applications, such as protective coatings, biomedical materials, electronic and optical devices, adhesion promoters, etc.

The thickness of the coatings obtained was above 10 nm in all cases as revealed by the fact that Ca and P were not detected by XPS and as confirmed by FIB-SEM cross-section imaging (Figure 4-6). The PEG-like layer thickness (Figure 4-7) progressively increased with the total plasma treatment time in a nearly linear trend.

The surface structure of the β -TCP bioceramic evaluated in this work is highly complex with rough topography (Figure 4-6 top), where crystal grains and sintering necks can be observed. The plasma coating did not alter the topography of the surface and the pores were not covered with any of the coatings evaluated. The porosity of β -TCP and its hydrophilic chemistry led to fast water absorption, which did not allow contact angle measurement (Table 4-1). For the shortest treatment SP10 the coating was probably partially uneven, and some areas remained partially uncoated, still allowing for water absorption. Following plasma treatments of a total of 20 min or more (DP10, TP10, QP10), the static contact angles of the surface of β -TCP raised to values between 120 and 126° as observed in Labay et al. [20]. This is shocking, considering that usually PEG-coatings are hydrophilic ($\theta_s < 90^\circ$), as confirmed by the contact angle values measured on flat silicon surfaces (Figure 4-4) with the same plasma coatings which varied between 74 and 79°.

Besides, dynamic contact angles were measured, which allowed calculating the contact angle hysteresis. The contact angle hysteresis is a measure for how well a drop of liquid sticks to the surface [31]. The hysteresis in contact angle obtained (Table 4-1) was rather high and very similar for all samples, indicating that the surface was heterogeneous. Considering the complex surface topography of β -TCP this can be attributed to roughness. This high hysteresis values are characteristic of surfaces where the drop does not roll-off easily [32], as confirmed by the pictures in Figure 4-4 showing pinning of the drop to the

surface.

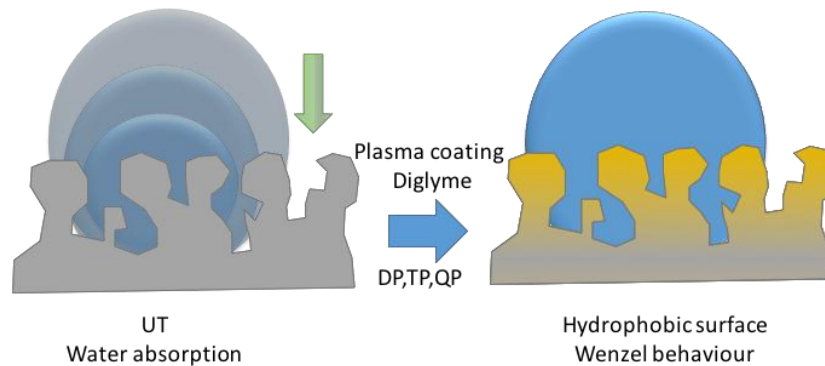


Figure 4-12 Representation of the wetting behaviour of β -TCP bioceramics before and after plasma polymerization of PEG-like layers.

All this was indication of wenzel's behavior [33] occurring on the surface of plasma coated β -TCP (depicted in Figure 4-12). The Wenzel relation ($\cos\theta^* = r \cos\theta$) predicts that roughness enhances wettability which allowed calculating the apparent surface to be of roughness (r) = 2.6 ± 0.4 for this bioceramic, and coping well with the SEM images (Figure 4-6).

Despite the great changes in surface chemistry altered wettability, the cytocompatibility was not compromised (Figure 4-9). Cell adhesion (6h of cell culture) to the surface of PEG-like coated β -TCP in all conditions evaluated was comparable to that of the UT sample. The same occurred for the proliferation of the cells, which was the same to that of naked β -TCP (except only for QQ10 at 24h and 7 days, where a minor decrease in the number of cells was registered).

Despite PEG being widely acknowledged for its antifouling properties, our polymer layer was deposited by plasma in such conditions that lead to rather different chemistry than conventional PEG (less amount of C-O groups, more crosslinking, presence of other moieties such as C=O) so it has a "reduced" PEG character. Similar results were found when seeding 3T3 fibroblasts on flat surfaces plasma coated employing also Diglyme, where those conditions leading to reduced PEG character of the coating displayed suitable cell morphology, and homogeneous growth of the cells on the substrates with these characteristics, while no attachment at all was observed when PEG coatings were produced so the PEG character was retained and antifouling properties were ensured [27].

This is further confirmed by the SEM images on the cells adhered to β -TCP (Figure 4-9) at different time points, which are very well extended on the surface of β -TCP for all coatings,

with visible filopodia which reflect their good attachment to the surface. Many parameters influence cell behavior on bioceramics [34], and parameters such as surface roughness, chemistry, solubility and crystallinity play a role. It seems clear that the thin layer produced here had suitable chemistry allowing, among others the protein adhesion required for further cell attachment, and therefore produced the minimum alterations in the biological behavior of the samples.

Two different antibiotics were selected in this work: gentamicin, a wide spectrum antibiotic that is widely employed in orthopedics, and ampicillin, which was selected for its wide spectrum of action and as reference for comparison with previous works [20], [35]. Both antibiotics followed distinct drug release profiles (Figure 4-10): On the one hand, ampicillin displayed burst release in the 1st hour of release from UT-D β -TCP, and the stationary stage was reached after only 7h. On the other hand, gentamicin followed a more progressive release from UT-D β -TCP, without reaching the stationary stage at least in the 24 h timeframe evaluated.

The recorded differences could be ascribed to the higher molecular weight and steric hindrance of gentamicin (Figure 4-1), impairing the diffusion from the β -TCP matrix.

The plasma coatings evaluated here in both cases induced a progressively reduced amount of drug released, following this order: UT-D \geq SP10-D > DP10-D > TP10-D \geq QP10-D

This could be explained by two different phenomena: i) etching processes occurring on the surface simultaneously to the plasma polymerization during plasma treatment, which might have eliminated a certain amount of the most superficial antibiotic adsorbed on the bioceramic; and ii) a barrier effect due to the polymer layer created. This copes well with the fact that lower amount was released when the plasma coating proceeded on for longer times (Figure 4-10d). Fortunately, the reactivity with the plasma phase did not revert in a denaturation of the antibiotics, as all samples showed suitable inhibition of the *Staphylococcus aureus* bacterial growth (Figure 4-11). In general after plasma processes aimed at modulation of drug release, the drugs keep their activity, as has been shown for different drugs (from anticancer to antibiotics), and varied plasma polymerization processes works [20], [36].

Fitting of the release profiles to the Kopcha model indicates that the release occurring for both antibiotics clearly follows a diffusion mechanism (as shown by a A/B ratio >1).

Of course, to control release from the plasma coating thicker layers need to be produced, as

shown for coatings on polymer films by Arefi-Khonsari et al. [37], [38] or in our case in bioceramics in Chapter 3. In fact, a certain reduction in the release rate was recorded in the release of ampicillin from the coatings obtained at longer plasma treatment times (DP10-D, TP10-D and QP10-D) as had also been observed in a previous work of the group evaluating the same drug for coatings produced in similar conditions [20]. As observed in that case, it is expected that longer treatments produce further reduction in the initial release rate due to increased cross-linking of the polymer.

Conclusions

This work investigated the effects of plasma polymerization on the modification of surface properties of β -TCP bioceramics for bone regeneration. Low pressure plasma polymerization of PEG-like polymers on microporous β -Tricalcium Phosphate (β -TCP) allowed obtaining coatings with low retention of the PEG character (high C/O ratio, grafting of end groups such as C=O and cross-linking of the polymer) which allowed avoiding the typical antifouling properties of the coating. Due to the significant roughness of the surface of β -TCP, following plasma coating the bioceramics showed a hydrophobic behavior, despite the wettability of the polymer layer produced. This was associated with Wenzel behavior, which allowed calculating the roughness ratio of the material, being around 2.6. The coating thickness (ranging from 10 nm to 40 nm) was directly dependent on the polymerization time, which in turn was related to the total amount of drug released. In general, it was observed that the longer the coating, the lesser the amount released (varying from close to 100% in the UT bioceramics to 80% in those with the longer (QP10) plasma coating. This is probably due to etching of the most superficial drug adsorbed on the surface during plasma processes. Moreover, for certain conditions the release profile started to be modified.

The two antibiotics evaluated (ampicillin and gentamicin) retained their antimicrobial activity intact after being released from the β -TCP substrates, confirming the suitability of the technique for coating the drug-loaded ceramic matrices.

Despite the great modification in wettability due to the PEG-like coating, the good cytocompatibility of β -TCP (adhesion and proliferation of SaOS-2) remained unaltered. The research undertaken allowed unraveling the characteristics of plasma coatings on calcium phosphate ceramics and advancing towards the design of drug delivery matrices with suitable biological and microbiological behavior.

References

- [1] "Osteomyelitis Symptoms, Treatment, Causes - What is the treatment for osteomyelitis? - MedicineNet." .
- [2] V. Delfosse, A. El Warrak, P. Clerfond, and B. Lussier, "Article Clinical investigation of local implantation of gentamicin-impregnated collagen sponges in dogs," *Can Vet J*, vol. 5252, pp. 627–630, 2011.
- [3] S. Seber, I. Günal, and E. Göktürk, "Antibiotic-impregnated xenografts in the treatment of chronic osteomyelitic cavities. Seven cases followed for 3 to 5 years.," *Int. Orthop.*, vol. 22, no. 3, pp. 197–9, 1998.
- [4] Z. Ruzszzak and W. Friess, "Collagen as a carrier for on-site delivery of antibacterial drugs.," *Adv. Drug Deliv. Rev.*, vol. 55, no. 12, pp. 1679–98, Nov. 2003.
- [5] J. Gaudias, "Les limites de l'antibiothérapie locale dans le traitement de l'infection ostéo-articulaire," *Eur. J. Orthop. Surg. Traumatol.*, vol. 4, no. 2, pp. 119–121, Jun. 1994.
- [6] M. Ouédraogo, R. Semdé, I. T. Somé, R. Traoré/Ouédraogo, I. P. Guissou, V. Henschel, J. Dubois, K. Amighi, and B. Evrard, "Monoolein–Water Liquid Crystalline Gels of Gentamicin as Bioresorbable Implants for the Local Treatment of Chronic Osteomyelitis: In Vitro Characterization," *Drug Dev. Ind. Pharm.*, vol. 34, no. 7, pp. 753–760, Jan. 2008.
- [7] A. J. Swieringa, J. H. M. Goosen, F. G. A. Jansman, and N. J. A. Tulp, "In vivo pharmacokinetics of a gentamicin-loaded collagen sponge in acute periprosthetic infection: Serum values in 19 patients," *Acta Orthop.*, vol. 79, no. 5, pp. 637–642, Jan. 2008.
- [8] A. M. Cruz, L. Rubio-Martinez, and T. Dowling, "New Antimicrobials, Systemic Distribution, and Local Methods of Antimicrobial Delivery in Horses," *Vet. Clin. North Am. Equine Pract.*, vol. 22, no. 2, pp. 297–322, Aug. 2006.
- [9] Z. Ruzszzak, "Effect of collagen matrices on dermal wound healing.," *Adv. Drug Deliv. Rev.*, vol. 55, no. 12, pp. 1595–611, Nov. 2003.
- [10] G. Hirsbrunner and A. Steiner, "Treatment of infectious arthritis of the radiocarpal joint of cattle with gentamicin-impregnated collagen sponges.," *Vet. Rec.*, vol. 142, no. 15, pp. 399–402, Apr. 1998.
- [11] B. Liu and D. Lun, "Current Application of β -tricalcium Phosphate Composites in Orthopaedics," *Orthop. Surg.*, vol. 4, no. 3, pp. 139–144, Aug. 2012.
- [12] A. A. Mirtchi, J. Lemaitre, and N. Terao, "Calcium phosphate cements: study of the β -tricalcium phosphate — monocalcium phosphate system," *Biomaterials*, vol. 10, no. 7, pp. 475–480, Sep. 1989.
- [13] J. Wang, W. Chen, Y. Li, S. Fan, J. Weng, and X. Zhang, "Biological evaluation of biphasic calcium phosphate ceramic vertebral laminae," *Biomaterials*, vol. 19, no. 15, pp. 1387–1392, 1998.
- [14] Y. L. Chang, C. M. Stanford, and J. C. Keller, "Calcium and phosphate supplementation promotes bone cell mineralization: implications for hydroxyapatite (HA)-enhanced bone formation.," *J. Biomed. Mater. Res.*, vol. 52, no. 2, pp. 270–8, Nov. 2000.
- [15] L. D. Silverman, L. Lukashova, O. T. Herman, J. M. Lane, and A. L. Boskey, "Release of gentamicin from a tricalcium phosphate bone implant," *J. Orthop. Res.*, vol. 25, no. 1, pp. 23–29, Jan. 2007.
- [16] M. Neumann and M. Epple, "Composites of Calcium Phosphate and Polymers as Bone Substitution Materials," *Eur. J. Trauma*, vol. 32, no. 2, pp. 125–131, Apr. 2006.
- [17] R. A. Perez, H.-W. Kim, and M.-P. Ginebra, "Polymeric additives to enhance the functional properties of calcium phosphate cements.," *J. Tissue Eng.*, vol. 3, no. 1, p. 2041731412439555, Jan. 2012.

- [18] R. Morent, N. De Geyter, T. Jacobs, S. Van Vlierberghe, P. Dubruel, C. Leys, and E. Schacht, *Plasma processes and polymers.*, vol. 6, no. suppl. 1. Wiley-VCH Verlag & Co. KGaA, 2004.
- [19] F. Benítez, E. Martínez, and J. Esteve, "Improvement of hardness in plasma polymerized hexamethyldisiloxane coatings by silica-like surface modification," *Thin Solid Films*, vol. 377–378, pp. 109–114, Dec. 2000.
- [20] C. Labay, J. Buxadera-Palomero, M. Avilés, C. Canal, and M. P. Ginebra, "Modulation of release kinetics by plasma polymerization of ampicillin-loaded β -TCP ceramics," vol. 49, no. 30, Jul. 2016.
- [21] M.-P. Ginebra, E. Fernández, F. C. M. Driessens, and J. A. Planell, "Modeling of the Hydrolysis of β -Tricalcium Phosphate," *J. Am. Ceram. Soc.*, vol. 82, no. 10, pp. 2808–2812, Dec. 2004.
- [22] F. Brétagne, M. Lejeune, A. Papadopoulou-Bouraoui, M. Hasiwa, H. Rauscher, G. Ceccone, P. Colpo, and F. Rossi, "Fouling and non-fouling surfaces produced by plasma polymerization of ethylene oxide monomer," *Acta Biomater.*, vol. 2, no. 2, pp. 165–172, 2006.
- [23] X. Deng, A. Nikiforov, D. Vujosevic, V. Vuksanovic, B. Mugoša, U. Cvelbar, N. De Geyter, R. Morent, and C. Leys, "Antibacterial activity of nano-silver non-woven fabric prepared by atmospheric pressure plasma deposition," 2015.
- [24] M. Allen, P. Millett, E. Dawes, and N. Rushton, "Lactate dehydrogenase activity as a rapid and sensitive test for the quantification of cell numbers in vitro.," *Clin. Mater.*, vol. 16, no. 4, pp. 189–94, 1994.
- [25] S. Bhatt, J. Pulpytel, M. Mirshahi, and F. Arefi-Khonsari, "Plasma co-polymerized nano coatings – As a biodegradable solid carrier for tunable drug delivery applications," *Polymer (Guildf.)*, vol. 54, no. 18, pp. 4820–4829, Aug. 2013.
- [26] K. (Ken) Ostrikov, U. Cvelbar, and A. B. Murphy, "Plasma nanoscience: setting directions, tackling grand challenges," *J. Phys. D. Appl. Phys.*, vol. 44, no. 17, p. 174001, May 2011.
- [27] E. Sardella, R. Gristina, G. S. Senesi, R. d'Agostino, and P. Favia, "Homogeneous and Micro-Patterned Plasma-Deposited PEO-Like Coatings for Biomedical Surfaces," *Plasma Process. Polym.*, vol. 1, no. 1, pp. 63–72, Jun. 2004.
- [28] R. D'Agostino and John Wiley & Sons., *Plasma processes and polymers*. Wiley-VCH, 2005.
- [29] C. Vautrin-UI, F. Roux, C. Boisse-Laporte, J. L. Pastol, A. Chausse, B. Grolleau, C. Nguyen, and G. Z. Cao, "Hexamethyldisiloxane (HMDSO)-plasma-polymerised coatings as primer for iron corrosion protection: influence of RF bias," *J. Mater. Chem.*, vol. 12, no. 8, pp. 2318–2324, Jul. 2002.
- [30] F. Arefi, V. Andre, P. Montazer-Rahmati, and J. Amouroux, "Plasma polymerization and surface treatment of polymers," *Pure Appl. Chem.*, vol. 64, no. 5, pp. 715–723, Jan. 1992.
- [31] C. J. van Oss, "A Review of: 'Wettability' J.C. Berg, ed. Marcel Dekker, New York, 1993; hardbound, pp. x + 531; \$195.00.," *J. Dispers. Sci. Technol.*, vol. 14, no. 6, pp. 717–718, Dec. 1993.
- [32] B. P. van der Wal, Static and dynamic wetting of porous Teflon® surfaces. s.n.], 2006.
- [33] R. N. Wenzel, "RESISTANCE OF SOLID SURFACES TO WETTING BY WATER," *Ind. Eng. Chem.*, vol. 28, no. 8, pp. 988–994, Aug. 1936.
- [34] S. Samavedi, A. R. Whittington, and A. S. Goldstein, "Calcium phosphate ceramics in bone tissue engineering: A review of properties and their influence on cell behavior," *Acta Biomater.*, vol. 9, no. 9, pp. 8037–8045, Sep. 2013.
- [35] C. Labay, J. M. Canal, M. Modic, U. Cvelbar, M. Quiles, M. Armengol, M. A. Arbos, F. J. Gil, and C. Canal, "Antibiotic-loaded polypropylene surgical meshes with suitable biological behaviour by plasma functionalization and polymerization.," *Biomaterials*, vol. 71, pp. 132–44, Dec. 2015.
- [36] S. Bhatt, F. Valamanesh, J. Pulpytel, R. Lo Dico, A. Baiyukha, I. Al-dybiat, M. Pocard, F.

Arefi-Khonsari, M. Mirshahi, S. Bhatt, F. Valamanesh, J. Pulpytel, R. Lo Dico, A. Baiyukha, I. Al-dybiat, M. Pocard, F. Arefi-Khonsari, and M. Mirshahi, "Radio-frequency plasma polymerized biodegradable carrier for <i>in vivo</i> release of cis-platinum," *Oncotarget*, vol. 7, no. 36, pp. 58121–58132, Sep. 2016.

[37] S. Bhatt, J. Pulpytel, and F. Arefi-Khonsari, "Low and atmospheric plasma polymerisation of nanocoatings for bio-applications," vol. 3, no. 2, pp. 63–83, Jun. 2015.

[38] S. Bhatt, J. Pulpytel, M. Mirshahi, and F. Arefi-Khonsari, "Catalyst-Free Plasma-Assisted Copolymerization of Poly(ϵ -caprolactone)-poly(ethylene glycol) for Biomedical Applications," *ACS Macro Lett.*, vol. 1, no. 6, pp. 764–767, Jun. 2012.

[39] Y. Ikada, "Surface modification of polymers for medical applications," *Biomaterials*, vol. 15, no. 10, pp. 725–736, 1994.

[40] P. . Chu, J. . Chen, L. . Wang, and N. Huang, "Plasma-surface modification of biomaterials," *Mater. Sci. Eng. R Reports*, vol. 36, no. 5, pp. 143–206, 2002.

[41] S. Yoshida, K. Hagiwara, T. Hasebe, and A. Hotta, "Surface modification of polymers by plasma treatments for the enhancement of biocompatibility and controlled drug release," *Surf. Coatings Technol.*, vol. 233, pp. 99–107, Oct. 2013.

[42] B. Nisol, G. Oldenhove, N. Preyat, D. Monteyne, M. Moser, D. Perez-Morga, and F. Reniers, "Atmospheric plasma synthesized PEG coatings: non-fouling biomaterials showing protein and cell repulsion," *Surf. Coatings Technol.*, vol. 252, pp. 126–133, 2014.

[43] J. Buxadera-Palomero, C. Canal, S. Torrent-Camarero, B. Garrido, F. Javier Gil, and D. Rodríguez, "Antifouling coatings for dental implants: Polyethylene glycol-like coatings on titanium by plasma polymerization.," *Biointerphases*, vol. 10, no. 2, p. 29505, Jan. 2015.

[44] S. Simovic, D. Losic, and K. Vasilev, "Controlled drug release from porous materials by plasma polymer deposition.," *Chem. Commun. (Camb.)*, vol. 46, no. 8, pp. 1317–9, Feb. 2010.

[45] K. Vasilev, N. Poulter, P. Martinek, and H. J. Griesser, "Controlled release of levofloxacin sandwiched between two plasma polymerized layers on a solid carrier.," *ACS Appl. Mater. Interfaces*, vol. 3, no. 12, pp. 4831–6, Dec. 2011.

[46] C. Canal, K. Khurana, S. Gallinetti, S. Bhatt, J. Pulpytel, F. Arefi-Khonsari, and M.-P. Ginebra, "Design of calcium phosphate scaffolds with controlled simvastatin release by plasma polymerisation," *Polymer (Guildf.)*, vol. 92, pp. 170–178, Jun. 2016.

[47] H. Yasuda, *Plasma polymerization*. Academic Press, 1985.

[48] H. Yasuda and T. Hsu, "Some aspects of plasma polymerization investigated by pulsed R.F. discharge," *J. Polym. Sci. Polym. Chem. Ed.*, vol. 15, no. 1, pp. 81–97, Jan. 1977.

[49] J. Friedrich, "Mechanisms of Plasma Polymerization - Reviewed from a Chemical Point of View," *Plasma Process. Polym.*, vol. 8, no. 9, pp. 783–802, Sep. 2011.

[50] A. Micheltore, P. Gross-Kosche, S. A. Al-Bataineh, J. D. Whittle, and R. D. Short, "On the effect of monomer chemistry on growth mechanisms of nonfouling PEG-like plasma polymers.," *Langmuir*, vol. 29, no. 8, pp. 2595–601, Feb. 2013.

[51] J. Trieschmann and D. Hegemann, "Plasma polymerization at different positions in an asymmetric ethylene discharge," *J. Phys. D. Appl. Phys.*, vol. 44, no. 47, p. 475201, Nov. 2011.

[52] D. Hegemann, "Macroscopic investigation of reaction rates yielding plasma polymer deposition," *J. Phys. D. Appl. Phys.*, vol. 46, no. 20, p. 205204, May 2013.

[53] Y. Li, B. W. Muir, C. D. Easton, L. Thomsen, D. R. Nisbet, and J. S. Forsythe, "A study of the initial film growth of PEG-like plasma polymer films via XPS and NEXAFS," *Appl. Surf. Sci.*, vol. 288, pp. 288–294, 2014.

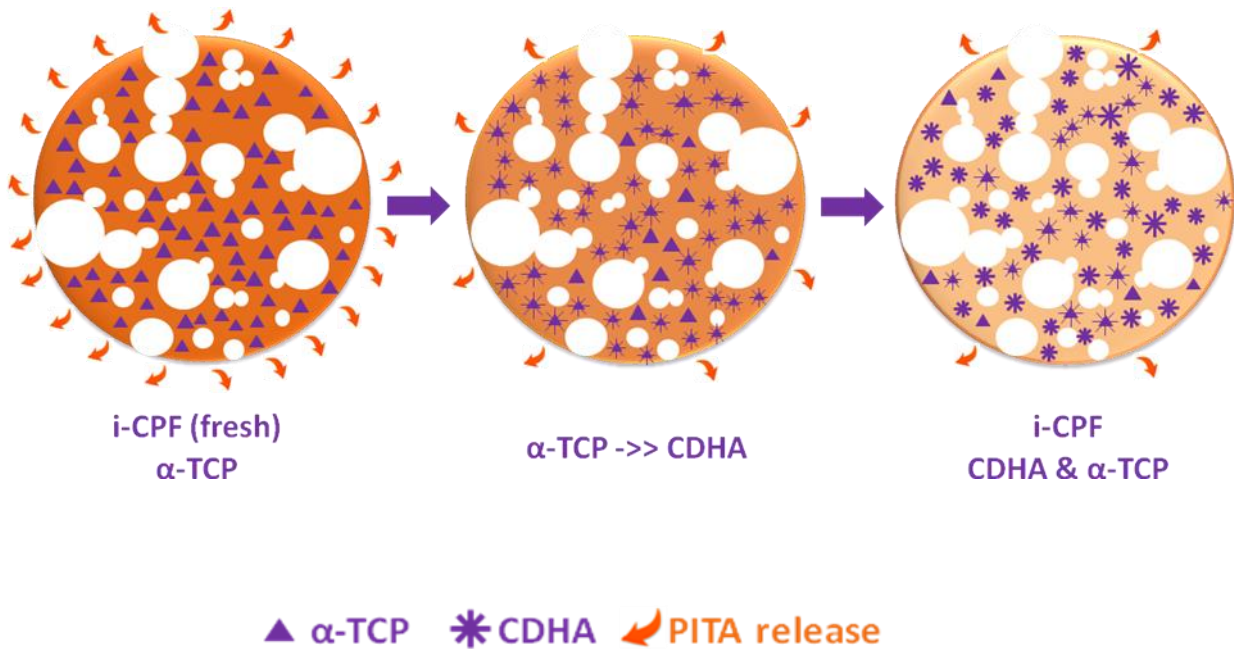
[54] R. Olayo, C. Ríos, H. Salgado-Ceballos, G. J. Cruz, J. Morales, M. G. Olayo, M. Alcaraz-Zubeldia, A. L. Alvarez, R. Mondragon, A. Morales, and A. Diaz-Ruiz, "Tissue spinal cord response in

rats after implants of polypyrrole and polyethylene glycol obtained by plasma," *J. Mater. Sci. Mater. Med.*, vol. 19, no. 2, pp. 817–826, Feb. 2008.

[55] A. S. Abednejad, G. Amoabediny, and A. Ghaee, "Surface modification of polypropylene membrane by polyethylene glycol graft polymerization," *Mater. Sci. Eng. C*, vol. 42, pp. 443–450, 2014.

Chapter 5

Injectable Calcium Phosphate Foams for the delivery of Pitavastatin as osteogenic and angiogenic agent



Abstract

Apatitic bone cements have been used as a clinical bone substitutes and drug delivery vehicle for therapeutic agents in orthopedic applications. This has led to their combination with different drugs with known ability to foster bone formation (BMPs, NPs or statins). Recent studies have evaluated Simvastatin for its role in enhanced bone regeneration, but its lipophilicity hampers incorporation and release to and from the bone graft.

In the study reported in this Chapter, Injectable calcium phosphate foams (i-CPF) based on alpha-tricalcium phosphate were loaded for the first time with Pitavastatin. The stability of the drug in different conditions relevant to this study, the effect of the drug on the scaffold's properties, the release profile, and the *in vitro* biological performance with regards to mineralization and vascularization were investigated. Pitavastatin did not cause any changes in both the micro and macro structure of the i-CPFs, which retained the biomimetic features. PITA-loaded i-CPFs showed a dose-dependent drug release, with early stage release kinetics clearly affected by the evolving microstructure due to the setting of cement. *In vitro* studies showed dose-dependent enhancement of mineralization and vascularization. Our findings contributes towards a design of controlled and low drug dosing bone grafts; i-CPFs loaded with PITA as osteogenic and angiogenic agent.

Introduction

Bone defects represent a major health burden, especially when they are of critical size and cannot heal following the usual regeneration mechanisms of bone[1]. In such cases bone grafting surgery is required, and in this context synthetic bone biomaterials have an increasing demand. Among the different biomaterials available, calcium phosphate cements (CPC) present several advantages that have fostered their study and application [2]–[4]. In particular, their composition mimicking the bone mineral phase, their ability to strongly bond with bone, their injectability and self-setting ability are some of their main assets [5]–[9]. Moreover, their intrinsic micro-nanoporosity makes them ideal candidates as drug delivery vehicles [10], [11], and have thus been studied in combination with different drugs including anti-inflammatories, antibiotics or anti-osteoporotic drugs [12]–[15].

Interconnected macroporosity is a key feature of synthetic bone grafts, since it allows circulation of nutrients and cell infiltration and enhances resorption and bone ingrowth.

Moreover, when injectable CPCs are used as matrices for the delivery of drugs or active molecules, the presence of interconnected macropores has been shown to significantly increase/modify drug delivery [14]. So far, a number of methods have been investigated to obtain macroporous CPCs [16]–[21]. In this work we will focus specifically the addition of biocompatible surfactants to obtain injectable calcium phosphate foams (i-CPF), a method that has been found adequate for obtaining stable scaffolds with interconnected macroporosity[17] .

Statins are extensively used drugs, employed mainly as inhibitors for the cholesterol biosynthesis. Additionally, they are known to present several pleiotropic effects, such as improving endothelial function, decreasing oxidative stress and inflammation, or inhibiting the thrombogenic response, among others [22]. Interestingly, Mundy et al. reported that they also played a role in bone formation, through the stimulation of BMP-2 expression [23]. This led to a wide investigation, focusing especially on simvastatin (SIM), as a potential drug for bone regeneration [23], [24]. However, the hydrophobic nature of SIM results into low oral bioavailability ($\leq 5\%$), due to extensive first-pass metabolism in the gastro-intestinal wall and high extraction in the liver [25]. The hydrophobic nature of SIM also hampers its uniform incorporation in water-based matrices, as is the case of CPCs, which are formed by a combination of powder and aqueous liquid phase.

With the aim of fostering bioavailability and ease of incorporation in CPCs, a more hydrophilic statin, Pitavastatin (PITA) has been investigated for the first time in this work, in combination with a foamed CPC. Due to higher oral absorption, oral bioavailability, and even solubility, PITA has a higher potency than SIM [26]–[28]. Moreover, although the studies on the pleiotropic effects of PITA are scarce [29], some findings suggest that it enhances bone turnover markers [30]; and gene expressions for mineralization [31]

The aim of the study that is reported in this Chapter was to explore the feasibility of incorporating PITA in i-CPFs as a strategy to foster the bone regenerative process at the defect site, using a lower dosage than SIM due to its higher potency. To this end, the effects of PITA on mesenchymal stem cells and on endothelial progenitor cells were evaluated, and the interactions of PITA with the physic-chemical properties of i-CPFs were assessed. Finally, the release kinetics from i-CPFs was evaluated.

Materials and methods

Pitavastatin stability

Pitavastatin Calcium ($C_{22}H_{23}FNO_4 \cdot 0.5Ca \cdot 2H_2O$; Tocris Bioscience, UK) was received in powder form and incorporated in the liquid phase with a solubility of 0.426 mg/l in water. The molecular structure of PITA; is shown in Figure 5-1. In the evaluation of the PITA's stability, two main factors were taken into account: pH and temperature. The temperature stability was evaluated with solutions of PITA prepared in Phosphate Buffer Saline (PBS) at different concentrations (5, 50 and 100 μ M) and stored at 5 °C and 37 °C with a pH of 6.5. Similarly, since during the setting reaction of i-CPF the pH reaches alkaline values of pH 9.5 and eventually shifts to neutral pH 7 during initial 24 h [32]. Therefore, PITA's stability was assessed at alkaline pH based on cement setting. PITA was dissolved in water (5, 25, 50, 75 and 100 μ M) and stored at 37 °C. Subsequently the pH of the PITA solutions (pH 6.5) was adjusted to pH 8 and pH 9.5 by addition of 0.01 M NaOH which affected the initial concentration for the solutions. The quantification of PITA solutions at various time points was carried out with High performance liquid chromatography (HPLC) in a Shimadzu HPLC system. A mobile phase of Acetonitrile: 0.1% phosphoric acid at a ratio of 50:50 (v/v), at a flow rate of 0.5 ml/min was passed through a C8 column (Shim-pack, Shimadzu). An injection volume of 10 μ L of the release sample was measured by photodiode array (PDA) at $\lambda_{max} = 245$ nm. 3 replicates were analyzed for each condition.

Evaluation of the effects of Pitavastatin on mesenchymal stem cells and endothelial progenitor cells in vitro

The osteogenic and angiogenic effects of PITA were evaluated in *in vitro* models with rat Mesenchymal stem cells (rMSCs) and endothelial progenitor cells (EPCs) respectively. Both cell types were extracted from femurs of young Lewis rats at the Institute for Bioengineering of Catalonia (IBEC), as in previous works [33]. Cell phenotypes were previously characterized by flow cytometry [34]. rMSCs cells were expanded in Advanced DMEM supplemented with 10% fetal bovine serum (FBS), 20 mM HEPES buffer solution, penicillin/streptomycin antibiotics (50 U/ml and 50 μ g/ml, respectively), and 2 mM L-glutamine (all from Invitrogen) at 37 °C with 5% CO₂ and 95% relative humidity. On the other hand, supernatant containing EPCs were centrifuged and re-suspended in EBM medium (Lonza) supplemented with EGM-2 BulletKit and 5% FBS. Both cell types were used from passage 4 for all the experiments. 10⁴ cells/well were seeded in 24 well plates

and cultured in their corresponding medium with PITA (0.1, 1 and 10 μM) and Tissue culture polystyrene (TCPS) was used as control. PITA was received in powder form and used as received to prepare a stock solution in Milli-Q water, which was further diluted to the final concentration of 0.1, 1 and 10 μM in cell culture medium.

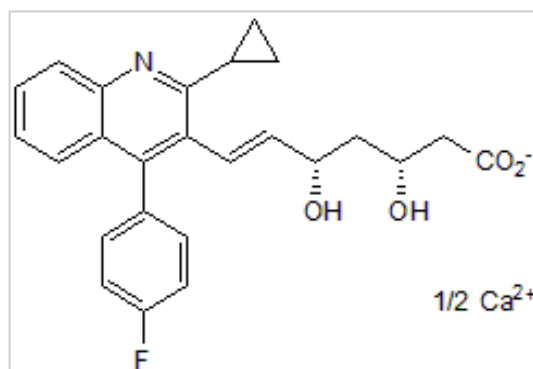


Figure 5-1 Chemical structure of the Pitavastatin used in this study.

The expression of osteogenic marker genes in rMSCs (BMP-2, Osteocalcin, Collagen-I) and vascularization genes in EPCs (VEGFA, VEGFR-1, VEGFR-2) were determined through RT-qPCR assay at various time points (6 and 24h, 3 and 7 days), Table 5-1. At each culture time, total RNA was extracted using RNeasy® Mini Kit (Qiagen, Hilden, Germany) as described in the manufacturer's instructions. Total RNA was quantified using a NanoDrop ND-1000 spectrophotometer (NanoDrop Technologies, Montchanin, DE, USA) and its quality was assured by agarose gel electrophoresis. 200 nanograms were retro-transcribed to cDNA using the QuantiTect Reverse Transcription Kit (Qiagen). cDNA products were further diluted and used as RT-qPCR templates. The RT-qPCR primers were designed, after specificity and intron span verification by Blast, using the Primer3 software (<http://rodo.wi.mit.edu/primer3/>) to amplify the specific genes for adhesion, ECM synthesis and bone remodelling (Table 1). Primers from genes that exhibited more than one transcript were selected from common regions. SYBR Green RT-qPCR analyses were carried out using the QuantiTect SYBR Green RT-PCR Kit (Qiagen) in an ABIPrism 7700 machine (Applied Biosystems, Foster City, CA, USA). Specificity of each RT-qPCR reaction was determined by melting curve analysis and by resolving the RT-qPCR products on 2% agarose gels. All samples were normalized by the expression levels of β -actin (reference gene) and fold changes (FC) were related to TCPS at 6 h of culture as follows:
$$\text{FC} = \frac{E_{\text{target}}^{\Delta Cq_{\text{target}}(\text{TCPS6h} - \text{Surface})}}{E_{\text{reference}}^{\Delta Cq_{\text{reference}}(\text{TCPS4h} - \text{Surface})}}$$
 (Pfaffl 2001), where C_q is the median value for the quantification cycle for the triplicate of each sample and E is the amplification efficiency, determined from the slope of the log-linear portion of the calibration curve, as: $E = 10^{-1/\text{slope}}$.

Preparation of pitavastatin loaded injectable calcium phosphate foams

α -TCP was used as a solid phase of i-CPFs and was obtained by heating in a furnace (CNR-58, Hobersal, Spain) in air a 2:1 molar mixture of calcium hydrogen phosphate (CaHPO_4 ; Sigma–Aldrich, USA) and calcium carbonate (CaCO_3 ; Sigma–Aldrich, USA) at 1400 °C for 15 h, followed by quenching in air. The α -TCP obtained was milled in an agate ball mill (Pulverisette 6, Fritsch GmbH, Germany) using 10 agate balls ($d = 30$ mm) for 15 min at 450 rpm; 2 wt.% of precipitated hydroxyapatite (HA; BP-E341, Merck, Germany) was added as a seed in the powder. 10 wt% Pluronic F-127 (Sigma Aldrich, USA) was blended with the solid phase for the preparation of the scaffolds. The liquid phase was a solution of 1 wt% of Polysorbate 80, herein Tween80 (Polysorbate 80, Sigma Aldrich, USA) in distilled water. PITA solutions were prepared at 50, 75, 100 and 200 μM by incorporating in the liquid phase.

Self-setting i-CPFs were foamed by mixing the solid and the liquid phase at 7000 rpm for 30 s using a domestic hand mixer. The foams were injected in Teflon cylindrical moulds of 6 mm x 12 mm and left to consolidate in 100 % relative humidity at 37 °C, followed by immersion in water at 37°C for 7 days to allow for complete reaction, prior to physico-chemical characterization.

Physic-chemical characterization of i-CPFs

The microstructure of the i-CPFs was characterized by field emission scanning electron microscopy (FESEM) (Neon 40, Zeiss, Germany). A fracture region was observed at 10 kV working voltage. Prior to observation, samples were Au-sputter coated (K950X, Emitech, US).

The Specific Surface Area (SSA) of i-CPFs was measured by Nitrogen adsorption in an ASAP 2020 (Micromeritics) with 6 cylindrical samples, using the Brunauer-Emmet-Teller (BET) method.

Helium pycnometry (AccuPyc 1330, Micromeritics, USA) was used to measure the skeletal density of i-CPFs and i-CPFs with 100 μM PITA.

Mercury intrusion porosimetry (MIP, AutoPore IV, Micromeritics, USA) was performed to determine the pore entrance size distribution (PESD) within the materials. Four cylindrical samples were introduced in the sample holder for the measurement, and a single measurement was performed for each composition.

Table 5-1 Table 1: DNA sequences of forward (fw) and reverse (rv) primers for the selected genes used for real – time qPCR.

Related Function	Gene Symbol	Gene Title	Primer sequences (5'-3')	Acc. No.	Amplicon size (bp)
Mineralization	OC	Osteocalcin	CCAGGGGATCTGGGTAGG-fw ATAGACTCCGGCGCTACCTC-rv	NM_013414.1	63
ECM component	COL1	Collagen-1	GCAGCTGACTTCAGGGATGT-fw CATGTTTCAGCTTTGTGGACCT-rv	NM_053304.1	94
Differentiation	BMP-2	Bone morphogenetic protein 2	CCCCTATATGCTCGACCTGT-fw AAAGTTCCTCGATGGCTTCTT-rv	NM_017178.1	137
Vascularization	VEGFA	Vascularization endothelial growth factor A	CGGAGAGCAACGTCACTATG-fw TGGTCTGCATTACATCTGC-rv	NM_031836.2	104
	VEGFR-1	Vascularization endothelial growth factor receptor-1	TGGAAAGCTCAGCGTACCTC-fw AGTTAGAAGGAGCCAAAAGAGTGT-rv	NM_019306.1	113
	VEGFR-2	Vascularization endothelial growth factor receptor-2	AAAGAGAGGGACTTTGGCCG-fw GTCGCCACTTGACAAAACCC-rv	NM_013062.1	143
House keeping	β -actin	Beta actin	CCCGCGAGTACAACCTTCT -fw CGTCATCCATGGCGAACT -rv	NM_031144.2	72

Micro-computed tomography, a 3-dimensional micro-computed (3D micro-CT) system used was TOMOLIBRIR and was developed at the Fraunhofer IZFP Saarbrucken, Germany to evaluate the three-dimensional (3-D) morphology of CPFs. The scanner was operated to obtain a voxel size of $4^3 \mu\text{m}^3$, at 100 kV and 9 W X-ray power with a data acquisition and reconstruction software, Volex. The samples employed were cylinders with 6 mm in diameter and 12 mm high. The 3-D volume was then reconstructed using Amira network (version 5.4.3).

Evaluation of Pitavastatin release

For drug release studies, i-CPFs were prepared with the liquid phase containing PITA at different concentrations (50, 75, 100 and 200 μM) as described in Sections 2.1 and 2.2. They were injected in 2 mm x 6 mm teflon moulds adapted from the USP ointment cell with only one open side allowing contact with the release medium. Prior to release, they were kept for 5 h in 100% relative humidity to have sufficient cohesion. The total amount of PITA loaded per sample was measured by weighing samples before release and calculating with respective concentration of PITA in the liquid phase using eq 1. (where, Wt. refers to weight)

$$\left(\frac{Wt_{\text{PITA liquid phase}}}{Wt_{\text{PITA liquid phase}} + Wt_{\text{solid phase.}} + Wt_{\text{liquid phase.}}} \right) \times Wt_{\text{PITA loaded scaffold}} = Wt_{\text{PITA per scaffold}} \text{ (eq. 1)}$$

Then release was conducted for 6 days by immersing the i-CPFs moulds in 5 ml of Phosphate Buffer Saline (PBS, pH=7.4) at 37°C with continuous stirring of 100 rpm, release was conducted for 6 days. At each time point 350 μL of release medium was withdrawn and replaced with 350 μL of fresh PBS. The amount of drug released was quantified by measuring the concentration of PITA in the release media collected at each time point with HPLC following the protocol described in the previous section. The cumulative release was plotted as a function of time after correcting the data for evaporation of PBS during 6 days. Additionally, the data for total percentage of PITA released was corrected for degradation occurred during setting, as detailed in section 3.1. Modeling was performed using the Korsmeyer Peppas (KP) model. The variable fitted is the quantity released M_t , normalized by the maximum quantity released M_∞ (eq. 2):

$$M_t = M_\infty \cdot k \cdot t^n \text{ (eq. 2)}$$

where k is a constant that accounts for structural parameters of the material and characteristics of the active principle such as the effective coefficient of diffusion. The

exponent n allows the identification of the mechanism controlling the release. Specifically, for a given geometry of the sample it allows discerning between a release controlled by Fickian diffusion, swelling/case II transport or an Intermediate situation. The KP model is applicable only up to 60% of the quantity released. The exponent n describes the shape of the curve. The quantity released as a function of time was thus fitted with the KP equation, and both the value of the exponent n and the correlation coefficient R² were reported.

Statistics

Statistical differences were determined using one-way ANOVA with Tukey's post hoc tests using minitab software. Statistical significance was considered when P < 0.05. Data are presented as mean ± standard deviation.

Results

Evaluation of PITA stability

The stability of PITA under the influence of temperature and pH as a function of time for 216 h (9 days) is reported in Figure 5-2. It was found that PITA in PBS was stable at both the temperatures of 5 and 37 °C (Figure 5-2, top), as no degradation was detected (P >0.05), allowing to perform the drug release assays at 37°C without risk of degradation of PITA, and if required, samples could be stored in the fridge. In contrast, it was observed that PITA was degraded at basic pH (Figure 5-2, bottom), particularly at high concentrations of 50, 75 and 100 µM. The degradation was found to be similar at pH 8 or 9.5, and the amount degraded in the solutions corresponds to ~8% in initial 24 h calculated with equation given below. The degradation of PITA was calculated with following reaction, further explained in discussion section (eq. 3):

$$\left(\frac{\text{Degradation (pH 9.5)}}{24 \text{ h}} \times 15 \text{ h} \right) + \left(\frac{\text{Degradation (pH 8)}}{24 \text{ h}} \times 9 \text{ h} \right) = \text{PITA degradation (24 h) i - CPFs (eq. 3)}$$

The degradation of PITA at pH 8 and pH 9.5 has been calculated as a function of time for initial 24 h (Table 5-2).

Table 5-2 Degradation of PITA at pH 8 and pH 9.5 with the function of time (t = 24 h) and total degradation when loaded in i-CPFs 24 h, calculated according to eq. (3).

	Degradation (%) (t = 24h)		PITA _{degradation} in i-CPFs setting reaction (%) (t = 24h)
	pH 8	pH 9.5	pH 9.5 → pH 7
5 μM	0	0	0
25 μM	0	0	0
50 μM	8.29	7.84	8.00
75 μM	7.26	6.59	6.83
100 μM	8.19	8.17	8.17

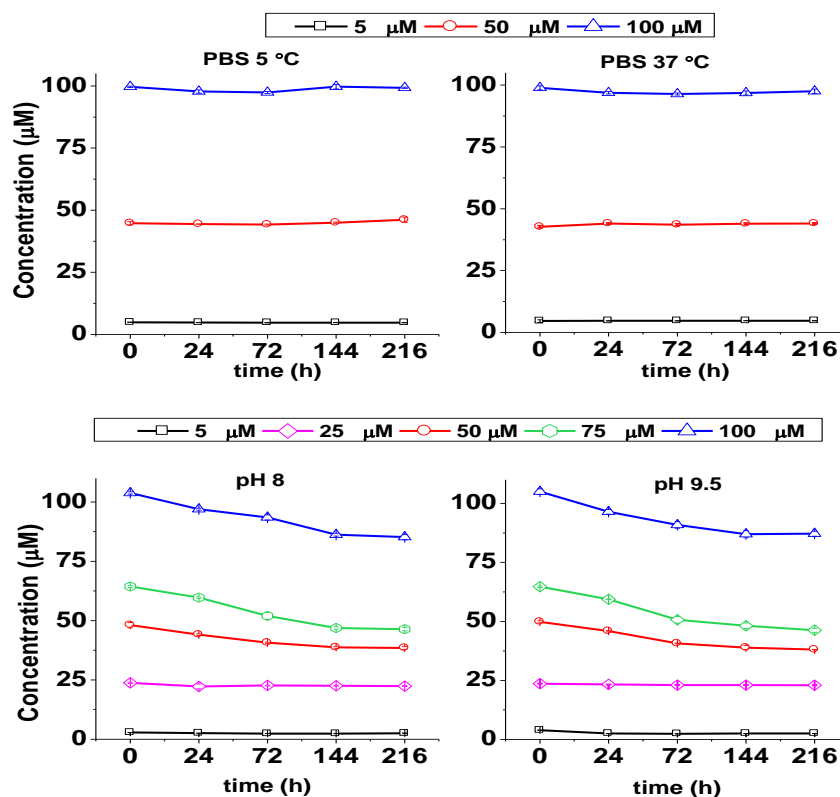


Figure 5-2 Influence of temperature (5 & 37 °C) (top) and pH (8 & 9.5) (37 °C) on the stability of PITA solutions at different concentrations (Standard deviation was calculated with three replicates, error bars are really small to be seen clearly).

Effects of Pitavastatin on mesenchymal stem cells and endothelial progenitor cells in vitro

The potential effects of PITA on the expression of some genes involved in bone regeneration were evaluated through RT-qPCR studies. The relative fold change in the expression by rMSCs of some osteogenic marker genes, namely OCN, collagen type 1 and BMP-2 is shown in Figure 5-3, left column. An over-expression of OCN was observed in presence of PITA at 72h, which was more marked for the 0.1 μ M dose. This concentration led also to an over-expression of OCN at early time points (6 and 24h) and to a significant increase in both Col type 1 gene expression at 72h compared to control, whereas no significant effect was observed for 1 μ M PITA. On the other hand BMP-2 gene expression was observed to be decreasing with progressing time yet it was significantly higher for both 0.1 μ M and 1 μ M PITA compared to the control at 72 h.

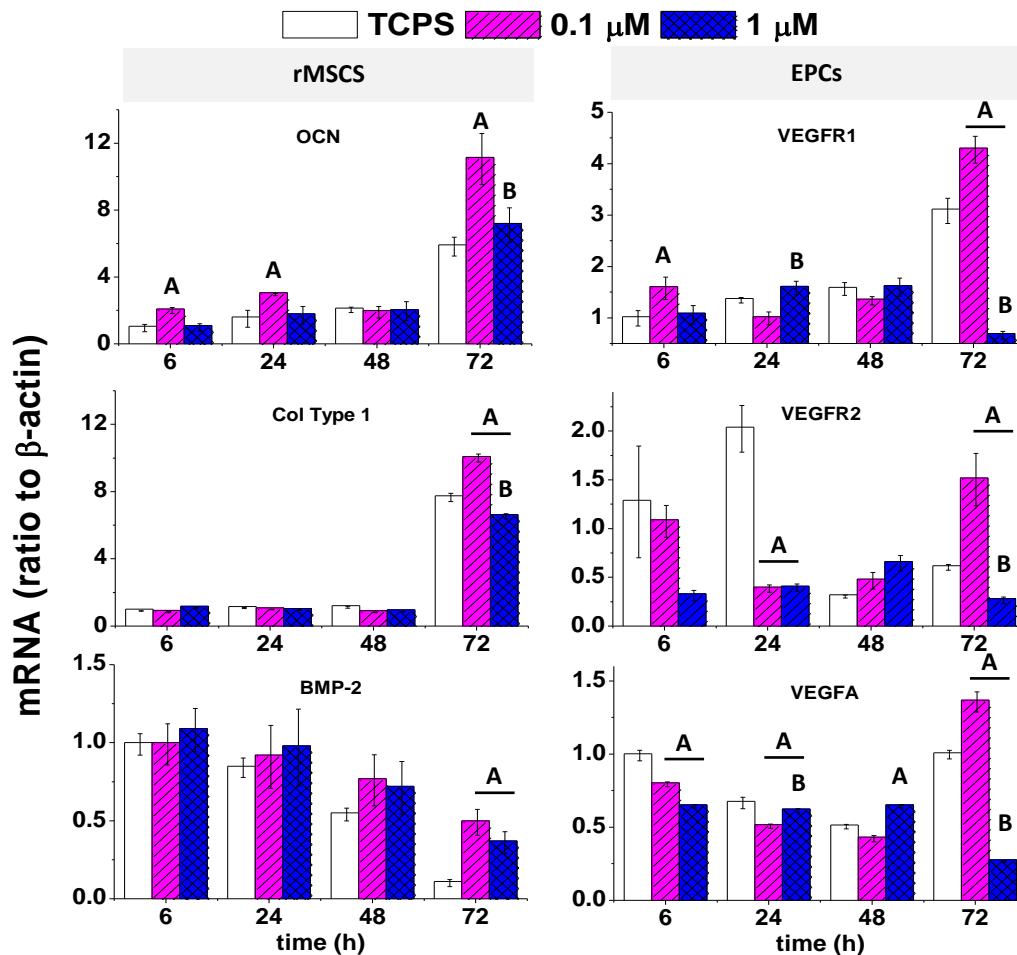


Figure 5-3 Influence of PITA on the gene expression of OCN, Col Type1, BMP-2 by rMSCs and VEGFR1, VEGFR2, VEGFA by EPCs and at 6, 24, 48 and 72 h. The statistical difference with TCPS and 0.1 μ M are represented as A and B respectively for each time point.

Concerning EPCs, the gene expression of VEGFA, VEGFR1, and VEGFR2 were studied, as an indication of the effect of PITA on vascularization, and the results are shown in the right column of Figure 5-3. For the initial hours of 6, 24 and 48 h, PITA showed lower expression for vascularization factors though it was more significant in case of VEGFA. Later on, presence of PITA at 0.1 μ M induced an over-expression of VEGFR1, VEGFR2 and VEGFA at 72h compared to control. In contrast, PITA at 1 μ M produced a statistical significant decrease on VEGFA, VEGFR1 and VEGFR2 gene expressions at 72h.

Synthesis and characterization of PITA loaded i-CPFs

PITA loaded i-CPFs were synthesized and their physic-chemical properties were evaluated as shown in Figure 5-4 and Table 5-3. The characterization of the microstructure was conducted with control i-CPF and PITA loaded i-CPF (100 μ M), highest concentration evaluated for degradation studies. The microstructure of the materials with and without PITA (100 μ M) in the bulk of i-CPFs, both displayed similar features. Entangled plate-like crystals derived from the dissolution-precipitation of α -TCP responsible for cement hardening were observed in the control and PITA loaded i-CPFs. The drug was completely solubilized in the liquid phase and CDHA was formed as a result of the hydrolysis of starting solid phase α -TCP in i-CPFs. The reconstruction of the μ CT scans allowed visualizing homogeneously distributed and interconnected porosity in i-CPFs with or without PITA as shown in Figure 5-4 (bottom). Additionally, Specific surface area (SSA), skeletal density and total porosity measured through MIP showed no significant differences due to the presence of the drug, as reflected in Table 5-3 and Figure 5-5.

Table 5-3 Specific surface area (SSA), skeletal density and Porosity of i-CPFS with and without PITA at 100 μ M, each measurement was conducted with 4 cylinders.

Materials	Specific surface area (m²/g)	Skeletal Density (g/cm³)	Total Porosity (%)
Control	7.89	2.34	74.39 \pm 3.2
100-PITA	7.98	2.07	78.01 \pm 2.8

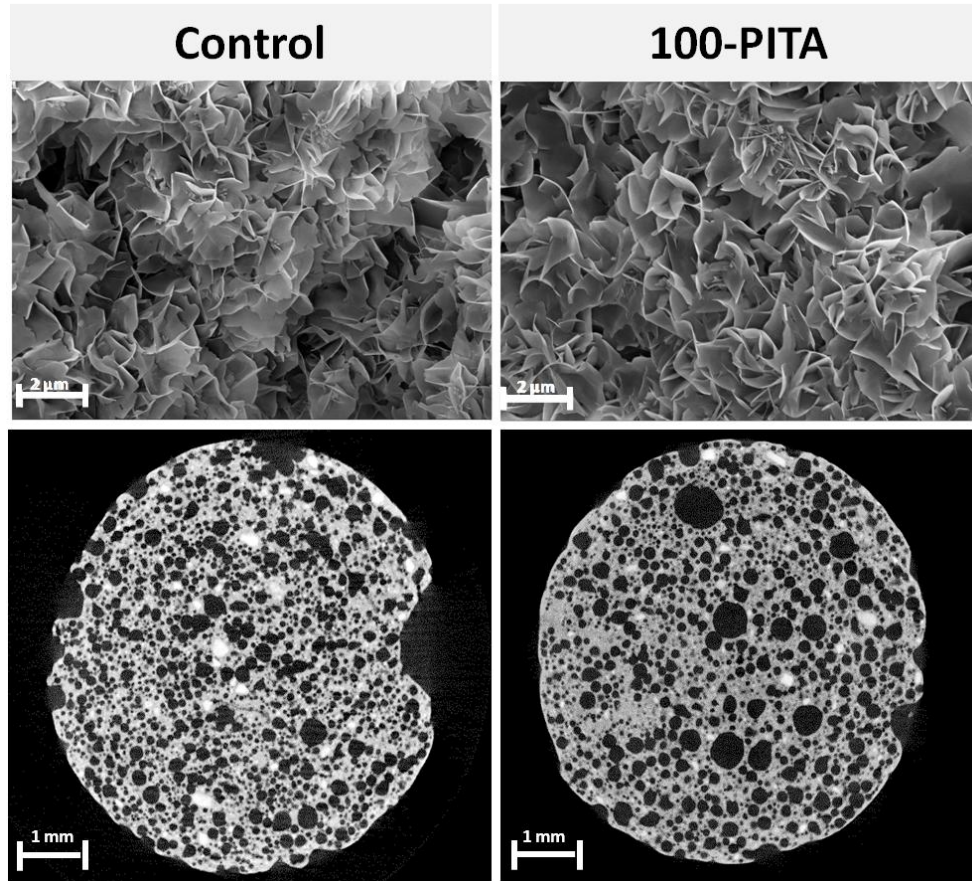


Figure 5-4 FESEM images of i-CPF of control and Pitavastatin loaded i-CPF with 100 μM h (top). μCT images of control i-CPF and Pitavastatin loaded i-CPF at 100 μM (bottom).

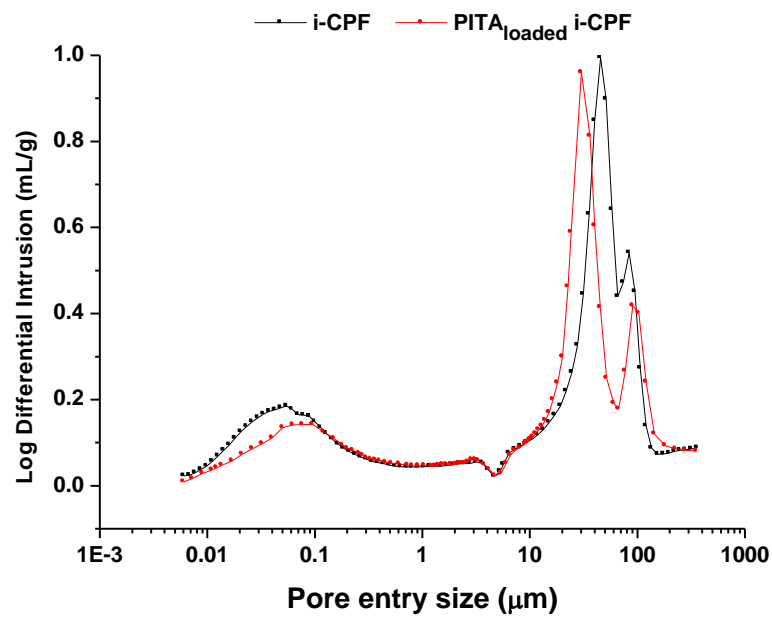


Figure 5-5 MIP pore size entry distribution (n=4) of i-CPF and PITA loaded i-CPF.

Pitavastatin release

The evaluation of the PITA release kinetics from i-CPFs was evaluated for different concentrations of drug added to the liquid phase of i-CPFs (50 μM (50-PITA), 75 μM (75-PITA), 100 μM (100-PITA) and 200 μM (200-PITA)) in PBS for 6 days as shown in Figure 5-6. The cumulative release of PITA showed two different phases. Initially, a burst release was found in the first 5 h, followed by a slow progressive release up to 72 h, later showed a tendency of stabilization. The release shows a dose dependent behavior from the initial time points as shown in the amplified image (Figure 5-6b). The maximum release obtained was for 200-PITA, $40.93 \pm 9.07\%$, in 72 h after corrected with PITA degradation and fitting parameters of KP model to interpret the release kinetics of the i-CPFs are reported in Table 5-4.

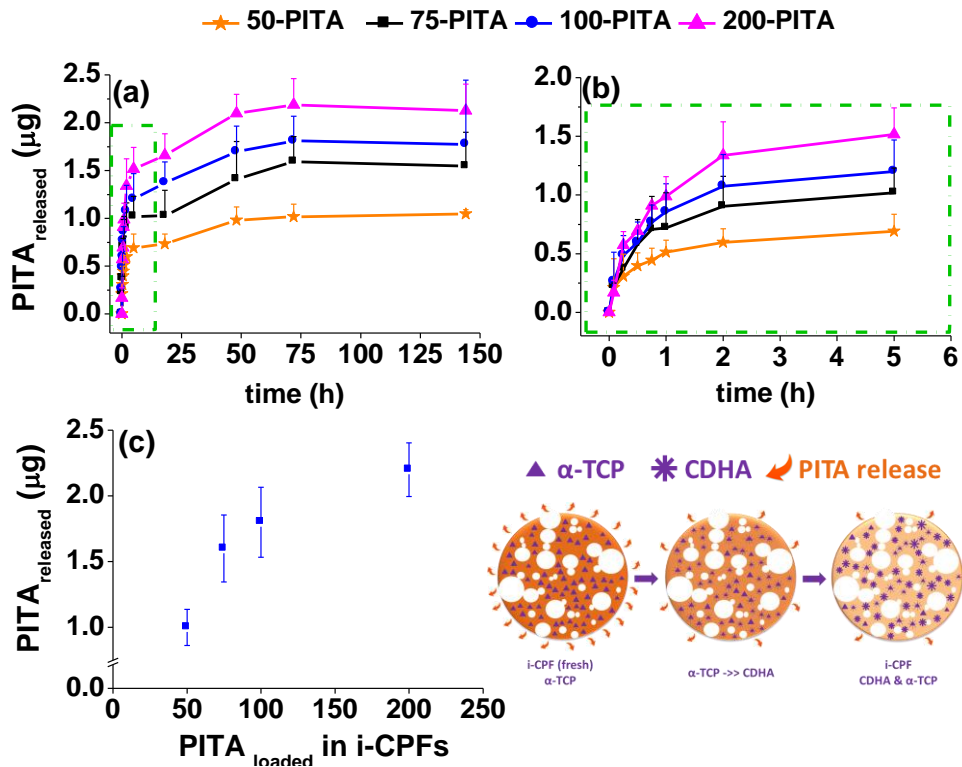


Figure 5-6 Release curves of i-CPFs containing different amounts of PITA for 6 days (a), zoom of the initial 5 hours (b) and total amount of PITA released by 72 h is plotted for each specimen of PITA loaded i-CPFs such as 50-PITA, 75-PITA, 100-PITA & 200-PITA (c) with a proposed scheme of the release of PITA during the setting reaction.

Table 5-4 Percentage of total release of PITA in each i-CPF specimen after 72 h and values of R² and n with Kosermeier Peppas model for the release kinetics.

i-CPFs	PITA _{released} (%)	Korsmeyer-Peppas (KP)	
		R ²	n
50-PITA	97.07 ± 10.95	0.9418	0.29
75-PITA	97.02 ± 17.81	0.8813	0.45
100-PITA	67.61 ± 13.51	0.8840	0.32
200-PITA	40.93 ± 9.07	0.9097	0.20

Discussion

Many studies have reported the benefits of statins, specially SIM, in bone formation as well as inhibition of bone resorption [23], [27], [29], [35], [36]. Within the family of statins, PITA presents some interesting properties, in particular its lower price, hydrophilic properties and its comparable efficiency compared to other statins (i.e. SIM) at much lower concentrations. Therefore, PITA has potential advantages in views of fostering bone regeneration in combination with bone substitutes. However, to the best of our knowledge, this potential application of PITA is still unexplored. In this work we addressed some aspects that are relevant for this potential application, namely, the stability of PITA under different conditions, its biological effects on MSCs and EPCs *in vitro*, and the feasibility of incorporating it i-CPFs, including the effect of the molecule on the properties of the calcium phosphate foams and the release kinetics of the drug.

PITA solutions in PBS were stable both at 5 and 37 °C for 9 days, which is interesting with regard to potential storage of samples, and also in views of the experimental conditions during cell cultures and release experiments.

The setting of calcium phosphate foams involves a dissolution-precipitation reaction, which entail a pH fluctuation. The dissolution of α-TCP initially increases the pH of the liquid medium, up to pH=9.5, slowly decreasing to pH=8 in 24 h [32]. Therefore, initial 24 h of the setting reaction acts as an alkaline environment for PITA. To evaluate whether this pH range could affect the stability of PITA, different PITA concentrations were exposed to

alkaline pH of either 8 or 9.5 (Figure 5-2). No degradation was found for the 5 and 25 μM PITA solution over 9 days of exposure. In contrast, at higher concentrations of 50, 75 and 100 μM , a significant degradation was recorded which increased with exposure time at both pHs. This implies that there will be a partial degradation of PITA due to the pH fluctuations during the setting reactions. To estimate the extent of this degradation, we can assume that, according to previous studies that assessed the pH evolution during the setting reaction [32], [37], when PITA is mixed with an i-CPF, it will be exposed to a pH \leq 9.5 for the initial 15h, and to a pH \leq 8 during the following 9h. With this in mind, the degradation associated to the pH fluctuations during the setting reaction for 24 h were calculated respectively as shown in section 3.1 and used for correction of final percentage of PITA released.

Apart from other beneficial effects, statins are described to promote in vitro angiogenesis and osteogenesis in a dose dependent manner [31], [38]–[41]. However, few studies have been conducted with PITA to demonstrate such effects. The present work was originally designed for three different concentrations of 0.1, 1 and 10 μM . It was found that 10 μM resulted in toxic effects on the cell culture with complete loss of cell viability in rMSCs and EPCs. Therefore, the study was continued with PITA concentrations in the cell culture medium of 0.1 μM (0.0475 $\mu\text{g/mL}$) and 1 μM (0.475 $\mu\text{g/mL}$) (Figure 5-3). The results showed an over-expression of genes associated to osteogenesis and vascularization with the lowest dosage of PITA (0.1 μM). Our findings of OCN and BMP-2 over-expression are in agreement with other studies where the bone anabolic effect of PITA was reported to stimulate OCN by inhibition of Rho-associated kinase and BMP-2 in human osteoblasts [31] and collagen [30]. It has been observed that present study observed similar results at 72 h with a concentration of 0.1 μM in rMSCs whereas previous work reported over expression at 48h with 1 μM in human osteoblasts. This difference can be explained as concentration may depend on type of cells as seen earlier in other studies with simvastatin and other statins [42]–[45]. Our results indicate that PITA induces mineralization, differentiation and osteogenesis in rMSCs. ,

In the case of EPCs, gene expression values for VEGF, VEGFR1 and VEGFR2 were observed for their key role in angiogenesis. VEGFA plays an important role of key regulator to promote growth of vascular endothelial cells and vessel growth, therefore an important marker for angiogenesis [46]. While VEGFA binds to two receptors of VEGFR1 and VEGFR2, it has been seen that role of VEGFR1 is still not well defined as it is known

as a 'decoy' receptor which regulate VEGFA in a negative fashion by interfering with binding between VEGFA and VEGFR2 [47]. On the other hand, recent studies claimed that VEGFR1 plays a role in recruitment of endothelial progenitors [48]. Therefore, role of VEGFR1 is still under debate. Whereas, VEGFR2 plays a key role in angiogenesis by enhancing effects of VEGFA by binding with it [49]. In present work, a significant increase had been observed in VEGFA, VEGFR2 and VEGFR1 at 72 h suggesting stimulation of vascularization by PITA. It is important to take into account that increase in VEGFR2 was three fold which is really essential for binding with VEGFA and stimulating angiogenesis. Similarly, PITA [50] and other statins [39], [51], [52] have been previously described to promote angiogenesis. Collectively, our data suggest that PITA has bone anabolic effects on both rMSCs and rEPCs, coping well with other studies, where 0.1 μM was also found to be the most effective dose [31], [41].

In addition to the bone anabolic effects just discussed, PITA being a hydrophilic molecule allows direct dissolution in the aqueous liquid medium used for i-CPFs synthesis. This is an advantage, as SIM requires an additional step to convert it from hydrophobic to hydrophilic by lactone ring opening, if solubility in an aqueous phase is desired [53]. In contrast, PITA can be directly incorporated in the aqueous phase of the self-setting foams to have a homogenous distribution throughout the foam volume, which can facilitate a sustained and a prolonged release. Drug incorporation in self-setting cements and foams can often result in modification of the setting times or alteration of the texture or porosity, among other parameters [14], [54], [55]. Therefore, characterization of macroporous i-CPFs was conducted for 100-PITA samples. As shown in Figure 5-4, it was found that PITA did not induce observable changes in the microstructure. Similarly, MIP pore size entry distribution was found to be similar for i-CPF as well as PITA loaded i-CPF (Figure 5-6.). SEM images showed plate like crystallites characteristic of the setting of α -TCP to calcium-deficient hydroxyapatite [56]. Also, reconstruction from the μCT scans allowed visualization of the interconnected macropores. The interconnected pores were seen clearly for control i-CPF as well as PITA (100 μM) loaded i-CPF. The skeletal density, total porosity and specific surface area were in accordance with previous results and displayed no significant differences among control i-CPF and PITA loaded i-CPF at 100 μM . These findings were in agreement with other studies for statins, where they showed that SIM did not alter phase composition or porosity of cements [57].

The concentration of PITA loaded in the i-CPFs was several times above the 0.1 μM

found to be fostering expression of angiogenic and mineralization genes. This was done with two considerations in mind: 1) the degradation of the drug due to the setting reaction that can be assumed to “inactivate” a ~6.5-8 % of the PITA incorporated in i-CPFs (as seen for 50, 75 and 100 μ M) during the period the setting proceeds at basic pHs between 8 and 9.5; and 2) in our release assays, having a detectable concentration of PITA had to be ensured (below 1 μ M was undetectable) , and studying the release behavior of i-CPFs (Figure 5-5) may allow extrapolating to adjust the concentration in future.

The behavior of initial burst release was in agreement with other findings showing fresh or pre-set for shorter time cements shows burst behavior [57]. The kosermeier peppas model was fitted to analyze the release kinetics but did not allow any conclusion due to limiting release mechanism as the parameter (n) was too low for the case of flat surfaces. On the other hand, some studies based on matrix tablets have shown that a lower value of $n < 4.5$ reflects a quasi-fickian diffusion behavior [58], [59]. . The profiles obtained can be ascribed to the evolving microstructure of the cement setting, which is responsible for the change in the elution regimes. Initially, the paste is just a suspension of α -TCP particles in aqueous solutions of PITA. As α -TCP precipitates to CDHA following the cement setting reaction, the network of CDHA crystals created progressively increases tortuosity, hindering the drug diffusion and reducing the release rate [57].

It has been observed that with 50-PITA released 0.2 μ g/mL which is still very high in comparison to findings of *in vitro* studies at 0.1 μ M PITA (0.0475 μ g/mL) for significant results. It is important to keep in account that release studies were designed with the aim of being in the detection range (1 μ M) of HPLC technique for PITA. However, with the observation of drug loading and release behavior, it is most susceptible that with extrapolation of data, a lower loading of PITA (5-10 μ M), will be respective to a release of 0.1 μ M similar to *in vitro* studies. Thereby, it opens a new pathway for future work on PITA loaded i-CPFs with cells *in vitro*.

When comparing the present findings with our findings of Chapter 3 on simvastatin loaded scaffolds [64]: a) PITA shows a much higher loading efficiency due to higher solubility than simvastatin, which gives an edge for incorporation of PITA through liquid phase b) Percentages released are much higher (~97 - 40 % PITA vs. 16 % Simvastatin in Chapter 3), and progressive, which can be explained by the fact that i-CPFs are evolving matrices, with a high amount of liquid phase where PITA is dissolved, so in the initial release timeframe, exchange with the release media is much more favored than with the set

macroporous CDHA samples [60]. PITA is efficient at lower dosages [61] so the progressive release behavior might allow to maximize the efficiency of the treatment .

Different release profiles are reported in the literature for SIM with calcium phosphate ceramics [62], premixed cement [63] and comparison of CDHA/ceramic [60], however, it is first time that PITA has been loaded with a calcium phosphate. The i-CPFs presented in this study exhibit a progressive release profile, corresponding to ~40% of the quantity loaded in 200-PITA and almost 97% released for 50-PITA and 75-PITA. The interconnected macroporosity (Figure 5-6b) of all these samples is expected to enhance, in addition, tissue colonization. The release profile of all samples stabilized after 72 h where probably a significant amount of α -TCP had transformed already to CDHA, hindering the diffusion of the drug trapped within the crystal structure as reflected in Figure 5-6. Moreover, the macroporosity of the i-CPFs investigated can be assumed to foster higher amounts of drug released to the media, in comparison with their non-macroporous homologues, as fluid exchange is fostered in this kind of samples with respect to dense cements [14].

Conclusions

First, PITA showed a stable behavior in PBS at different working temperatures of 37 °C (scaffold preparation; release kinetics) and 5 °C (*in vitro* studies). On the other hand, pH 8 and pH 9.5 resulted in progressive degradation of PITA at higher concentrations of 50, 75 and 100 μ M. Second, i-CPFs and PITA loaded i-CPFs both exhibited similar interconnected macroporous structure with no significant changes in microstructure (Plate like crystallites), SSA, total porosity, pore size distribution and skeletal density. Third, PITA application in solution resulted in enhancement of gene expressions of OCN, collagen type 1 and BMP-2 in rMSCs indicating towards mineralization and differentiation. In case of EPCs, gene expressions of VEGFA, VEGFR2, and VEGFR1 were enhanced by 72 as verified by RT-PCR as indicators of angiogenesis. Finally, PITA loaded i-CPFs followed release kinetics according to the evolving microstructure of the scaffold in the initial hours with a burst release which slowly progressed in a dose-dependent manner. Design of the i-CPFs as a drug delivery system loaded with PITA, an osteogenic and angiogenic promoter, allowing very low dosages, with the fact that it does not alter the attractive biomimetic features of the i-CPFs studied here makes them a captivating alternative for versatile bone grafts.

References

- [1] P. P. Spicer, J. D. Kretlow, S. Young, J. A. Jansen, F. K. Kasper, and A. G. Mikos, "Evaluation of bone regeneration using the rat critical size calvarial defect," *Nat. Protoc.*, vol. 7, no. 10, pp. 1918–1929, Sep. 2012.
- [2] W. Brown and L. Chow, "A new calcium-phosphate setting cement," *J. Dent. Res.*, vol. 62, no. 19, pp. 672–672, 1983.
- [3] R. Z. LeGeros, "Calcium phosphate-based osteoinductive materials.," *Chem. Rev.*, vol. 108, no. 11, pp. 4742–53, Nov. 2008.
- [4] M. P. Ginebra, M. Espanol, E. B. Montufar, R. A. Perez, and G. Mestres, "New processing approaches in calcium phosphate cements and their applications in regenerative medicine.," *Acta Biomater.*, vol. 6, no. 8, pp. 2863–73, Aug. 2010.
- [5] S. V. Dorozhkin, "Calcium orthophosphate cements for biomedical application," *J. Mater. Sci.*, vol. 43, no. 9, pp. 3028–3057, Mar. 2008.
- [6] M. Bohner, "Calcium orthophosphates in medicine: from ceramics to calcium phosphate cements," *Injury*, vol. 31, no. SUPPL. 4, pp. D37–D47, Dec. 2000.
- [7] S. Deb, Orthopaedic bone cements. .
- [8] M. Bohner, U. Gbureck, and J. E. Barralet, "Technological issues for the development of more efficient calcium phosphate bone cements: A critical assessment," *Biomaterials*, vol. 26, no. 33, pp. 6423–6429, Nov. 2005.
- [9] M. Bohner, L. Galea, and N. Doebelin, "Calcium phosphate bone graft substitutes: Failures and hopes," *J. Eur. Ceram. Soc.*, vol. 32, no. 11, pp. 2663–2671, Aug. 2012.
- [10] M. Espanol, R. A. Perez, E. B. Montufar, C. Marichal, A. Sacco, and M. P. Ginebra, "Intrinsic porosity of calcium phosphate cements and its significance for drug delivery and tissue engineering applications.," *Acta Biomater.*, vol. 5, no. 7, pp. 2752–62, Sep. 2009.
- [11] D. Pastorino, C. Canal, and M.-P. Ginebra, "Multiple characterization study on porosity and pore structure of calcium phosphate cements," *Acta Biomater.*, vol. 28, pp. 205–214, Dec. 2015.
- [12] M.-P. Ginebra, T. Traykova, and J. A. Planell, "Calcium phosphate cements: competitive drug carriers for the musculoskeletal system?," *Biomaterials*, vol. 27, no. 10, pp. 2171–7, Apr. 2006.
- [13] E. Verron, I. Khairoun, J. Guicheux, and J.-M. Bouler, "Calcium phosphate biomaterials as bone drug delivery systems: a review.," *Drug Discov. Today*, vol. 15, no. 13–14, pp. 547–52, Jul. 2010.
- [14] D. Pastorino, C. Canal, and M.-P. Ginebra, "Drug delivery from injectable calcium phosphate foams by tailoring the macroporosity-drug interaction.," *Acta Biomater.*, vol. 12, pp. 250–9, Jan. 2015.
- [15] M.-P. Ginebra, C. Canal, M. Espanol, D. Pastorino, and E. B. Montufar, "Calcium phosphate cements as drug delivery materials.," *Adv. Drug Deliv. Rev.*, vol. 64, no. 12, pp. 1090–110, Sep. 2012.
- [16] A. Almirall, G. Larrecq, J. . Delgado, S. Martínez, J. . Planell, and M. . Ginebra, "Fabrication of low temperature macroporous hydroxyapatite scaffolds by foaming and hydrolysis of an α -TCP paste," *Biomaterials*, vol. 25, no. 17, pp. 3671–3680, 2004.
- [17] E. B. Montufar, T. Traykova, C. Gil, I. Harr, A. Almirall, A. Aguirre, E. Engel, J. A. Planell, and M. P. Ginebra, "Foamed surfactant solution as a template for self-setting injectable hydroxyapatite scaffolds for bone regeneration.," *Acta Biomater.*, vol. 6, no. 3, pp. 876–85, Mar. 2010.
- [18] R. A. Perez, H.-W. Kim, and M.-P. Ginebra, "Polymeric additives to enhance the functional

properties of calcium phosphate cements.," *J. Tissue Eng.*, vol. 3, no. 1, p. 2041731412439555, Jan. 2012.

[19] R. P. del Real, E. Ooms, J. G. C. Wolke, M. Vallet-Regí, and J. A. Jansen, "In vivo bone response to porous calcium phosphate cement," *J. Biomed. Mater. Res. Part A*, vol. 65A, no. 1, pp. 30–36, Apr. 2003.

[20] S. del Valle, N. Miño, F. Muñoz, A. González, J. A. Planell, and M.-P. Ginebra, "In vivo evaluation of an injectable Macroporous Calcium Phosphate Cement," *J. Mater. Sci. Mater. Med.*, vol. 18, no. 2, pp. 353–361, Feb. 2007.

[21] S. Takagi and L. C. Chow, "Formation of macropores in calcium phosphate cement implants," *J. Mater. Sci. Mater. Med.*, vol. 12, no. 2, pp. 135–139, Feb. 2001.

[22] J. K. Liao and U. Laufs, "Pleiotropic effects of statins.," *Annu. Rev. Pharmacol. Toxicol.*, vol. 45, pp. 89–118, Jan. 2005.

[23] G. Mundy, "Stimulation of Bone Formation in Vitro and in Rodents by Statins," *Science (80- .)*, vol. 286, no. 5446, pp. 1946–1949, Dec. 1999.

[24] I. Garrett, G. Gutierrez, and G. Mundy, "Statins and Bone Formation.," *Curr. Pharm. Des.*, vol. 7, no. 8, pp. 715–736, May 2001.

[25] S. Vickers, C. A. Duncan, I. W. Chen, A. Rosegay, and D. E. Duggan, "Metabolic disposition studies on simvastatin, a cholesterol-lowering prodrug.," *Drug Metab. Dispos.*, vol. 18, no. 2, pp. 138–45, 1990.

[26] R. Y. A. Mukhtar, J. Reid, and J. P. D. Reckless, "Drug focus," *Int. J. Clin. Pract.*, vol. 59, no. February, pp. 239–252, Feb. 2005.

[27] N. Horiuchi and T. Maeda, "Statins and bone metabolism.," *Oral Dis.*, vol. 12, no. 2, pp. 85–101, Mar. 2006.

[28] Y. Saito, "Pitavastatin: an overview.," *Atheroscler. Suppl.*, vol. 12, no. 3, pp. 271–6, Nov. 2011.

[29] Y. Zhang, A. D. Bradley, D. Wang, and R. A. Reinhardt, "Statins, bone metabolism and treatment of bone catabolic diseases.," *Pharmacol. Res.*, Jan. 2014.

[30] T. Majima, A. Shimatsu, Y. Komatsu, N. Satoh, A. Fukao, K. Ninomiya, T. Matsumura, and K. Nakao, "Short-term effects of pitavastatin on biochemical markers of bone turnover in patients with hypercholesterolemia.," *Intern. Med.*, vol. 46, no. 24, pp. 1967–1973, Jan. 2007.

[31] K. Ohnaka, S. Shimoda, H. Nawata, H. Shimokawa, K. Kaibuchi, Y. Iwamoto, and R. Takayanagi, "Pitavastatin Enhanced BMP-2 and Osteocalcin Expression by Inhibition of Rho-Associated Kinase in Human Osteoblasts," *Biochem. Biophys. Res. Commun.*, vol. 287, no. 2, pp. 337–342, 2001.

[32] C. Canal, D. Pastorino, G. Mestres, P. Schuler, and M.-P. Ginebra, "Relevance of microstructure for the early antibiotic release of fresh and pre-set calcium phosphate cements.," *Acta Biomater.*, vol. 9, no. 9, pp. 8403–12, Sep. 2013.

[33] a Aguirre, a González, J. a Planell, and E. Engel, "Extracellular calcium modulates in vitro bone marrow-derived Flk-1+ CD34+ progenitor cell chemotaxis and differentiation through a calcium-sensing receptor.," *Biochem. Biophys. Res. Commun.*, vol. 393, no. 1, pp. 156–61, Feb. 2010.

[34] A. Aguirre, J. A. Planell, and E. Engel, "Dynamics of bone marrow-derived endothelial progenitor cell/mesenchymal stem cell interaction in co-culture and its implications in angiogenesis," *Biochem. Biophys. Res. Commun.*, vol. 400, no. 2, pp. 284–291, Sep. 2010.

[35] A. Moshiri, A. M. Sharifi, and A. Oryan, "Role of Simvastatin on fracture healing and osteoporosis: a systematic review on in vivo investigations," *Clin. Exp. Pharmacol. Physiol.*, vol. 43, no. 7, pp. 659–684, Jul. 2016.

- [36] S. R. Shah, C. A. Werlang, F. K. Kasper, and A. G. Mikos, "Novel applications of statins for bone regeneration," *Natl. Sci. Rev.*, vol. 2, no. 1, pp. 85–99, Mar. 2015.
- [37] M.-P. Ginebra, E. Fernandez, F. C. M. Driessens, and J. A. Planell, "Modeling of the Hydrolysis of β -Tricalcium Phosphate," *J. Am. Ceram. Soc.*, vol. 82, no. 10, pp. 2808–2812, Dec. 2004.
- [38] T. Maeda, a Matsunuma, T. Kawane, and N. Horiuchi, "Simvastatin promotes osteoblast differentiation and mineralization in MC3T3-E1 cells.," *Biochem. Biophys. Res. Commun.*, vol. 280, no. 3, pp. 874–7, Jan. 2001.
- [39] T. Maeda, T. Kawane, and N. Horiuchi, "Statins augment vascular endothelial growth factor expression in osteoblastic cells via inhibition of protein prenylation.," *Endocrinology*, vol. 144, no. 2, pp. 681–92, Feb. 2003.
- [40] T. Maeda, A. Matsunuma, I. Kurahashi, T. Yanagawa, H. Yoshida, and N. Horiuchi, "Induction of osteoblast differentiation indices by statins in MC3T3-E1 cells.," *J. Cell. Biochem.*, vol. 92, no. 3, pp. 458–71, Jun. 2004.
- [41] H. Kaji, J. Naito, Y. Inoue, H. Sowa, T. Sugimoto, and K. Chihara, "Statin suppresses apoptosis in osteoblastic cells: role of transforming growth factor-beta-Smad3 pathway.," *Horm. Metab. Res.*, vol. 40, no. 11, pp. 746–51, Nov. 2008.
- [42] Y. Qi, T. Zhao, W. Yan, K. Xu, Z. Shi, and J. Wang, "Mesenchymal stem cell sheet transplantation combined with locally released simvastatin enhances bone formation in a rat tibia osteotomy model," *Cytotherapy*, vol. 15, no. 1, pp. 44–56, Jan. 2013.
- [43] K. H. Baek, W. Y. Lee, K. W. Oh, H. J. Tae, J. M. Lee, E. J. Lee, J. H. Han, M. Il Kang, B. Y. Cha, K. W. Lee, H. Y. Son, and S. K. Kang, "The Effect of Simvastatin on the Proliferation and Differentiation of Human Bone Marrow Stromal Cells," *J. Korean Med. Sci.*, vol. 20, no. 3, p. 438, Jun. 2005.
- [44] T. Maeda, A. Matsunuma, T. Kawane, and N. Horiuchi, "Simvastatin Promotes Osteoblast Differentiation and Mineralization in MC3T3-E1 Cells," *Biochem. Biophys. Res. Commun.*, vol. 280, no. 3, pp. 874–877, Jan. 2001.
- [45] S. Ruiz-Gaspa, X. Nogues, A. Enjuanes, J. C. Monllau, J. Blanch, R. Carreras, L. Mellibovsky, D. Grinberg, S. Balcells, A. Díez-Perez, and J. Pedro-Botet, "Simvastatin and atorvastatin enhance gene expression of collagen type 1 and osteocalcin in primary human osteoblasts and MG-63 cultures," *J. Cell. Biochem.*, vol. 101, no. 6, pp. 1430–1438, Aug. 2007.
- [46] N. Ferrara, H.-P. Gerber, and J. LeCouter, "The biology of VEGF and its receptors," *Nat. Med.*, vol. 9, no. 6, pp. 669–676, Jun. 2003.
- [47] R. L. Kendall and K. A. Thomas, "Inhibition of vascular endothelial cell growth factor activity by an endogenously encoded soluble receptor.," *Proc. Natl. Acad. Sci. U. S. A.*, vol. 90, no. 22, pp. 10705–9, Nov. 1993.
- [48] S. Hiratsuka, K. Nakamura, S. Iwai, M. Murakami, T. Itoh, H. Kijima, J. M. Shipley, R. M. Senior, and M. Shibuya, "MMP9 induction by vascular endothelial growth factor receptor-1 is involved in lung-specific metastasis.," *Cancer Cell*, vol. 2, no. 4, pp. 289–300, Oct. 2002.
- [49] F. Shalaby, J. Rossant, T. P. Yamaguchi, M. Gertsenstein, X.-F. Wu, M. L. Breitman, and A. C. Schuh, "Failure of blood-island formation and vasculogenesis in Flk-1-deficient mice," *Nature*, vol. 376, no. 6535, pp. 62–66, Jul. 1995.
- [50] R. Maas, C.-C. Huang, J.-S. Chen, T.-C. Wu, H.-B. Leu, P.-H. Huang, T.-T. Chang, S.-J. Lin, J.-W. Chen, H. Yip, K. Kluge, B. Schäfer, D. Hossfeld, W. Fiedler, H. Drexler, A. Caruso, S. Kittner, D. Lackland, J. Lichtman, L. Lisabeth, D. Makuc, G. Marcus, A. Marelli, D. Matchar, C. Moy, D. Mozaffarian, M. Mussolino, G. Nichol, N. Paynter, and E. Soliman, "Pharmacotherapies and their influence on asymmetric dimethylarginine (ADMA)," *Vasc. Med.*, vol. 10, no. 1 suppl, pp. S49–S57, Jul. 2005.

- [51] Y. Zhang, R. Zhang, Y. Li, G. He, D. Zhang, and F. Zhang, "Simvastatin augments the efficacy of therapeutic angiogenesis induced by bone marrow-derived mesenchymal stem cells in a murine model of hindlimb ischemia," *Mol. Biol. Rep.*, vol. 39, no. 1, pp. 285–293, Jan. 2012.
- [52] M. Frick, J. Dulak, J. Cisowski, A. Józkwicz, R. Zwick, H. Alber, W. Dichtl, S. P. Schwarzacher, O. Pachinger, and F. Weidinger, "Statins differentially regulate vascular endothelial growth factor synthesis in endothelial and vascular smooth muscle cells," *Atherosclerosis*, vol. 170, no. 2, pp. 229–236, 2003.
- [53] A. T. Serajuddin, S. A. Ranadive, and E. M. Mahoney, "Relative lipophilicities, solubilities, and structure-pharmacological considerations of 3-hydroxy-3-methylglutaryl-coenzyme A (HMG-CoA) reductase inhibitors pravastatin, lovastatin, mevastatin, and simvastatin.," *J. Pharm. Sci.*, vol. 80, no. 9, pp. 830–834, Sep. 1991.
- [54] M. Bohner, J. Lemaître, P. Van Landuyt, P. Y. Zambelli, H. P. Merkle, and B. Gander, "Gentamicin-loaded hydraulic calcium phosphate bone cement as antibiotic delivery system.," *J. Pharm. Sci.*, vol. 86, no. 5, pp. 565–72, May 1997.
- [55] A. Ratier, I. . Gibson, S. . Best, M. Freche, J. . Lacout, and F. Rodriguez, "Setting characteristics and mechanical behaviour of a calcium phosphate bone cement containing tetracycline," *Biomaterials*, vol. 22, no. 9, pp. 897–901, May 2001.
- [56] S. Gallinetti, C. Canal, and M.-P. Ginebra, "Development and Characterization of Biphasic Hydroxyapatite/ β -TCP Cements," *J. Am. Ceram. Soc.*, vol. 97, no. 4, pp. 1065–1073, Apr. 2014.
- [57] G. Mestres, K. Kugiejko, D. Pastorino, J. Unosson, C. Öhman, M. Karlsson Ott, M.-P. Ginebra, and C. Persson, "Changes in the drug release pattern of fresh and set simvastatin-loaded brushite cement," *Mater. Sci. Eng. C*, vol. 58, pp. 88–96, 2016.
- [58] T. Haque, U. Mesbah, S. Talukder, K. Laila, M. S. Fatema, M. Islam, and R. Selim, "Model Dependent and Independent Approaches to Compare In vitro Release Profiles from Ethylcellulose and Eudragit L100 Based Matrix Tablets."
- [59] S. Basak, B. Jayakumar Reddy, and K. Lucas Mani, "Formulation and release behaviour of sustained release ambroxol hydrochloride HPMC matrix Tablet," *Indian J. Pharm. Sci.*, vol. 68, no. 5, p. 594, 2006.
- [60] C. Canal, K. Khurana, S. Gallinetti, S. Bhatt, J. Pulpytel, F. Arefi-Khonsari, and M.-P. Ginebra, "Design of calcium phosphate scaffolds with controlled simvastatin release by plasma polymerisation," *Polymer (Guildf)*, vol. 92, pp. 170–178, Jun. 2016.
- [61] S. Hayes, "Remington: The Science and Practice of Pharmacy, volume I and volume II. Twenty-second edition," *J. Med. Libr. Assoc.*, vol. 102, no. 3, pp. 220–221, Jul. 2014.
- [62] J. Chou, T. Ito, M. Otsuka, B. Ben-Nissan, and B. Milthorpe, "The effectiveness of the controlled release of simvastatin from β -TCP macrosphere in the treatment of OVX mice," *J. Tissue Eng. Regen. Med.*, vol. 10, no. 3, pp. E195–E203, Mar. 2016.
- [63] M. Montazerolghaem, K. Ott, and Montazerolghaem et al, "Sustained release of Simvastatin from premixed injectable Calcium Phosphate Cement," *J. Biomed. Mater. Res. A*, pp. 1–8, Mar. 2013.
- [64] C. Canal, K. Khurana, S. Gallinetti, S. Bhatt, J. Pulpytel, F. Arefi-Khonsari, and M. P. Ginebra, "Design of calcium phosphate scaffolds with controlled simvastatin release by plasma polymerisation," *Polym. (United Kingdom)*, vol. 92, pp. 170–178, 2016.

Chapter 6 Conclusions

This thesis deals with the development and investigation of novel strategies for improved tunable release from calcium phosphates as drug delivery vehicles. Two kinds of drugs are investigated: antibiotics, and statins. The main findings are summarized below:

Regarding the use of plasma polymerization to modulate SVA release from Calcium phosphate scaffolds

- This work has allowed setting proof of concept of the possibility to fine tune drug release of simvastatin acid (SVA) as osteogenic and angiogenic drug, incorporated in 3D ceramic scaffolds (CDHA & β -TCP) with a dry plasma polymerization process using biocompatible plasma polymers, PCL-co-PEG (1:4).
- The thickness and structure of the polymer coatings obtained is highly dependent on the texture of the materials, in particular on its SSA. Due to its much higher SSA, thinner polymer layers were deposited on CDHA, allowing for the diffusion of the drug and leading to progressive and controlled drug release with respect to the uncoated biomaterial. On the other hand, β -TCP's distinct textural features led to thicker polymer layers, which acted as a barrier impairing SVA release within the timeframe evaluated.
- On CDHA, long plasma polymerization times implied an initial blocking of the release, followed by a slow release pattern, while short treatment times allowed a slow, controlled release.
- The mode of deposition (continuous or pulsed wave) allowed to further control the plasma polymer layers produced. Thus, the plasma coatings evaluated were found to be suitable for tuning the drug release from bone biomaterials, allowing to produce ceramic dosage forms combining delayed release, followed by controlled delivery of drugs.

Regarding fundamentals of plasma polymerization on β -TCP for drug release

- Plasma polymerization of PEG-like polymers on microporous β -Tricalcium Phosphate (β -TCP) allowed obtaining coatings with low retention of the PEG character (high C/O ratio, grafting of end groups such as C=O and cross-linking of the polymer) which allowed avoiding the typical antifouling properties of the coating
- Due to the significant roughness of the surface of β -TCP, following plasma coating the bioceramics showed a hydrophobic behavior, despite the wettability of the polymer layer produced. This was associated with Wenzel behavior, which allowed calculating the apparent surface of the material being around 2.6.
- The coating thickness was directly dependent on the polymerization time, which in turn was related to the total amount of drug released. In general it was observed that the coatings produced decreased the amount of drug released, a part of which was hypothesized to be due to etching of the most superficial drug adsorbed on the surface during plasma processes. Moreover, for certain conditions the release profile started to be modified.
- The two antibiotics evaluated (ampicillin and gentamicin) retained their antimicrobial activity intact after being released from the β -TCP substrates, confirming the suitability of the technique for coating the drug-loaded ceramic matrices.
- Despite the great modification in wettability due to the PEG-like coating, the good cytocompatibility of β -TCP (adhesion and proliferation of SaOS-2) remained unaltered. The research undertaken allowed unraveling the characteristics of plasma coatings on calcium phosphate ceramics and advancing towards the design of drug delivery matrices with suitable biological and microbiological behavior.

Regarding PITA as osteogenic and angiogenic promoter loaded in i-CPFs as drug delivery vehicles

- Pitavastatin (PITA) was incorporated for the first time to calcium phosphate bone grafts, in particular in injectable calcium foams (i-CPFs) and no modifications were recorded on the physic-chemical properties of the i-CPFs. In particular, i-CPFs maintained its injectability, cohesion and interconnected macroporosity with no significant changes in microstructure and related parameters (SSA, total porosity and skeletal density).
- PITA exhibited a time-dependent degradation at basic pHs for concentrations above 50 μM (between 6.8% and 8.2%), which is important to take into account in the preparation of PITA-laden calcium phosphate cements. Conversely, solutions of PITA in PBS were shown to be stable at of 5 $^{\circ}\text{C}$ and 37 $^{\circ}\text{C}$.
- The in vitro effects of PITA on rMSCs and EPCs were clearly dose-dependent, with an optimum value found at 0.1mM. The osteogenic properties of PITA were investigated with rMSCs and showed enhancement of gene expression for OCN, Col type 1 and BMP-2, indicating the promotion of mineralization and differentiation. Moreover, using the same concentration, PITA-treated, EPCs showed increased over-expression of VEGFA, VEGFR1, VEGFR2, indicating an enhancement of vascularization and angiogenic properties.
- Finally, PITA-loaded i-CPFs followed a release kinetics that matched to the evolving microstructure of the scaffold in the initial hours due to setting, with a dose-dependent release which reached between 40% and 97% of the initial loaded amount depending on the initial concentration loaded. Therefore, the drug loading in the i-CPFs may easily be scaled to the suitable range with optimum biological activity. The combination of PITA with the i-CPFs studied in this work is a promising alternative for versatile bone grafts, which gather the interesting anabolic properties of the drug with the biomimetic features of the CDHA carrier.

